The
University
Of
Sheffield.

Switchable adhesion between oppositely charged polyelectrolytes

by

Rita La Spina

Submitted for the degree of Doctor of Philosophy

Department of Physics and Astronomy

December 2009

To my parents

"The nature of rain is the same, but it makes thorns grow in the marshes and flowers in the garden"

Arabic proverb

Abstract

Adhesion is a well-studied phenomenon, mainly for its industrial importance. We consider a smart water-based adhesive that is switchable, i.e. the adhesion may be turned on and off by an environmental trigger, in this case the pH.

The interaction investigated is between a weak polyacid hydrogel of poly(methacrylic acid) (PMAA) and poly[2-(dimethyl amino)ethyl methacrylate] (PDMAEMA, a weak polybase) chemically grafted to planar silicon substrates (brushes) by atom transfer radical polymerisation.

The interaction between PDMAEMA and PMAA is of great interest because it represents a situation where a surface adhesive (a polybase in contact with a polyacid) can be turned on and off simply by changing the external environment. In particular we observe that at pH less than 2, there is no significant interaction between the brush and hydrogel, whereas above pH 3, there is strong adhesion comparable to epoxy glue. The interaction between the brush and the gel is pressure sensitive so that the adhesion energy is a function of the applied load.

To understand the mechanism involved in the pressure sensitive behaviour we performed neutron reflectivity experiments of the brush in contact with the hydrogel after known pressures were applied. Comparison of the conformations of brushes of different thicknesses but with the same applied pressure shows that the interaction between the brush and hydrogel takes place at the interface and is mainly due to electrostatic interactions between the carboxylic group of the hydrogel and the amino group into the brush. Viscoelastic dissipation in the hydrogel also contributes to the total work of adhesion.

Declarations

I declare that this thesis is the result of my own work except where the work of others is cited, either explicitly or via the list of references.

No part of this dissertation has been submitted for a degree, diploma or other qualification at any other University.

Rita La Spina

December 2009

Acknowledgements

This thesis is the result of a collaboration between different people who have contributed with their different expertise.

I would like to thank Mark Geoghegan for his excellent supervision, support, patience, and friendship during these years of PhD;
The scientific meetings in front of a coffee or beer have been helpful in developing brilliant ideas and strategy to deal with the project. He gave me the opportunity to grow as a more independent researcher and at the same time to experience the "scientific world" allowing me to participate to international conferences and industrial meeting and be aware of scholarships and awards.
In particular I thank him for introducing me to the "amazing" world of the neutron reflectivity without which my life would have no meaning....

I also acknowledge Michael Tomlinson for his great help in the chemistry part of the project such as the synthesis of brush and ATRP and especially for sharing his positive attitude about work and life. He has been the psychological (spiritual) support in the very difficult period of my PhD. I learnt from him how to look at things in a rational way without forgetting or hiding the spontaneous passion and dramatic parts of my character.

I am extremely grateful to Arnaud Chiche for introducing me to the "obscure" world of adhesion and for his patience and support and full availability. He has been the "key" person in the development of the project from improving the machine to make the experiments, to the treatment of the data. I shall never forget the long conversations on MSN about adhesion when the rest of the office thought I was not really doing any work... and I am sure it was the same for him!

I would like to thank Lorena Ruiz Pérez for her help when I arrived in Sheffield, and in particular, for explaining to me (in Italian!) the project and for familiarizing me with the new physics and chemistry labs and environments.

A big thanks goes to the mechanical workshops in the Physics department, in particular to Simon Dixon and to the Daniel Jackson in the glass workshop in the Chemistry department for contributing to the project with practical ideas and for his advice and suggestions as well as making the components of the experimental set-up. (Simon's ingenuity in finding utility for bicycle pumps in a scientific project still amazes me!)

I am very grateful to the Polyfilm young and experienced researchers for the collaboration and the good time together during several meetings in different parts of Europe. A special thanks goes to Prof. Liliane Léger for her advice during at the real starting point of the project when I was pretty much lost. Of course, I acknowledge the European Union for funding.

I cannot forget Mark's group for the friendly time spent together: Johann, Ana, Zhenyu, Pierre, Matt, Ateyyah, Yu Pen, Ana-Lorena, and Youmna and in particular Maryam for her help in the AFM experiments and Steve for preparing the brush samples.

In the chemistry department I would like to thank Professor Tony Ryan and Professor Chris Hunter for allowing me to use their labs.
I am grateful to the postdocs for suggestion and help during these years: Andy, Alan, Lekshmi, Tsvetelin, Tanja, Jonathan, in particular Steve Carter to prepare some brush sample in Physics department, and Andy, Collin, Paul, Simon in Chemistry department.

At the Rutherford Appleton Laboratory (ISIS) I would like to thank Sean Langridge and in Laboratoire Léon Brillouin, CEA at Saclay (France) Alain Menelle and Fabrice Cousin, for providing assistance with the neutron reflectivity experiments; and Mike Weir to share the pain and the pleasure of the beamtime in Saclay and ISIS.

During my PhD I spent 5 months at the Max-Planck-Institut für Metallforschung in Stuttgart in Germany. A special thanks goes to Professor Stanislav Gorb for his hospitality in his group and proving all the assistance to perform the experiments and

finishing an important part of my project and to his friendly group. I really enjoyed my time in Germany and it would not be possible without the presence of colleagues and friends: Martina, Henrik, Marlene, Dagmar, Elena, Alexander, Julia, Ellen, Florian, Blythe, Melanie, Steffen and in particular Conny, who looked after me during all my time in Stuttgart. Thanks are also due to the DAAD for funding this collaboration.

My time in Sheffield would not be so great without the presence of good friends always there in the good and bad moments that characterized the life. They are and will be always reference points and for how we are spread around the world the friendship is and will be always there. I will start with "my soulmate" Parvaneh, Christa, Frank, CMA, Jessica, Chris, Warren, Dennison, Mentxu, Luka, Steve, Céline, Dava, Susana, Richard, Christian, Hazel, Jaume, Yogi, Jo, Penelope, Enrique, Lorna, Brett, Damien, Véro, Julien, Pierre, Rafel, MariaRocio, Carlos, Lars, Iñigo.
And I cannot forget the Italian and Sicilian community in Sheffield, starting from Danieluzzo mio (BELLO!!!), Giovannuzzo, Marinella, Serenella, Francesca, Caterina, Roxana, Melchiorre, Valeria, Cristina, Federica, Federico, Alessandra, Valentina, and my pen-friend Sachin.
A big thanks goes to Richard Webb and all my friends at the Astronomy Art Group for many enjoyable evenings being "creative".

Most of all I want to thank my parents and brothers for their support in this long journey, called a PhD, and especially my parents, for allowing me to make my own decisions in life, even if they were not always happy about them! For this reason and for their constant support and love during my first 30 years on this planet, I dedicate this thesis to them.

Introduction

In this study, we are investigating the adhesion between poly[2-(dimethyl amino)ethyl methacrylate] (PDMAEMA, a polybase) chemically grafted to planar silicon substrates by atom transfer radical polymerisation, with a hydrogel of poly(methacrylic acid) (PMAA).

Adhesion is a well-studied phenomenon, mainly due to its industrial importance. There are several reasons that make adhesion science an interesting field nowadays. One is the need to move away from organic solvents on account of their environmental unfriendliness, but maintaining the same adhesion properties. Another is the desire to improve adhesion with "smart" behaviour, a capability being researched by many groups interested in bio-mimetic behaviour [1].

I present experiments which describe different form of smart water-based adhesion that is both switchable (the adhesion may be turned on and off) and reversible (adhesion on/off cycling is possible). The method is both inexpensive and requires a very small amount of material, in contrast with other forms of water-based adhesives, which require a high particulate content in order to achieve reasonable adhesion. In fact, this adhesion is nearly as strong as epoxy glue, when it is "on" .The only requirement is for a pH trigger; the adhesion is sensitive to pH and the adhesion can be turned off when the pH is lowered to acidic conditions.

This *in situ* switchable adhesion, where the adhesion can be turned on and off changing the pH environment, expands the variety of applications for also medical purpose because a wide range of biocompatible polymers can be used. Other applications include the process of sticking/unsticking labels from different types of containers, making the recycling process more efficient. Other applications are in the field of microfluidics, controlled wetting, lubrication, and adhesion.

In the literature, there are examples of tuning the properties of polyelectrolytes by changing the environment, such as using mixed polymer brushes that swell and collapse in selective solvents [2] by variation of the pH environment [3].

There are examples of interactions between electrolyte molecules and polymers with the same and oppositely charges in solution, including the study of biomolecules such as DNA [4], amino acids [5], interacting surfactants [6]; but, as far we are aware, there is only one example of a macroscopic interaction between oppositely charged polyelectrolytes. This study was performed by the group of Osada [7] in 1999 by bringing a PAMPS gel, [poly(2-acrylamido-2-methylpropanesulfonic acid)] into contact with a PDMAPPA-Q gel, [quaternized poly(N-[3-(dimethylamino)propyl] acrylamide]. This was part of a rheological study of the interaction between polyelectrolytes. In the case of PAMPS and PDMAPPA-Q, however, the gels would not slide over each other, but rather would adhere, and were thus fractured in the rheometer. The adhesion between these oppositely charged polyelectrolyte was not measured.

We here describe the interaction between oppositely charged polyelectrolytes in water solution, and focus on the interaction between weak polyelectrolytes. In particular, we are interested in the interaction between a pH responsive brush polymer grafted on an inorganic substrate and an oppositely charged hydrogel.

A polymer brush is a polymer layer attached with one end to the surface. If the grafting density of the polymer on the surface is high enough, the chains start to repel each other and they can be stretched away from the surface, making a brush shape rather like the bristles on a brush.

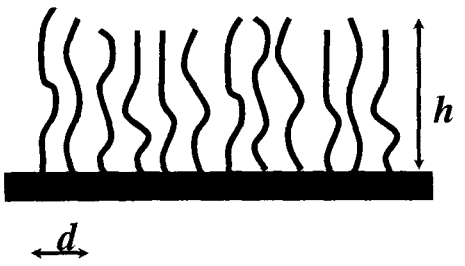

Fig 1 Schematic representation of a polymer brush anchored on substrate. *d* is the distance between to anchoring point and *h* is the thickness of the polymer layer.

In our case we are studying pH responsive PDMAEMA weak polyelectrolyte brush that may be characterised by a wettability transition and change in conformation as a function of the pH environment [6].

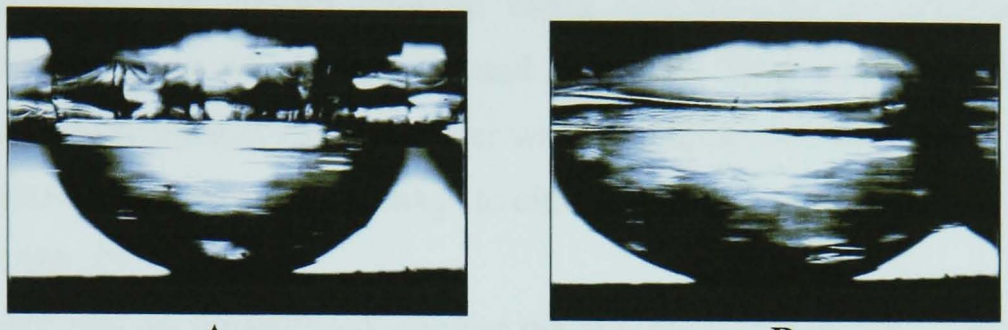

Fig 2 A) shows the swelling of a PMAA hydrogel lens at pH 2. B) shows the swelling of the hydrogel at pH 10. The comparison of the two pictures shows that the hydrogel is more collapsed in acid (pH 2) than when equilibrated in basic solution (pH 10).

The external media that we are considering is a crosslinked hydrogel, synthesised from a weak polyacid, the poly(methacrylic acid) (PMAA). This kind of gel is elastic and pliable when hydrated and is capable of large deformations in some pH environments. Also, an environmental change from acidic to basic pH induces in the gel a physical transition from hydrophobic to hydrophilic behaviour and vice versa [8].

The interaction between a polymer brush and an external network was already studied by O' Connor and McLeish who introduced the term of molecular Velcro™ [9] where the network plays the role of loops and the polymer brush acts as hooks. Theoretically [9] and experimentally [10-12] it has been shown that polystyrene (PS) brushes and gels and poly(dimethylsiloxane) (PDMS) brushes and gels can form molecular Velcro™; but it is not possible to separate the two parts, because after being in contact, the chains cannot disentangle because it is entropically forbidden, and the only way to detach the two parts is by bond breakage.

The challenge in this project is the development of a new way to measure adhesion between oppositely charge polyelectrolytes, to design a new adhesive, to be able to work under water with a strength comparable to epoxy resins, which is switchable and reversible, so that the adhesion can be tuned on and off and back on again as a function of the pH [13].

Upon examining the contact between brush and hydrogel at different pH, we recognize a pH region where the brush and gel do not interact with each other, and a region where they interact strongly under which condition it is difficult to remove the gel from the brush without any damage to either or both components as was shown by Gong in 1999 [7].

As a second step we investigated whether the process is switchable or whether it was forming a type of molecular Velcro™ [9], i.e. impossible to disentangle without bond breakage. We discovered that after changing the pH, the brush and gel would come apart without damaging either of the components.

The experimentally observed phenomena are:

- at pH less than 2, there is no significant interaction between the brush and hydrogel, whereas above pH 3, there is a strong adhesion which is comparable to that of an epoxy with a silanated glass [14] ;
- the adhesive interaction between the brush and gel above pH 3 can be reversed if immersed in a solution at pH 1 [13].

We also discovered that the interaction between the brush and hydrogel is pressure sensitive and that the work of adhesion is a function of the applied load.

We studied the mechanism involved in the adhesion between the brush and the hydrogel. Looking at the structure of the topology of the two polymers, brush and network, we figured out two that the main mechanisms of interaction, are either a surface and/or an interdigitation effect.

- Interfacial (surface) effect

  The applied force produces an increase in the contact area between the brush and hydrogel, creating more surface available for electrostatic or hydrogen bond interactions between the amino and carboxylic groups of the polybase and polyacid respectively.

- Interdigitation effect

  The Velcro™ [9] effect could be another mechanism involved where an increasing in applied load generates an interdigitation of the brush into the hydrogel.

The experimental data suggest that the dominant mechanism of interaction between the brush and the hydrogel is the interfacial effect which is likely to be between the

amino group of the brush side chains and the carboxylic groups of the PMAA hydrogel; there is no clear evidence of any interpenetration mechanism of the brush chains into the hydrogel. The contribution of hydrogen bonding is negligible in comparison to the electrostatic interaction. In general, the amount of charged groups is a function of the number degree of polymerisation and in the case of the brush it is proportional to the thickness of the polymer layer.

The switchable behaviour of the brush-gel system is triggered by the variation of pH in acid condition such as pH 1. In this pH condition, the brush is charged and swollen while the hydrogel is collapsed and uncharged. This shows that the driving force, generating the switchable behaviour, is the decreased amount of charges on the hydrogel which consequently reduces the electrostatic attraction between the brush and the hydrogel.

This thesis is divided into two parts:

The first part is related to the theoretical background concerning the adhesion theory, in Chapter 1. The chemistry and the physics of brushes and hydrogel for neutral polymers are described in Chapter 2, and for polyelectrolyte brushes and hydrogels in Chapter 3.

The second part is related to the experimental results. Chapter 4 focuses on the sample preparation and on the experimental techniques used in this project. Chapter 5 is related to the study of adhesion between the brush and the hydrogel, including the phenomenological effect and the mechanism of interaction. Chapter 6 concerns experiments where we calculate the real value of adhesion between the brush.

1. Creton, C. and S. Gorb, *Sticky feet: From animals to materials.* Mater. Res. Soc. Bull., 2007. **32**: p. 466-468.
2. Sidorenko, A., et al., *Switching of polymer brushes.* Langmuir, 1999. **15**: p. 8349-8355.
3. Geoghegan, M., et al., *The pH-induced swelling and collapse of a polybase brush synthesized by atom transfer radical polymerization.* Soft Matter, 2006. **2**: p. 1076-1080.
4. Davies, M.L., et al., *Cation fluorene-based conjugated polyelectrolytes induce compaction and bridging in DNA.* Biomacromolecules, 2009. **10**: p. 2987-97.
5. Mecca, T., et al., *Polycationic calix[8]arenes able to recognize and neutralize heparin.* Org. Biomol. Chem., 2006. **4**: p. 3763-3768.
6. Wesley, R.D., et al., *Structure of polymer/surfactant complex formed by poly(2-(dimethylamino)ethyl methacrylate) and sodium dodecyl sulfate.* Langmuir, 2002. **18**: p. 5704-5707.
7. Gong, J.P., G. Kagata, and Y. Osada, *Friction of gels. 4. Friction on charged gels.* J. Phys. Chem. B, 1999. **103**: p. 6007-6014.
8. Ruiz-Pérez, L., et al., *The conformation of poly(methacrylic acid) chains in dilute aqueous solution.* Macromolecules, 2008. **41**: p. 2203-2211.
9. O'Connor, K.P. and T.C.B. McLeish, *"Molecular Velcro": Dynamics of a constrained chain into an elastomer network.* Macromolecules, 1993. **26**: p. 7322-7325.
10. Deruelle, M., L. Léger, and M. Tirrell, *Adhesion at the solid-elastomer interface: Influence of the interfacial chains.* Macromolecules, 1995. **28**: p. 7419-7428.
11. Geoghegan, M., et al., *The kinetics of penetration of grafted polymers into a network.* Macromolecules, 1999. **32**: p. 5106-5114.
12. Vilmin, T., et al., *Interdigitation between surface-anchored polymer chains and an elastomer: Consequences for adhesion promotion.* Europhys. Lett., 2004. **68**: p. 543-549.
13. La Spina, R., et al., *Controlling network-brush interactions to achieve switchable adhesion.* Angew. Chem. Int. Ed., 2007. **46**: p. 6460-6463.
14. Woerdeman, D.L., et al., *Characterization of glass–epoxy adhesion using JKR methods and atomic force microscopy.* Composites A, 1999. **30**: p. 95-109.

Contents

Chapter 1

Adhesion theories

1.1 Introduction

The word adhesion comes from the Latin word adhaerere, that is a compound of ad (to) + haerere (stick) [1]. This word was used by Lucretius to describe the fact that iron sticks to a magnet. The meaning of the word adhesion, in this context, is straightforward and indicates the phenomenon that or the state in which two parties are attached together. The ASTM D 907 (American Society for Testing And Materials) definition indicates that adhesion is "the state in which two surfaces are held together by interfacial forces, which may consist of valence forces, interlocking forces or both". The mechanism of adhesion is a multidisciplinary subject that involves surface chemistry, physics, rheology, stress analysis and, nowadays, the physics and chemistry of polymers. Industries in building, engineering and biomedical fields are investigating the adhesion of polymers, and besides, industries, such as aerospace and automobiles are moving their interest from metals and metal components to polymer and epoxy resins because they are cheaper and lighter and present good mechanical properties. The "adhesion" between two bodies is strictly dependent on the strength of the interface due to physical and chemical properties and topology of the surface; the "adherence" takes in account the bulk characteristics [2]. The "adherence" can be measured, but the "adhesion" only if the bulk is perfectly elastic. The chemical composition, the roughness, the polarity and the surface free

energy of the external polymer layer is studied using techniques such as time-of-flight secondary ion mass spectroscopy (ToF-SIMS) [3], atomic force microscopy (AFM) [4], scanning electron microscopy (SEM) [5], attenuated total reflectance infrared spectroscopy (ATR-IR) [5], and optical contact angle measurements [6]. The mechanism of adhesion and the adhesion strength of the materials at the interface are studied using some direct adhesion techniques such as pull-off tests [7], peel tests [8], lap [9] and shear tests [10]. These techniques are destructive because they measure the force or energy required to separate the surfaces involving breakage, tear and delamination of the surfaces but give information about the limit of material applicability but do not reveal any information about the physical chemistry characteristics of the surface and interface. The full characterization of the polymer adhesion combines the use of direct adhesion measurements and surface techniques. The main contributions of adhesion mechanisms are mechanical coupling, molecular bonding and thermodynamic adhesion.

Mechanical coupling is based on interlocking (hook and eye) between the substrate and the adhesive, such as glue on wood. Other researchers consider that the key parameter is the roughness of the surfaces, which increases the area of contact between the substrate and the adhesive [11]. If very high or even porous materials are brought into contact, the main mechanism of interaction is interlocking. If the materials present low roughness, the area of contact of the surfaces increases compared to smooth surfaces, and indeed the adhesion increases. This phenomenon is observed when liquid glue, which transforms into a solid by polymerization, crosslinking or drying, is applied on a surface. In the case of soft adhesive it is important to create a good contact firstly between the surfaces; the roughness plays an important role, during the debonding process, especially for soft adhesive, because it increases the points of contact and consequently the energy to separate the two surfaces. In this case, there is an optimal roughness value that balances good contact between the surfaces and the increase of energy to separate them [12].

The molecular bonding contribution requires the adhesion between the substrate and the adhesive to be due to intermolecular forces such as short-range interactions, dipole-dipole and van der Waals forces, and/or chemical interactions, such as covalent bonds, between the two surfaces. This mechanism requires that the surfaces be in intimate contact but often the presence of defects, cracks and air bubbles decreases the

strength of adhesion at the interface [13]. Another contribution is the thermodynamic mechanism of adhesion based on equilibrium processes at the interface. The surfaces, exposed in different environment, try to arrange the orientation of the molecules into the surface to minimize the surface free energy, affecting the strength of adhesion at the interface [14]. This is important, for example, in the coatings field.

A final contribution concerns the rheological mechanisms of adhesion based on interdiffusion and consequently interpenetration of the polymer chains across the interface improving the strength of adhesion. The process is favourable at temperatures higher than the glass transition temperature due to the higher mobility of the polymer chains, e.g. the use of block copolymers to heal the interface between immiscible polymers [15]. The linking polymer at the interface produces an extra cost of energy to separate the surface because the polymer chains would be stretched and dissipate energy when the surfaces are separated [16]. The polymer chains at the interface have to be long enough to interact with the bulk by entangling with the melt for glassy polymers [15], or co-crystallize with at least 2 lamellae [17] or entangle with the polymer network in the case of elastomeric materials [18].

1.2 Adhesion theories

The phenomenon of stickiness has been always experienced by humans. The sticky resin from pine trees has been used in numerous applications from adding friction to violin strings to a binding agent for fragile archaeological items. Going back to Palaeolithic times, early man used resin to fashion spears for hunting by gluing stone and bone to wooden sticks to make spears [19]. The study of the contact mechanism has a more recent origin dating back to 1882 from an article by Hertz [20]. The interest in studying the contact mechanism was quite practical. Due to the increase of industrial development, understanding the contact of train wheels on the steel rails became an important problem [21]. In this particular example, the force to deform the contact is much larger than the adhesion forces and the latter is neglected. If, however, the bodies in contact are deformable, the adhesion forces become important; Johnson, Kendall and Roberts in 1971 studied this phenomenon [22]. They considered the case of two spheres in contact interacting via adhesion forces. They showed mathematically the dependence of the adhesion energy on the radius of contact, the

radius of curvature of the lens, the load applied and the elastic modulus of the lens. This article has had a huge impact in the scientific and engineering community. Its relevance may even become greater nowadays when scientific studies are leading to a more thorough understanding of the behaviour of nanostructures. The adhesive forces become much more important as the size of the contact and the stiffness of material decrease.

1.2.1 Role of the interface

Adhesion, in its fundamental meaning, is defined as the interaction between atoms or molecules at the interface. The interaction can have different origins such as van der Waals or non-covalent bond forces, chain interpenetration, or chemical bonds across the interface [23, 24]. Long distance forces are intrinsic characteristics of the material and can be quantified by their surface and interfacial energies. The surface energy is the quantity of energy required to create a unit of surface, a, between the interface. If the second phase is vacuum or air, this energy is called surface energy; if it is a different phase this energy is called interfacial energy. Thermodynamically, the surface can have a lower free energy when it is in contact with a second phase than when it is by itself in the vacuum [25]. To form this new area the system has to break bonds on the surface and create new ones with the other phase. The value of surface energy depends of the kind of bonds that have to be broken. On the suggestion of Fowkes [26] the surface energy can be expressed as the sum of all bond contributions:

$$\gamma = \gamma^d + \gamma^p + \gamma^h \tag{1.1}$$

where γ^d are the dispersion forces, γ^p the polar forces, and γ^h hydrogen bonding. Thermodynamically, the surface energy is defined as

$$\gamma = \left(\frac{\partial G}{\partial A}\right)_{T,P}, \tag{1.2}$$

where A is the area created and G is the surface Gibbs free energy.

The surface energy leads to the definition of the work of cohesion and the work of adhesion. The work of adhesion is the work done on the system when two different bodies, forming an interface of unit area, are separated reversibly to create two new interfaces of unit area.

Mathematically the work of adhesion between two bodies denoted (1) and (2) can be described as

$$W_{adh} = \gamma_1 + \gamma_2 - \gamma_{1,2}, \tag{1.3}$$

where γ_1 and γ_2 are the surface energies in phases 1 and 2, respectively, and $\gamma_{1,2}$ is the interfacial energy.

If the two phases are identical, $\gamma_1 = \gamma_2 = \gamma$, and $\gamma_{1,2} = 0$, the energy required to separate the two components is known as the work of cohesion and it is mathematically expressed as

$$W_{coh} = 2\gamma. \tag{1.4}$$

The most frequently used way to calculate the surface energies of solid surfaces is through contact angle measurement [2]. The technique is based on the measurement of the angle between a droplet of liquid and a surface. When the droplet is added on the surface, different interfaces are created: solid-liquid, liquid-vapour and solid-vapour, Fig 1.1.

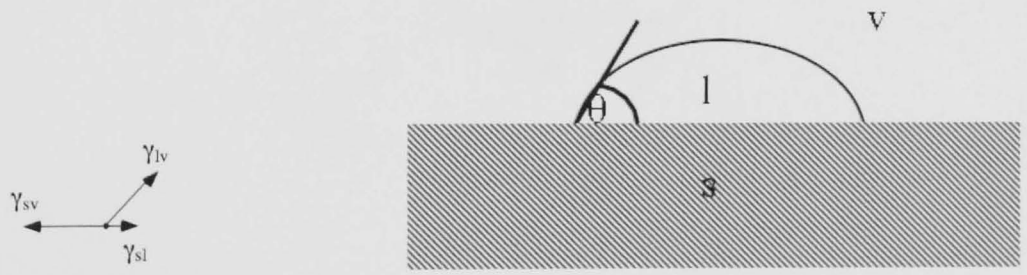

Fig 1.1 Schematic representation of a drop of (l) liquid in equilibrium with its vapour (v) on a solid (s) substrate for contact angle experiments. The surface and interfacial energies, γ_{sv}, γ_{lv}, γ_{sl} act in the direction indicated.

These force balance of these interfacial energies results in Young's equation [27]

$$\gamma_{lv}\cos\theta = \gamma_{sv} - \gamma_{sl} \tag{1.5}$$

Where γ_{lv} indicate the liquid-vapour surface tension, γ_{sv} the solid-vapour surface tension and γ_{sl} the solid-liquid surface tension.

To calculate the interfacial interaction between two solid bodies in contact, contact mechanism theories have been developed. The contact mechanism theories take into account the elastic modulus and roughness of the materials, geometry of the surface, chemical and physical bonding, and chain interpenetration [2, 28].

1.2.2 Hertz theory

Hertz [20, 21] considered the behaviour of two elastic smooth bodies in contact pressed against each other. Assuming that there are no interfacial attraction forces between the two surfaces, he demonstrated that the size and the shape of the contact depend on the elastic deformation of the two bodies.

The model considers the interaction between two spheres, radius R_1 and R_2 with elastic moduli E_1 and E_2, respectively, compressed by a force P.

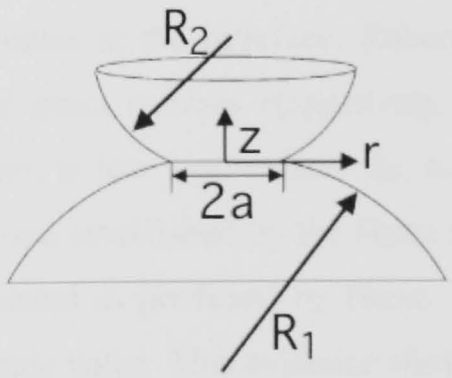

Fig 1.2 Representation, taken from Shull [21], of two spheres in contact of radius R_1 and R_2 having a contact area of radius a.

The relationships linking the change of contact radius, a_0, and the displacement, δ, as a function of the radius of curvature R, elastic constant of the system and force applied P are:

$$a_0^3 = \frac{PR}{K}, \tag{1.6}$$

$$\delta = \frac{P}{Ka} = \frac{a_0^2}{R}, \tag{1.7}$$

$$\frac{1}{R} = \frac{1}{R_1} + \frac{1}{R_2}, \text{ and} \tag{1.8}$$

$$\frac{1}{K} = \frac{3}{4}\left[\frac{1-\nu_1^2}{E_1} + \frac{1-\nu_2^2}{E_2}\right], \tag{1.9}$$

where ν_1 and ν_2 are Poisson's ratios for the two spheres in contact. Equation 1.6 is known as the Hertz equation and it can be used in the case of a sphere in contact with a flat surface by considering the flat surface as a sphere of infinite radius.

For the Hertz model, one assumes that the bodies are isotropic, frictionless, that their shapes can be approximated to a half sphere and the contact radius, a_0, is much smaller than the curvature radius of the bodies, R. Adhesive forces are neglected; consequently, the contact radius is zero at zero load as indicated in the equation.

The Hertz theory is not completely consistent with some experimental results. For example, Bradley found that two silica spheres in contact with a force P, required a force bigger than P to pull them apart [29]. This behaviour was explained through the presence of the attractive forces at the interface. Roberts and Kendall [22] , using smooth rubber spheres and glass spheres respectively, noted the same effect. In particular they found out that, at low load values, the radius of contact between the spheres was larger than the one established by the Hertz theory. At high compressive load values, the system behaved as predicted by Hertz. At a load close to zero, the contact area approached a finite value. This evidence showed that interfacial attractive forces appear more evidently as the load is close to zero. These forces may be modelled as additional forces acting at the interface.

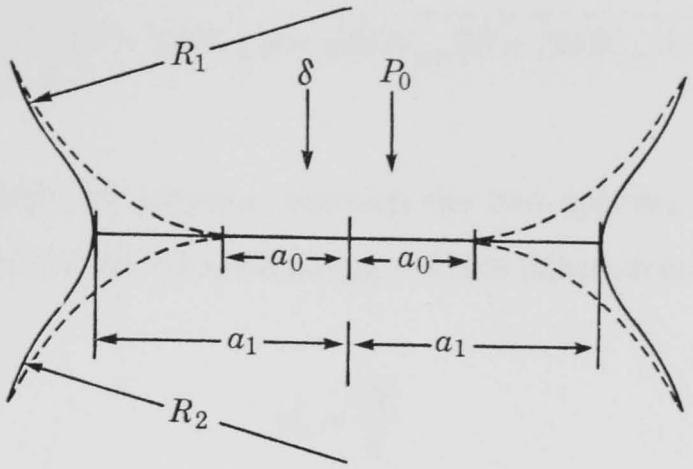

Fig 1.3 Comparison of the radius of contact predicted by Hertz, a_0, and by JKR a_1. The attractive forces at the interface enlarge the area of contact between the two elastic solids, making $a_1 > a_0$. The image is taken from [22].

The presence of extra attractive forces influences the stress distribution at the interface. The Hertz theory assumes that the stress distribution at the interface is a maximum at the centre of contact and then decreases closer to the edge [30].

Johnson et al. [22] calculated the stress distribution, in the presence of adhesive forces, by adding to the Hertz stress distribution a non-physical infinite tensile stress at the edge. The radius of contact, in the presence of attractive forces, is larger than the radius of contact for the Hertz calculation as shown in Fig 1.3.

1.2.3 JKR theory

The JKR theory, named after its three discoverers Johnson, Kendall and Roberts, was published in 1971 [22]. It describes two smooth elastic spheres of radius R_1 and R_2 and elastic moduli E_1 and E_2 in contact. The JKR model assumes that the attractive forces between the surfaces are short-range interactions and they act only inside the contact area. The assumptions for the system are the same as the Hertz model except that the attractive forces between the surfaces are taken into consideration. When the interfacial attractive forces are considered, the contact radius, a, is a function of the radius of curvature, elastic modulus, force applied and the work of adhesion between the two spheres, considering that $R = R_1$ and R_2 is infinite as for the Hertz model, and results in

$$a^3 = \frac{R}{K}\left(P + 3\pi W_{adh} R + \sqrt{6\pi W_{adh} RP + (3\pi W_{adh} R)^2}\right) \tag{1.10}$$

where W_{adh} is the work of adhesion between the two spheres. The equation is an extension of the Hertz model. Assuming $W_{adh} = 0$, the equation reverts to:

$$a_0^3 = \frac{PR}{K}. \tag{1.11}$$

The introduction of the adhesion forces in the interaction between the two surfaces in contact influences the variation of the force applied and removed as a function of the area of contact as shown in Fig 1.4, adapted from the thesis due to A. Chiche [31] .

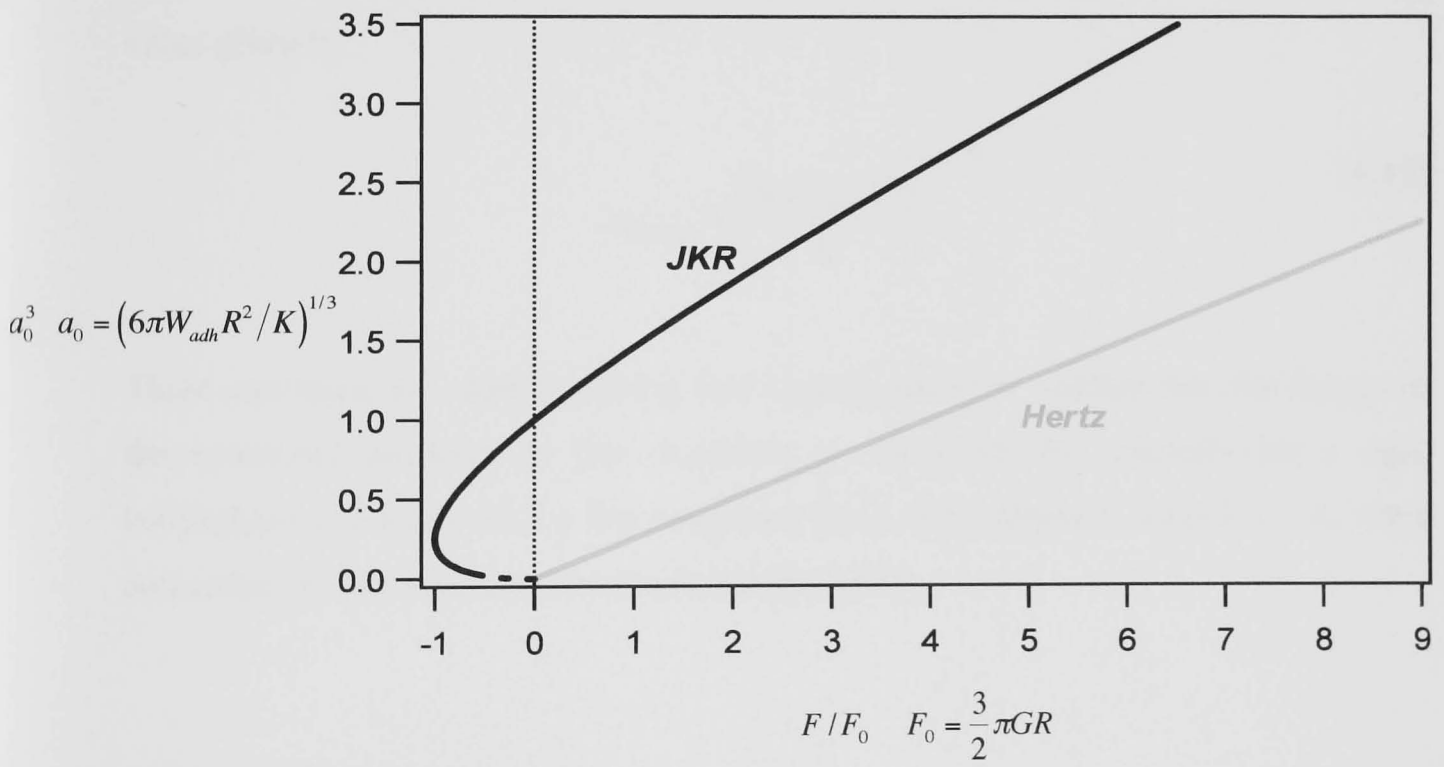

Fig 1.4 Variation of normalized cubed contact radius a^3/a_0^3 as a function of the normalized loading/unloading forces F/F_0 in the Hertz and JKR models when two elastic spheres are brought into contact. For the Hertz model, the force and the cube of the contact radius have a linear relationship; when the contact area is zero the force is zero too, showing that there are no adhesion forces involved during the loading and unloading. In the JKR model, the relationship between the force and the area is not linear. When the lens is close to the surface but, $F/F_0 = 0$, a^3/a_0^3 assumes a finite value due to the attractive forces between the two surfaces. The same effect is observed during

the unloading process, the force is zero but the area of contact assumes a finite value due to the adhesive forces acting between the surfaces. To separate the two surfaces, the force must be negative. The dashed line in the graph is not observed in real systems because the lens is separated from the surface before reaching the 0 value of radius.

When the load applied is negative, the contact radius decreases until a separation of the spheres takes place. This separation occurs when the load reaches a critical tensile value, called pull off force, $P_{pull\text{-}off}$ given by

$$P_{pull-off} = -\frac{3}{2} W_{adh} \pi R \tag{1.12}$$

The equation shows that the pull-off force is independent of the elastic moduli of the materials. The JKR model predicts that at zero load, the contact radius has a finite value given by

$$a_{0(JKR)} = \left(\frac{6\pi W_{adh} R^2}{K} \right)^{1/3} \tag{1.13}$$

These equations are valid assuming that contact radius is smaller than the height of the compliant material. If this condition is not valid, for example for a rigid hemisphere in contact with a flat compliant layer of thickness h, with $h << a$, some corrections to the equations have to be applied [32].

1.2.4 DMT theory

In 1975 Derjaguin, Muller and Toporov, (DMT), proposed a new theory [28] for rigid spheres. They proposed that long-range attractive forces act outside the contact area where the surfaces are not far apart. The attractive forces are modelled using the Lennard-Jones potential and the deformation is in agreement with the Hertz model.
In the DMT model, the contact radius, a_{DMT}, is a function of the radius of curvature, elastic modulus, force applied and the work of adhesion according to

$$a^3_{(DMT)} = \frac{R}{K}\left(P + 2\pi W_{adh} R\right) \tag{1.14}$$

If a negative load is applied, the critical force $P_{c(DMT)}$ to pull apart the two surfaces is given by

$$P_{c(DMT)} = -2\pi W_{adh} R \tag{1.15}$$

As for the JKR model, the pull-off force in the DMT model is independent of the elastic moduli.

The DMT model also predicts a finite value for the contact radius at zero load,

$$a_{0\ (DMT)} = \left(\frac{2\pi W_{adh} R^2}{K}\right)^{1/3}. \tag{1.16}$$

A comparison between the respectively pull-off forces in the JKR and DMT models, equations 1.12 and equation 1.15 reveals a discrepancy. Both equations are independent of the moduli and could be valid in the case of rigid spheres or elastic material giving a different value of the pull-off force. This apparent contradiction was resolved by Tabor [28], showing that both the JKR and DMT models are both valid but describe two different extreme situations. The JKR model can be used in the case of a soft lens with large curvature radius, while the DMT model is applicable to a solid lens with a small radius. According to Tabor, the transition between JKR and DMT can be established by the dimensionless parameter μ.

$$\mu = \left(\frac{R W_{adh}^2}{K^2 z^3}\right)^{1/3} \tag{1.17}$$

In the equation W_{adh} is the work of adhesion and z is the equilibrium distance in the Lennard-Jones potential. JKR analysis can be used when the dimensionless parameter μ is greater then 5, and the DMT analysis for μ less then 0.1. μ represents the ratio of the elastic deformation consequently to the adhesion for the surface forces [21].

Another dimensionless parameter, called the transition parameter λ, was introduced by Maugis [28] and is related to μ by

$$\lambda = 1.157\mu. \tag{1.18}$$

The Maugis-Dugdale model (MD), built on the Dugdale approximation, assumes that the adhesion between the spheres and the surface, outside the contact area, has a constant stress over some length regime. The MD model is based on numerical calculation and appears to be a general case of the JKR and DMT theories and can be applied for all values of λ. For $\lambda = 0.1$, the MD model is closer to the DMT curve, for $\lambda = 5$, it approaches the JKR curve [28].

The MYD model, developed by Muller, Yushchenko and Derjaguin, [28] includes the short-range and long-range attraction forces acting inside and outside the contact area the adhesion process.

The graph below shows a comparison of the force, stress, and shape profiles of the different adhesion models discussed.

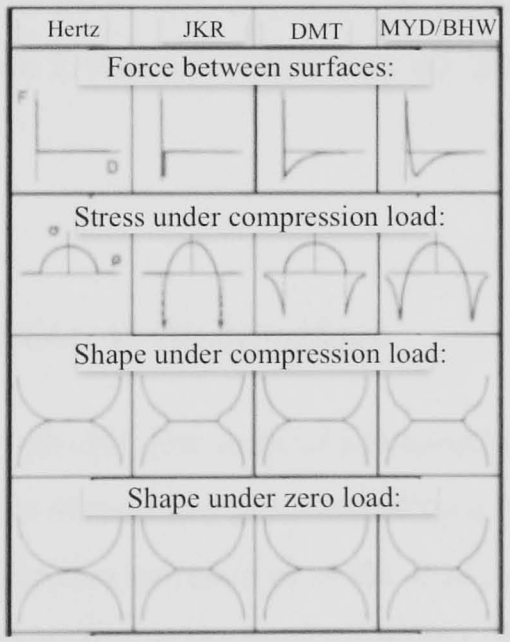

Fig 1.4 Force, shape, stress between two elastic spheres in contact, as predicted by the different adhesion theories. The figure is taken by Horn, et. al. [30].

In the case of the Hertz model, Fig 1.4, column 1, the two spheres are treated as rigid bodies, frictionless and smooth, without any attractive forces between the surfaces

and they separate at zero load. The stress distribution is compressive which means that it is greater at the centre of contact and lower at the edges.

For the JKR model, the two spheres have the same characteristics as for the Hertz model, but they have attractive forces acting between the two bodies, at least when the two bodies are in contact. These forces lead the area of contact to be larger than for the Hertz model. The JKR model restricts the interaction force acting only at contact; consequently the edge of contact assumes a contact angle of 90°, because any interaction between the two bodies acting on lengths greater than zero would deform the shape of contact to lead to a contact angle different from 90°, and so the force diverges at the edge of contact as shown in Fig 1.4 in the stress distribution for the JKR model. To avoid this discontinuity of interaction at the edge of contact, the Dugdale cohesive zone is applied at the edge of contact; the Dugdale cohesive zone considers that the distance between the lens and the substrate goes gradually from 0, at the edge of contact, to a high value. The distance between the surface and the lens must be smaller than the interaction length. In this condition, the model presents a more realistic situation.

For the DMT model, the two spheres have attractive forces acting only outside the area of contact where the surfaces are still close to each other; inside the area of contact, the model assumes a Hertzian shape and no forces affect the surface of contact [30].

1.3 Fracture propagation at the interface

The experimental set-up to calculate the work of adhesion between a flat surface and a hemispherical lens comprises several key parts including a load control system, which controls the rate of the application or removal of the load, and a camera to record the change of the contact area or radius as the load is applied. The radius of the lens must be known while the elastic modulus may be calculated separately or during the performance of the experiments.

In a general experiment, the flat surface is positioned on a stage and the second surface, usually of hemispherical shape, is moved by a motor in contact with the flat surface. When the load is applied (loading regime) the work of adhesion and the

elastic properties of the lens can be calculated by fitting to the JKR equation because the contact radius and any loads applied are known. If the experiment is run until equilibrium is reached, the work of adhesion is specifically the thermodynamic work of adhesion in the loading regime, W. In this stage, the contact area between the two surfaces increases enhancing the load amount. Subsequently, the load is removed and the contact area decreases until the lens is detached from the flat surface.

This process is called fracture or crack propagation because the contact perimeter can be viewed as a crack. During the unloading, the adhesion energy can be calculated for each point but the thermodynamic work of adhesion, W_{ul} can be calculated only when the system reaches equilibrium. Two different values of adhesion energy can be measured in the loading and the unloading regime. If $W_{ul} > W_l$, the contact between the two surfaces has generated interfacial bonding such as van der Waals forces, hydrogen or covalent bonding, or chain interpenetration. To detach the lens and propagate the fracture, it is necessary to use larger forces than in the loading process [33]. If $W_{ul} = W_l$, the two surfaces have no interaction and the stored energy given to the system during the loading is released during the unloading process. The meaning of the work of adhesion, in a non-equilibrium state, is the energy cost to open the interface, or specifically, the amount of energy to separate two surfaces. It is normally indicated by G and it is known as the energy release rate.

The fracture propagation rate or the crack velocity, v, is defined as the variation of the contact radius a as a function of the time, given by

$$v = -\frac{da}{dt}. \tag{1.19}$$

The negative sign indicates that an advancing crack corresponds to a decrease of contact radius with the time. In the loading regime, $v < 0$, which corresponds to an increase of the contact radius with time.

The relation between the crack propagation rate and the energy cost of opening the interface can be illustrated by the following example: consider a piece of adhesive tape stuck on a piece of paper that has to be removed. If the tape is pulled too fast, the crack is forced to propagate faster and opening the paper-adhesive tape interface can cost more than ripping the paper. Consequently the paper breaks before the interface is open. To avoid this, the tape has to be removed slowly. This example leads to the

conclusion that: if the crack propagates at high speed, the system needs more energy. Mathematically the relation between G and v is given by an empirical formula [34-36];

$$G = G_0\left(1+\left(\frac{v}{v_0}\right)^m\right), \tag{1.20}$$

where G_0 represents the minimum energy to propagate the crack at zero speed; v_0 is the normalization coefficient of the speed and m is a coefficient usually close to 0.5 if the temperature of the material is near its glass transition, T_g. In another range of temperature it can assume a different value.

The value of G_0 cannot be smaller than W_{ul} because W_{ul} is the thermodynamic minimum energy cost to open the interface and it may be $W_{ul} = G_0$. Larger values of G_0 can be related to an interaction at the interface such as short distance interactions that occurs during the contact.

1.3.1 Stress distribution

Another important parameter to consider when two bodies are in contact is the stress distribution. In section 1.2.4, the stress distribution has been mentioned only because the contact mechanism quantification may not involve any knowledge about the stress distribution.

For the Hertz model, where no adhesion forces are considered, the stress distribution for frictionless contact during compression process, is described by

$$\sigma_{zz}^{H} = -\frac{3P_H}{2\pi a^2}\left(1-\left(\frac{r}{a}\right)^2\right)^{1/2}, \tag{1.21}$$

where r indicates the radial distance from the axis of symmetry of the contact, P_H is the load applied, and a is the contact radius. The negative sign, in the contact mechanism convention, indicates that the stress is compressive.

If adhesive forces are considered, the system develops a tensile stress and the actual load is less than the one applied.

The equation can be written in this case by considering P, the tensile force to the contribution as ($P < P_H$)

$$\sigma_{zz}^{adh} = \frac{P_H - P}{2\pi a^2}\left(1-\left(\frac{r}{a}\right)^2\right)^{-1/2}. \tag{1.22}$$

In the case of JKR model, the stress distribution is given as a summation of the two contributions,

$$\sigma_{zz}^{JKR} = \sigma_{zz}^{H} + \sigma_{zz}^{adh}. \tag{1.23}$$

The stress distribution in the case of no adhesive forces, adhesive forces and a combination of the two is shown in the pictures below.

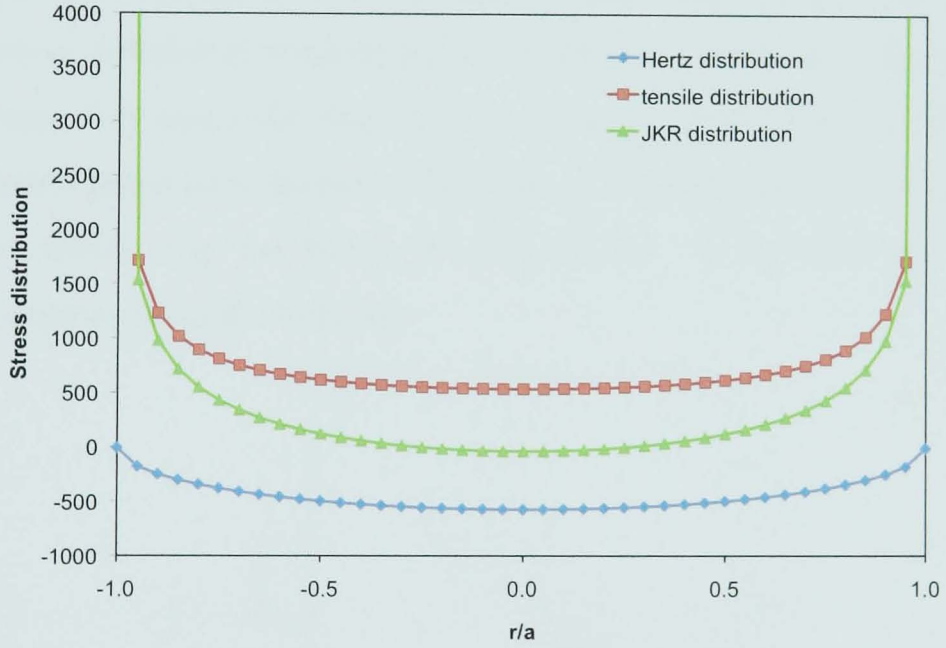

Fig 1.5 Comparison of the stress distribution for two bodies in contact for the Hertz model, in the presence of adhesive forces, i.e. tensile stress, and in the JKR model, i.e. the sum of the two components.

In the case where there are no adhesive forces, the stress distribution is larger in the centre of the contact and decreases towards the edge. The presence of adhesive forces reduces the stress distribution at the contact area making an infinite stress at the interface.

Silberzan et al. [37] describe the stress distribution for a PDMS surface and lens in contact after being soaked in chloroform and dried in modest vacuum conditions at 60°C. These adhesion experiments, using the JKR equation, show a sharp hysteresis between the loading and unloading process. The value of the work of adhesion in the loading regime was W_l =39 mJ/m^2 and the elastic modulus was K_l =0.40 MPa. In the unloading regime, the work of adhesion was W_{ul} =328 mJ/m^2 and the elastic modulus was K_{ul} =1.10 MPa. The difference of the values of work of adhesion in the two regimes was explained by the formation of hydrogen bonds between the oxidized Si-OH group at the contact. What is more important to point out is the difference in the value of modulus in the loading and unloading processes. This is not *a priori* obvious because the modulus is a bulk property. Silberzan et al considered that the JKR model may not be valid for this system because the application of increasing force could induce more or a different bonding process at the interface. Consequently, the work of adhesion may vary along the interface as a function of the contact radius. To prove this they investigated how the stress distribution at the interface varies as a function of the contact radius. Fig 1.6 shows the dependence of the adhesion energy in the unloading regime along the interface.

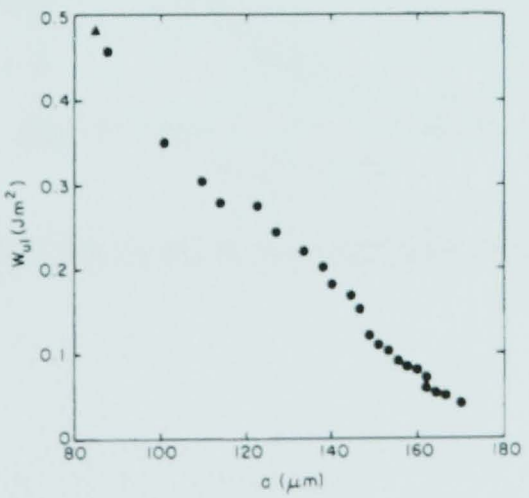

Fig 1.6 This graph, taken from the paper of Silberzan et al. 1994 [37], shows the dependence of the work of adhesion in the unloading regime as a function of the contact radius in the case of a PDMS lens and PDMS surface in contact.

The relationship between the stress distribution as a function of the contact supposes that the yield of the hydrogen bonds reaction at the interface is larger at the maximum contact area, which corresponds to the point of application of greatest loads. The stress at radius r at the maximum radius of contact a_{max} is given by

$$\sigma(r) = \left(\frac{3KW_l}{2\pi a_{\max}}\right)^{1/2} \frac{1}{\left(1-\frac{r^2}{a_{\max}^2}\right)^{1/2}} - \frac{3Ka_{\max}}{2\pi R}\left(1-\frac{r^2}{a_{\max}^2}\right)^{1/2} \qquad \textbf{(1.24)}$$

where the first term, which is always greater than zero, is the tensile stress and the second is the compressive stress from the Hertz theory, and acts against the tensile stress.

To explain the weight of the two contributions to the final stress shown, Fig 1.7 shows a graph from Silberzan's paper, which shows that the value of adhesion energy in the unloading regime is lower at the edge but increases drastically moving to the centre of contact where the compressive stress is dominates.

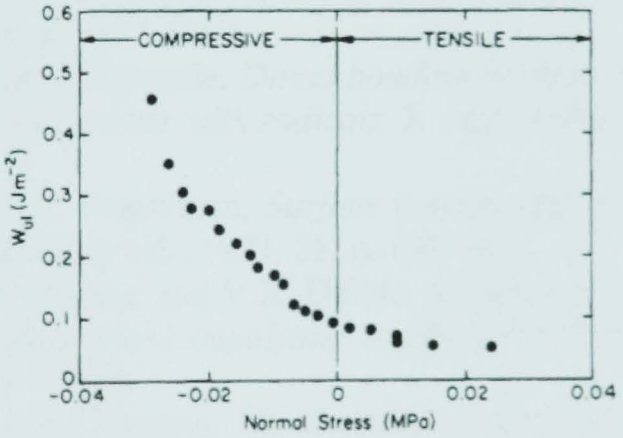

Fig 1.7 This graph, taken by [37], shows W_{ul} as a function of stress and contact position.

1. Onions, C.T., *The Oxford Dictionary on Enghish Etimology.* Clarendon Press, Oxford, 1966.
2. Awaja, F., et al., *Adhesion of polymers.* Prog. Polym. Sci., 2009. **34**: p. 948-968.
3. Vicherman, J.C. and D. Briggs, *Surface analysis by mass spectroscopy.* United Kingdom: IM Publications and Surface Spectra Limited, 2001.
4. Vicherman, J.C., *Surface analysis: the principal techniques.* West Sussex: Wiley, 2003.
5. Reed, S.J.B., *Electron microprobe analysis and scanning electron microscopy in geology.* Cambridge: Cambridge University Press, 1996.
6. Slep, D., et al., *Effect of an interactive surface on the equilibrium contact angles in bilayer polymer films.* Langmuir, 2000. **16**: p. 2369-2375.
7. Varenberg, M. and S. Gorb, *A beetle-inspired solution for underwater adhesion.* J. R. Soc. Interface, 2008. **5**: p. 383-385.
8. McGuiggan, P.M., et al., *Peel of an adhesive from a temperature-gradient surface.* Int. J. Adhes. Adhes, 2008. **28**: p. 185-191.
9. Khoee, S., et al., *An investigation into the improvement of adhesive strength of polyimides by incorporation of elastomeric nanoparticle.* J. Colloid Interface Sci., 2009. **336**: p. 872-878.
10. Kim, S.B., et al., *Development of aqua epoxy for repair ans strengthening of RC structural members in underwater.* Constr. Build. Mater., 2009. **23**: p. 3079-3086.
11. Kinloch, A.J., *The science of adhesion, Part 1 Surface and interfacial aspects.* J. Mater. Sci. , 1980. **15**: p. 2141-2166.
12. Chiche, A., P. Pareige, and C. Creton, *Role of surface roughness in controlling the adhesion of a soft adhesive on a hard surface.* C. R. Acad. Sci. IV-Physics, 2000. **1**: p. 1197-1204.
13. Mutsuda, M. and H. Komada, *Direct bonding between Poly(oxy-2,6-dimethyl-1,4-phenylene) and rubber with radicals.* J. Appl. Polym. Sci., 2005. **95**: p. 53-59.
14. Lipatov, Y. and A. Feinerman, *Surface tension and free energy of polymers.* Adv. Colloid Interface Sci., 1979. **11**: p. 195-233.
15. Creton, C., H.R. Brown, and V.R. Deline, *Influence of chain entanglement on the failure modes in block copolymer toughened interfaces.* Macromolecules, 1994. **27**: p. 1774-1780.
16. Lake, G.J. and A.G. Thomas, *The strength of highly elastic materials* Proc. R. Soc. Lond. A, 1967. **300**: p. 108-119.
17. Benkoski, J.J., P. Flores, and E.J. Kramer, *Diblock copolymer reinforced interfaces between amorphous polystyrene and semicrystalline polyethylene.* Macromolecules, 2003. **36**: p. 3289-3302.
18. Woerdeman, D.L., et al., *Characterization of glass–epoxy adhesion using JKR methods and atomic force microscopy.* Composites A, 1999. **30**: p. 95-109.
19. Packham, D.E., *Handbook of adhesion* 2nd ed. Wiley 2005.
20. Hertz, H., *Über die Berührung fester elastischer Körper.* J. Reine u Angew. Math., 1881. **92**: p. 156-171.
21. Shull, K.R., *Contact mechanics and the adhesion of soft solids.* Mater. Sci. Eng., 2002. **R36**: p. 1-45.
22. Johnson, K.L., K. Kendall, and A.D. Roberts, *Surface energy and the contact of elastic solids.* Proc. R. Soc. London A, 1971. **324**: p. 301-313.

23. Amiel, C., et al., *Adsorption of hydrophilic-hydrophobic block copolymers on silica from aqueous solutions.* Macromolecules, 1995. **28**: p. 3125-3134.
24. Israelachvili, J.N., *Intermolecular and Surface Forces*. 2nd ed. 1991, London: Academic Press.
25. Kumar, G. and K.N. Prabhu, *Review of non-reactive and reactive wetting of liquids on surfaces.* Adv. Colloid Interface Sci., 2007. **133**: p. 61-89.
26. Huttinger, K.J., S. Hohmann-Wien, and G. Krekel, *A method for the determination of the acid-base interactions and the work of adhesion at the solid-liquid interface.* J. Adhesion Sci. Technol., 1992. **6**: p. 317-331.
27. Young, T., *An essay on the cohesion of fluids.* Phil. Trans. R. Soc. London, 1805. **95**: p. 65-87.
28. Shi, X. and Y. Zhao, *Comparison of various adhesion contact theories and the influence of dimensionless load parameter.* J. Adhesion Sci. Technol., 2004. **18**: p. 55-68.
29. Bradley, R.S., *The cohesive force between solid surfaces and the surface energy of solids.* Phil. Mag., 1932. **13**: p. 853-862.
30. Horn, R.G., J.N. Israelachvili, and F. Pribac, *Measurement of the deformation and adhesion of solids in contact.* J. Colloid Interface Sci., 1987. **115**: p. 480-492.
31. Chiche, A., *Debonding of a soft adhesive: Cavitation and crack propagation.* PhD Dissertation, 2003 (Laboratoire PPMD ESPCI, Paris, France).
32. Shull, K.R., et al., *Axisymmetric adhesion tests of soft materials.* Macromol. Chem. Phys., 1998. **199**: p. 489-511.
33. Pollock, H.M., D. Maugis, and M. Barquins, *The force of adhesion between solid surface in contact.* Appl. Phys. Lett., 1978. **33**: p. 798.
34. Gent, A.N. and J. Schultz, *Effect of wetting on the strength of adhesion of viscoelastic materials.* J. Adhesion, 1972. **3**: p. 281-294.
35. Andrews, E.H. and A.J. Kinloch, *Mechanism of adhesive failure. (I).* Proc. R. Soc. London A, 1973. **332**: p. 385-399.
36. Maugis, D. and M. Barquins, *Fracture mechanics and the adherence of viscoelastic bodies.* J. Phys. D: Appl. Phys., 1978. **11**: p. 1989-2023.
37. Silberzan, P., et al., *Study of the self-adhesion hysteresis of a siloxane elastomer using the JKR method.* Langmuir, 1994. **10**: p. 2466-2470.

Chapter 2

Brush and hydrogel

2. Introduction

Coating a surface is an important area of technology for industrial purposes because it is a means of modifying the physical chemistry characteristics of the surface of a material [1-3]. The surface is the outermost layer of a material and is always created when a material is fractured with the breaking of chemical bonds. For this reason it is often very reactive and is characterized by a high energy which can be reduced by the adsorption of atoms or molecules from the ambient environment, or alternatively atoms at the surface may be rearranged to allow additional bonding of the surface atoms [4]. Polymers are good candidates for surface modification because they can form films with a wide variety of functional groups, and they have mechanical properties that they can be tailored. The use of polymers as coatings has different applications such as in the photolithographic field [5], in the adhesion between surfaces [4], lubricants [6], colloidal stabilizers [7], anti fouling coatings [8], in electronics [9], protection against erosion, amongst others.

Traditionally, to coat a surface, the polymer layer is physically attached to the surface by spin casting or solution dip-coating. The polymer is bound on the surface through non-covalent bonds, such as van der Waals interactions between the polymer layer and the surface [4] and the film can easily be desorbed if exposed to harsh conditions. Very often there is a temporal decrease in mechanical properties.

To overcome this problem, the polymer film can be chemically attached to the surface through covalent bonds using two methods, namely the "grafting to" method, where

the polymer is grown in solution and after attached to the surface, or the "grafting from" method, where the polymer is grown directly from the surface [10].

These two synthetic routes can be used to produce a polymer brush with defined properties.

A gel, on the other hand, can be considered a polymer with a three-dimensional network where the chains are connected through cross link points [11]. The cross-linker can have a physical nature if the chains are associated together by hydrogen bond and van der Waals interactions, or a chemical nature if the polymer chains are linked through covalent bonds to molecules with at least two or more reactive groups. The linked polymer chains create a molecule with a high molecular weight and the gel does not break up in many solvents but it can however absorb good solvents. Hydrogels are a particular kind of gel that swell in water, and are wet and soft but conserve their solid structure. A hydrogel can be made of polymers often known as "smart polymers" or "intelligent polymers" [12, 13], because in response to small changes in environmental conditions such as temperature, pH, solvent [14], electric fields [15], they exhibit a large changes in chemical and physical properties such as changing hydrophilicity and hydrophobicity, and dimensional size. These changes in properties are reversed when the stimulus is reversed.

In this chapter we are focusing on the synthesis of polymer brushes and hydrogels and their swelling behaviour in solution.

2.1 Characteristics of a brush layer

A polymer brush is a layer of polymer chains attached by one end to a flat surface [16, 17]. If the grafting density of the polymer, which is a measure of the distance between two neighbouring chains, is high enough, the chains start to repel each other and can stretch away from the surface [18], resembling the bristles on a brush.

Polymer brushes are applied as new adhesive materials [19, 20], protein-resistant surfaces [21], compatibilizers between surfaces [16], and biomimetic materials for drug delivery [22].

The behaviour of a polymer chain in solution as opposed to a polymer grafted onto a surface can be dramatically different. Whereas, in the first case, the polymer chains

are free to move around, in the second case, they are constrained by the surface. The main parameters controlling the conformation of polymer in solution are [11, 17]: the quality of the solvent, which influences the monomer-monomer interactions, the chain stiffness and the degree of polymerisation *N*.

In a good solvent, the interaction between monomer and solvent molecules dominate, and the entropy drives the polymer chains to maximize their interaction with the solvent. Consequently, the polymer chains form an expanded coil conformation. By contrast, in a poor solvent, the entropy drives the chains to minimize their contact with solvent molecules, and consequently the polymer assumes the conformation of a collapsed globule. In the case of a theta solvent, where the interaction between polymer and solvent is equal to the monomer-monomer interaction, the polymer chains assume an intermediate conformation between good and poor solvents. This also the case for the polymer melts. The radius of gyration, R_g, [11], describes the dimensions of a polymer chain in solution as a dependence on the quality of the solvent. Table 2.1 summarizes the R_g for a polymer chain in different solvent conditions.

solvent	$\boldsymbol{R_g}$
Good solvent	$R_g \sim N^{3/5}$
Poor solvent	$R_g \sim N^{1/3}$
Melt/Theta solvent	$R_g \sim N^{1/2}$

Table 2.1 Dependence of the radius of gyration on the number of polymerisation index for single polymer chains in solution in good, poor and melt/theta solvent conditions.

The dependence of the radius of gyration of a single chain in solution is a function of the degree of polymerisation and is obtained using scaling theory. R_g shows less dependence on N (or equivalently molecular weight) under poor solvent conditions and an increasing dependence in the case of theta and good solvents.

The conformation of end-tethered polymer chains [11] is governed by the degree of polymerisation N, and by an extra parameter, the grafting density of chains on the surface, σ, which is the number of polymer chains grafted per unit area of the substrate.

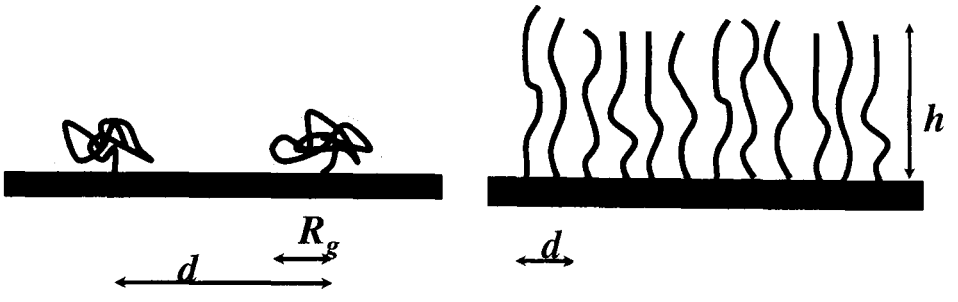

Fig. 2.1 Schematic representation of a polymer chain anchored on a surface in a "mushroom conformation" (on the left) and in a stretched "brush conformation" (on the right). *d* is the distance between adjacent anchor points and R_g is the radius of gyration of the chains. If $d > R_g$, the chains are far apart and they assume a mushroom conformation. If $d < R_g$, the chains are so close to each other that they start to repel each other, stretching in the *z* direction forming a brush conformation of height *h*.

For small grafting densities, where the average distance between the anchor point, *d*, is greater than the radius of gyration ($d > R_g$), the chains are far from each other and, as long as there is no any special interaction with the substrate, the conformation of the chain is analogous to a single chain in dilute solution, at least away from the substrate.

Under good solvent conditions, the chains try to maximize contact with the solvent molecules keeping chain stretching to a minimum. This behaviour results in the formation of a random coil in solution and, in the case of a polymer chain constrained by one end to the surface, is called a mushroom conformation.

As the grafting density of chains increases, the repulsive interaction between monomer units becomes large enough that the chains stretch from the surface giving a brush conformation of height, *h*.

There is a limit of grafting density after which the polymer chains start to interact, passing from the mushroom to the brush regime. This threshold value scales as $\sigma \sim N^{6/5}$ and is calculated using Flory theory [23]. The film is shown to be in a mushroom conformation for grafting densities less than this threshold value, otherwise a brush conformation results.

The grafting density of the polymer chain influences the height *h* of the polymer brush as shown by Alexander [24] and de Gennes [25] in their scaling theory.

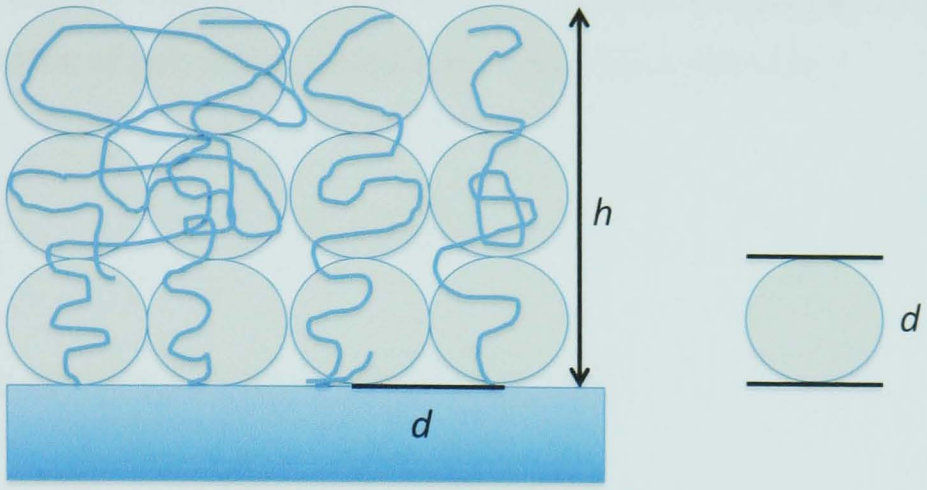

Fig. 2.2 Representation of the Alexander and de Gennes model. The polymer chains are stretched from the surface and each grafted chain can be subdivided into blobs of diameter *d*. The height of the brush, i.e. film thickness, is given by *h*.

At relatively low grafting density when the brush is in the semi-dilute regime, the brush chains are uniformly attached to the surface with a grafting density of σ. Each chain, with a degree of polymerisation N, is divided in blobs of diameter d, that contain a number of monomers N_b lower than N so that $\frac{h}{d}N_b = N$ where h is the height of the brush.

The dimensionless grafting density is given by:

$$\sigma_0 = \frac{a^2}{d^2}, \tag{2.1}$$

where σ_0 represents the fractional area of substrate that is covered by the grafted chains. a is the Kuhn length or the effective monomer size.

Inside each blob, we have N_b monomers and the distance between two polymer segments inside blob is given by

$$d = aN_b^{3/5}, \tag{2.2}$$

We are assuming that inside a blob the chains behave like a polymer in a good solvent with $N_b^{3/5}$ scaling behaviour for their size [26].

If we consider that the volume of each blob is d^3, (without considering the prefactors), the volume fraction of polymer ϕ_b inside every blob is given by [11]

$$\phi_b \approx N_b \frac{a^3}{d^3}, \tag{2.3}$$

and substituing equation 2.2 into equation 2.3 we have

$$\phi_b \approx \frac{a^3}{d^3}\left(\frac{d}{a}\right)^{5/3} = \sigma_0^{2/3}. \tag{2.4}$$

Equating the two forms of ϕ_b and extending it for all blobs, ϕ, forming one polymer chain we have

$$\phi = N\frac{a^3}{hd^2} = N\frac{a\sigma_0}{h}. \tag{2.5}$$

The thickness of the layer is obtained by equalize the equation 2.4 and 2.5 and rearranging them respect to brush thickness

$$h \approx Na\sigma_0^{1/3}. \tag{2.6}$$

From these relations it can be concluded that the size of grafted chains exhibits a stronger dependence on N compared to free polymer chains in solution, for which the size scales as $N^{3/5}$.

When R_g is larger than the grafting density, the chains tend to overlap forming the concentrated brush regime. The free energy of the system is given by the contributions of the stretching of the polymer chains and repulsion between the chains,

$$\Delta G = \Delta G_{int} + \Delta G_{el}, \tag{2.7}$$

where ΔG_{int} and ΔG_{el} are respectively the interaction term due to repulsion energy between two neighbouring chains and an elastic term due to loss of entropy for stretching the chains. The balance of these two terms determines the thickness of the polymer brush at equilibrium.

Using the Flory theory [26], ΔG_{int} and ΔG_{el} can be expressed mathematically as

$$\frac{G_{chain}(h)}{K_B T} = \upsilon \frac{N^2 \sigma_0}{h a^2} + \frac{h^2}{N a^2}, \tag{2.8}$$

where T is the absolute temperature, and ν is the excluded volume constant. The excluded volume [27] is defined as the volume *effectively* occupied by a segment of a polymer. It means that two polymer segments cannot be in the same place at the same time due to the repulsion forces.

The derivative of this equation with respect to the thickness of the brush layer in solution is given by

$$h = N(\upsilon \sigma_0)^{1/3}. \tag{2.9}$$

This equation shows the same dependence as for the semi dilute regime but, in this case, the stretching of the chains is driven by the osmotic pressure that expands the chains until equilibrium is reached.

It should be highlighted that this relationship is valid only for a neutral polymer, and consequently, it is not valid for charged polyelectrolytes.

When the brush is in poor solvent conditions, the chains remain in a collapsed state. In particular, at low grafting density, the single chains remain apart but, as σ increases, they interact with each other forming collapsed aggregates of various sizes and shapes. The de Gennes [25] theory assumes that all the brush chains are stretched at the same height forming a step like-profile. Other theories and experimental results confirm that the height of the brush follows this scaling theory, described above, but the amount of polymer as a function of the distance from the substrate depends on the vertical distance of the polymer chains from the graft surface and assumes a parabolic profile [28].

A polymer brush can be deposited on a surface via physisorption ("grafting to" method) or via chemisorption [16] ("grafting to" and "grafting from"). We discuss each of these in turn.

2.1.1 Physisorption

Normally the methods used to physisorb [17] a polymer on a surface are spin-casting or solution dip coating. The disadvantage of using these techniques is that the film is anchored to the surface using long-range and weak van der Waals interactions, which may desorb under harsh conditions.

For this reason, it is much more beneficial to attach the polymer on the surface using a chemical bond. The film is more stable and it can be used for various purposes.

In the case of physisorption of polymer brushes, a pre-synthesized block copolymer [29], in which one of the blocks has a strong interaction with the surface and acts like an anchor on the surface for the second block, is attached to the surface. The second block interacts more strongly with the solvent than with the surface so it floats in the solvent making a polymer brush. Polymer brushes synthesised with this method present some limitations to their use because the layer is reversibly attached to the surface by long-range and weak van der Waals interactions. The layer cannot reach high grafting density due to steric factors during the deposition of the polymer chain and the layer has a molecular weight determined by the polymer deposited. There are a limited number of chemical groups that may be used to functionalise the brush, because the side groups could interact with the surface via electrostatic or hydrophobic interactions or they could interact with the polymer forming covalent bonds. These factors make the use of these surfaces for most applications difficult.

2.1.2 Chemisorption

The chemisorption process involves short ranges interaction and covalent bonds between the film and the substrate.

There are two methods used to graft a polymer to a solid substrate: "grafting to" method and "grafting from" method as shown in Fig 2.3.

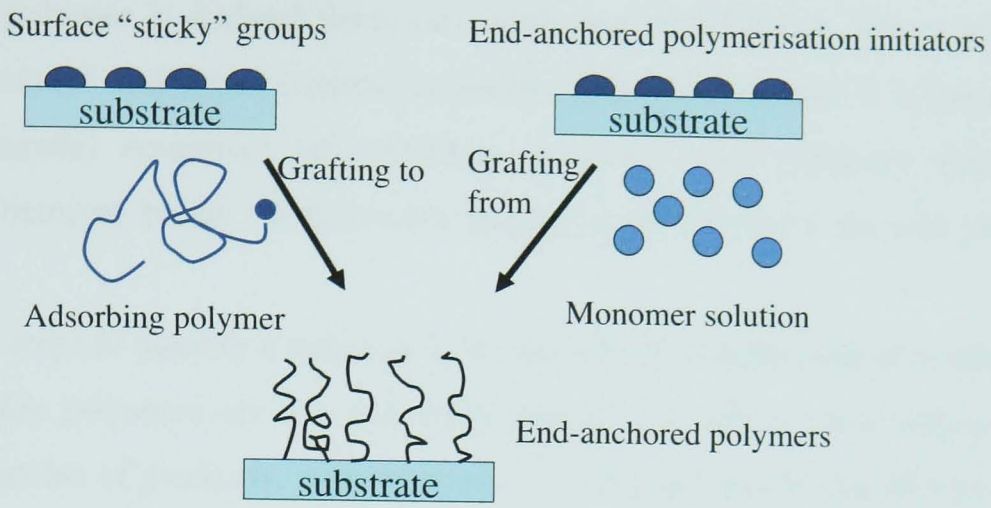

Fig 2.3 Schematic illustration of the "grafting to" and "grafting from" method for the synthesis of a polymer brush.

In the "grafting to" method, the polymer is grown *ex situ* with a specific functionalized end. Afterwards the polymer is added in contact with the substrate and, under appropriate condition, reacts with the surface.

In the "grafting from" method, the surface is functionalized with initiator molecules and then a polymer is grown from the surface.

There are differences in the properties of the final film using the two methods:

the "grafting to" method produces a film with a low grafting density and a low thickness, typically in the order of 3~10 nm [30, 31]. The polymer, in order to react with the surface, needs to diffuse into the polymer film, and, if the polymer has a larger molecular weight, the grafting density is low due to the large entropic barrier for packing/extending the chains [32]. The "grafting from" method is an alternative route of synthesis of a polymer brush with important advantages.

Polymer brushes synthesised via "grafting from" methods are covalently attached to the surface and the advantages of this method is the larger grafting density [33] of the polymer layer in comparison to the "grafting to" method. In the "grafting from" method the surface is functionalized with an initiator molecule and then the polymer layer is grown from the surface. A more detailed description of the "grafting from" mechanism will be explained in section 2.2.2.

2.2 Polymer classification and Synthetic methods

The word polymer is derived from the Greek words polumeros where πολυ (polu), meaning "many" and μέρος (meros) meaning "parts". A polymer is a large molecule (macromolecule) composed of repeating structural units typically connected by covalent chemical bonds. Well-known examples of polymers include plastics and proteins.

One of the ways to classify a polymer is to consider the mechanism of synthesis [34].

Condensation polymers are any polymers formed through a condensation reaction; small molecules of products, such as water or methanol and hydrochloridic acid, are released during the reaction. Examples of condensation polymers include polyamides, polyacetals and polyesters.

Addition polymers are any polymers formed by an addition reaction, where the monomers react together via rearrangement of bonds without the release of any small molecules. Examples of addition polymers include the reaction of unsaturated monomers like ethylene or acetylene, alicyclic compounds like Nylon 6 and polyethylene oxide.

Addition polymers can be synthesised using different routes that can be categorized by: free radical addition polymerisation and living addition polymerisation, and these are described in more detail in sections 2.2.1 and 2.2.2.

2.2.1 Free radical polymerisation

The free radical mechanism can be divided into three stages:

- initiation,
- chain propagation, and
- chain termination.

Initiation is the stage where free radicals, that start the polymerisation, are created. The initiator is normally a molecule that under condition of light or heat can be break down in radicals. Radicals are unstable species that react easily on account of their unfilled bonds.

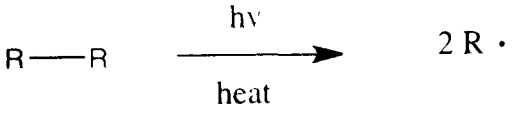

The second stage is the propagation where the initiator radicals react with the monomers with the following equilibrium.

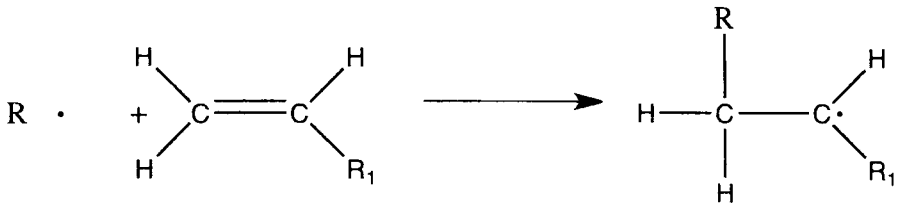

The radicals are unstable and they react with a monomer that has a double bond formed by a σ bond and a π bond. The free radical uses one electron from the π bond to form a covalent bond with the carbon atom. The other electron moves to the second carbon atom, turning the whole molecule into a radical. The new radical is formed on the carbon of the double bond that can better stabilize the radical with substitute groups such as a methyl group or phenyl group. During the polymerisation process, the growing chains can collide with another species, XY, transferring the radical active centre.

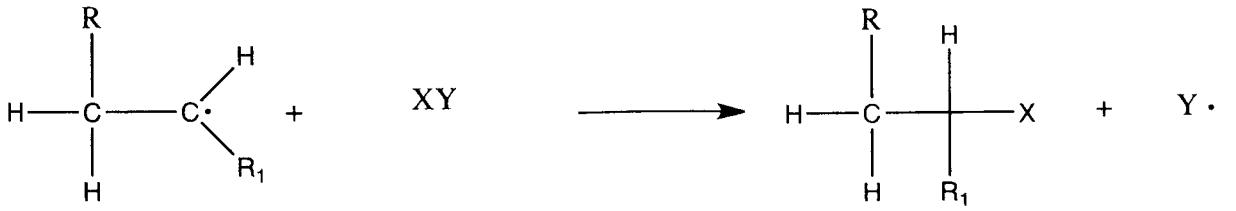

This process is called chain transfer and it is dependent on the strength of the XY bond.

In principle, the reaction should be finished when all the monomer is consumed but this outcome is very unlikely. In reality there are some side reactions that contribute to the termination of the reactions. Termination typically occurs in two ways: combination and disproportionation.

Combination occurs when two radicals join together and form a single chain. This mechanism stops the chain's growing. Termination by combination is shown in the diagram

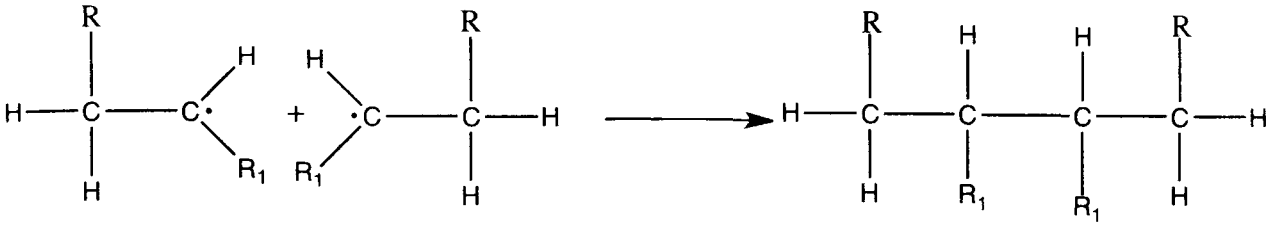

Disproportionation occurs when a free radical strips a hydrogen atom from an active chain forming a single bond in one molecule and a double bond in the other. This mechanism as well stops chain growth. Another reason for termination can be the reaction of the radical with an impurity.

Termination by disproportionation is shown in the scheme below

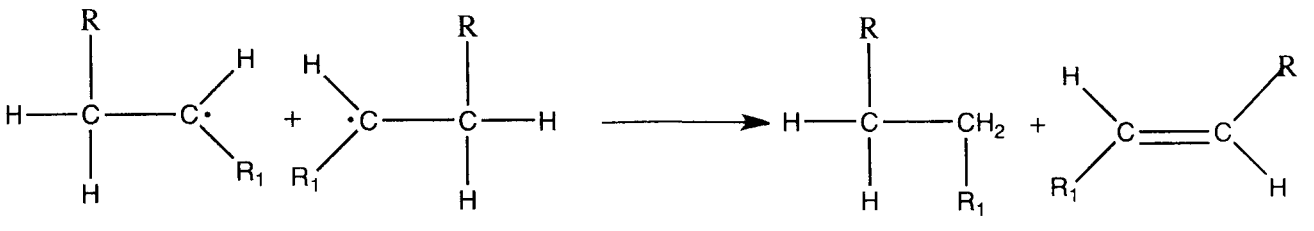

Polymers synthesised using free radical polymerisation are characterized by an unpredictable molecular weight and high polydispersity because the kinetics of the initiator reaction is much slower than the propagation one.

2.2.2 Living / controlled polymerisation

Another way to synthesise polymers is by living or controlled polymerisation [10]. This method in comparison to radical polymerisation gives a polymer with the possibility of a pre-determined molecular weight, a low polydispersity and a wide range of polymer topology. It can be used with a wider range of monomers with special functional groups. Fig 2.4 lists these characteristics.

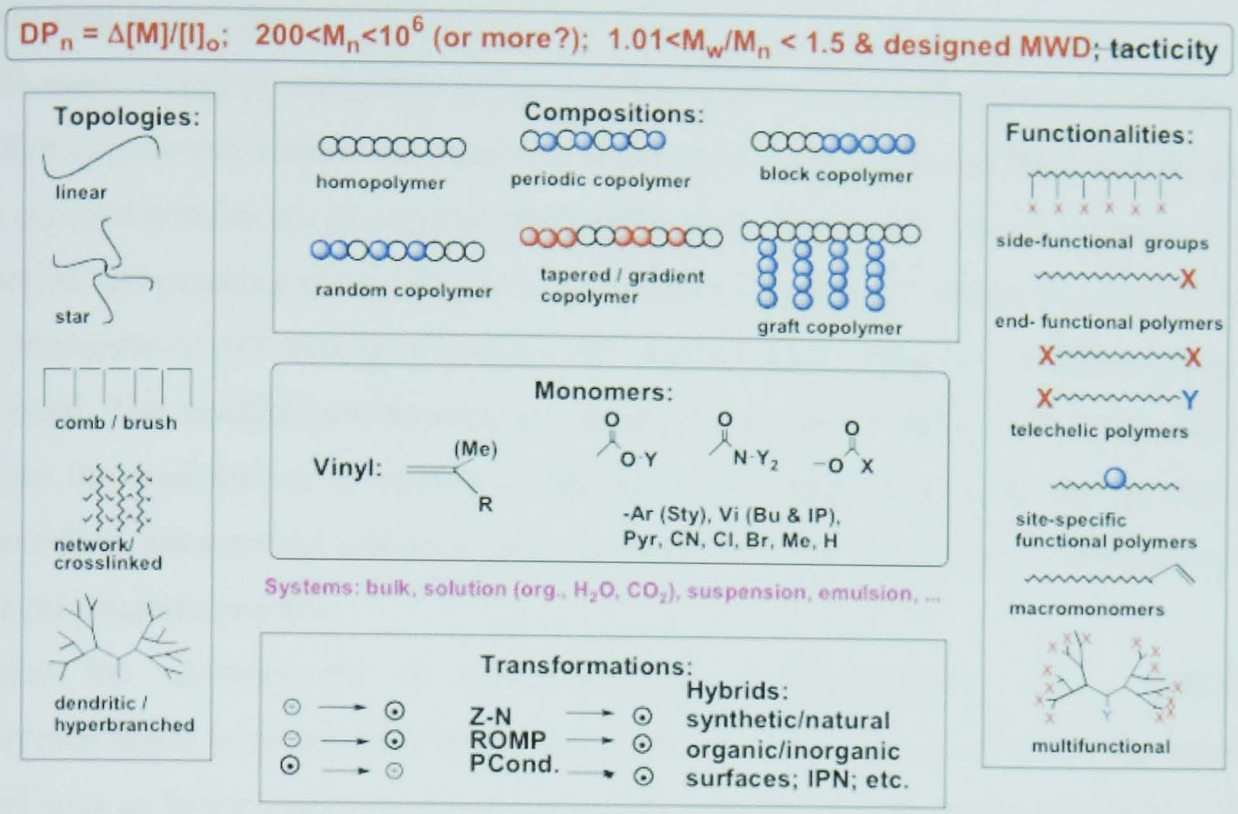

Fig.2.4 Summary of polymer architectures and types that can be synthesised using living controlled polymerisation. The graph is taken from http://www.chem.cmu.edu/groups/maty/about/research/02.html retrieved 27-11-2009.

CRP, control radical polymerisation, has attracted the attention of the both academia and industry because materials with a specific set predefined properties can be prepared [35]. The applications are in the fields of coatings, adhesives, electronics, and biomaterials.

Living polymerisations, discovered by Szwarc in 1956 [36], indicates a polymer synthesis route where the chain termination step and the chain transfer reaction are absent. The living nature of the process can be demonstrated by the re-initiation of the chain growth with the addition of further monomers when the first synthesis is finished. Because of this, it is possible to synthesise block copolymer with a defined polymerisation index and narrow molecular weight distribution [10].

The disadvantage of a pure living polymerisation for growing polymer brushes is the restricted number of monomers, the low reaction temperatures, the long time required for the reaction, and the extreme sensitivity to impurities and water. Consequently, (with few exceptions) the reaction has to be conducted in special glassware with

rigorous purification, drying of the reagents and the process is very expensive for industrial approaches.

The name living or controlled polymerisation indicates that during the synthesis the polymer grows at a more constant rate than for the free radicals method, for example. In selected conditions, during the propagation process, there is a low concentration of "active" propagating chains and a large number of "dormant" chains that are not able to propagate or self-terminate because they are reversible capped to a radical group or a metal. The equilibrium between the dormant and active chain is dynamic and the more the equilibrium is shifted to the dormant species the more the reaction is controlled, because the initiation process becomes more significant in comparison to the propagation process.

Since the development of controlled/living polymerisations, many different polymerisation schemes have been introduced for the synthesis of polymer brushes [10] such as living anionic polymerisation, living cationic polymerisation, living ring-opening polymerisation (ROP), ring-opening metathesis polymerisation (ROMP), nitroxide-mediated polymerisation (NMP), reversible addition-fragmentation chain transfer polymerisation (RAFT), and atom-transfer radical polymerisation (ATRP). Many industrially important polymers are synthesized via ROP, which has been used in the "grafting from" method with monomers like lactones, lactides, and lactic acid, producing potentially important biodegradable polymers. Polymer brushes may also be synthesized via ROMP for the creation of polymers with electrical properties.

NMP, RAFT and ATRP are the three major CRP processes because they are suitable for a wider variety of monomers, solvents and can be performed under more reasonable reaction conditions like room temperature and with less rigorous cleanliness. They are classified like radical polymerisation and they follow similar fundamental reaction schemes, based on the reversible end-capping of growing polymer radical chains. NMP relies on a nitroxide reversible leaving group, RAFT on a dithiol ester, and ATRP on transition metal halide complexes [10, 35, 37].

A controlled polymerisation process should respect these features

First order kinetic behaviour; the concentration of the monomer decreases linearly as a function of the time and, if there is no termination reaction, the concentration of the propagation species is constant until the completion of the reaction.

Pre-determinable degree of polymerisation; the number average molecular weight of

the polymer should be a linear function of the monomer conversion. This implies that the initiation stage is fast enough that all the chains start to grow at the same time and there are no transfer chain reactions.

Narrow molecular weight distribution; this implies that all the chains are grown at the same time and there are no termination or chain transfer reactions.

Long-lived polymer chain; this feature implies that the chains have their active centre alive until the completion of the reaction and, if some more monomer is added, the reaction should resume, allowing the growth of block copolymers.

2.3 ATRP

ATRP is the most widely used "controlled"/living radical reaction due to its flexibility and ease of use. The name indicates the similarity in the reaction mechanism between ATRP and Kharasch reaction or well known ATRA [35], atom transfer radical addition.

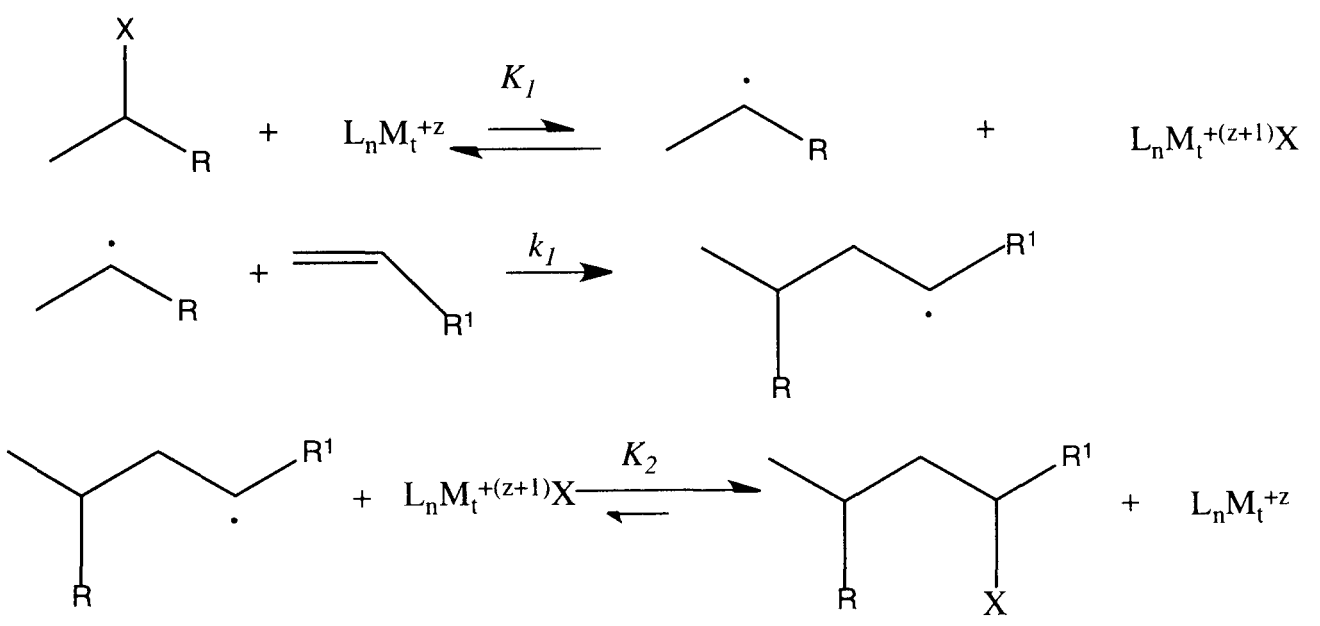

Fig 2.4 Mechanism of the Kharasch reaction where a metal species, *M*, catalizes the cleavage of the carbon–halogen (C–X) bond generating a radical species that reacts with an olefin.

ATRP has attracted the attention of industry and academia in comparison to other CRP's because it requires a simpler set-up, generally inexpensive products, and a low concentration of catalysts. Also ATRP is suitable for many types of polymers

including acrylates, methacrylates, styrenes, vinylpyridines, acrylonitrile, and acrylamides. The mechanism of the initiation and propagation consists of the following stages [38]:

Initiation (halogen exchange):

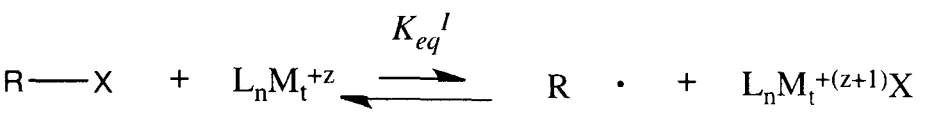

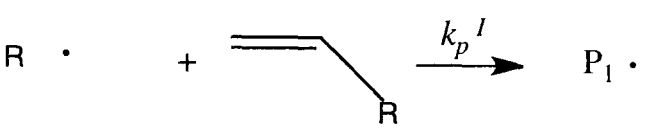

Controlled propagation:

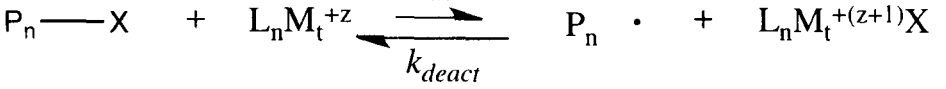

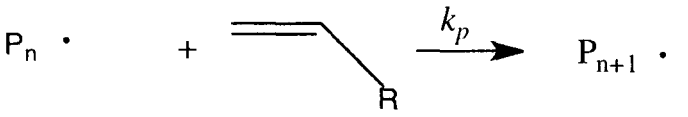

Termination:

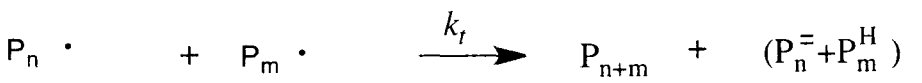

In a classical radical polymerisation the propagation step is much faster than the initiation step as described in the section 2.2.1, and consequently the polymer has a wide polydispersity index, PDI. In the ATRP reaction, the initiator, and afterwards the monomer is bound to a halogen species that keeps the species P-X mostly inactive, lie in a dormant state. A transition metal, the catalyst, in the lower oxidation state, is added under salt and it reacts with a ligand L, forming a stable complex. In the

initiation stage, the catalyst is oxidized in the higher oxidation state and forms a complex with a co-ordinated halide ligand. This exchange of the halogen between the dormant species and the transition metal in the higher state of oxidation results in the formation of the propagation radicals R.

This initiation reaction is the sum of several equilibria and k_{act} indicates the rate of formation of the active radical and k_{deact} indicates the rate of formation of the dormant species, k_p is the rate of propagation of the polymerisation and k_t the rate of termination reaction. When the reaction is in progress, the rate of termination reaction is diminished due to the fact that the radicals are always trapped in the activator or deactivator process and capped with the halogen. This is called the persistent radical effect (PRE) [39] and the equilibrium is strongly shifted toward the dormant species ($k_{act} << k_{deact}$). In this condition, the rate of initiation is much larger then the rate of propagation and this is why the polymer chains grow at a more constant rate than in traditional radical polymerisation. To reach a polymerisation with a narrow PDI it is necessary to increase the efficiency of the initiation stage and reduce the rate of termination before the persistent radical effect is established. This can be accomplished by adding to the reaction mixture the higher state transition metal (complex) that allows us to establish an instantaneous control and reduces the fraction of polymer of low molecular weight [38].

Atom transfer (overall equilibrium):

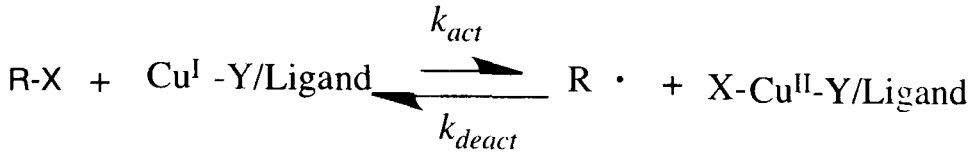

Contribution reactions:

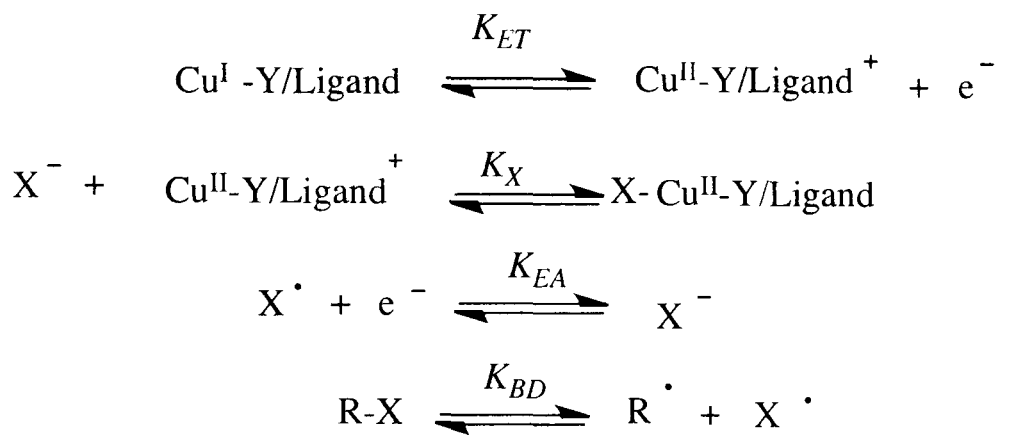

Fig 2.5 Representation of the equilibria in an ATRP reaction. The equilibrium reaction is the overlap of several reversible equilibria: the homolysis of the bond R-X (K_{BD}), the alkyl halide, two redox process, the oxidation of the complex transition metal at the higher oxidation (K_{ET}), and the reduction of the halide (K_{EA}) and the heterolytic cleavage of the Cu-X bond (K_X). Each single reaction contributes to the global K_{ATRP}, and for this reason it is important to understand the role of each single component.

An ATRP system is composed of the monomer, an initiator with a transferable halogen, a catalyst (a complex of a ligand with a transition metal). Other important factors are the reaction temperature and the solvent.

Monomer; a wide variety of monomers has been used for growing brushes by ATRP, including styrene, methacrylate, methacrylamides, and acrylonitrile. Each monomer, for its unique chemical structure, has its intrinsic equilibrium constant between the active and the dormant species [38]. The atom transfer equilibrium constant, in the absence of side reactions, can be defined

$$K_{ATRP} = \frac{k_{act}}{k_{deact}} = K_{ET} K_{EA} K_{BD} K_X . \qquad (2.10)$$

The magnitude of this constant, K_{ATRP}, establishes the polymerisation rate. If the value

of the equilibrium constant is too small, the reaction will not occur or occur very slowly because the equilibrium is completely shifted towards the dormant species. If the value of the equilibrium constant is too high, the reaction will be not controlled because the high concentration of active species will lead to a rapid termination. However, the overall equilibrium is a function not only of the kind of monomer but strongly depends on the quantity and reactivity of the catalyst.

Initiators; in ATRP, the typical initiator molecules are the alkyl halide (R-X).

The choice of the initiator is important for a controlled reaction because it determines the number of growing polymer chains if transfer and termination reactions are negligible. The concentration of the initiator can be related to the degree of polymerisation DP by [10]

$$DP = \frac{[M_0]}{[initiator]} \times conversion. \qquad \textbf{(2.11)}$$

The role of the initiator is to selectivity exchange halide between the growing chain and the metal complex. The halides normally used are bromine and chlorine. C-F is not used because it has a very strong bond and C-I is not used because it has a weak bond and it is not really selective.

Catalyst; the catalyst [40] is the most important component in the ATRP process since it determines the equilibrium of halide exchange between the dormant and the active species, and consequently the rate of reaction propagation. The most common catalyst is copper for the broad range of monomers that can be used but there are examples of ATRP reactions with metals such as Ti, Mo, Re, Fe, Ru, Os, Rh, Co, Ni, and Pd. A good catalyst has to satisfy several prerequisites: the metal has to have two accessible oxidation states separated by one electron, a good affinity for the halide, and its complex with the ligand should be really strong.

The activity of the catalyst has to be associated not only to the redox potential of the metal also the halidophilicity of the transition metal complex. To ensure a better control of the reaction, the transition metal complex has to be at least partially soluble in the reaction medium in a way that the concentration of the activator Cu^{1+} and deactivator Cu^{2+} can be defined. The equilibrium between Cu^{1+} and Cu^{2+} is oxygen sensitive and all the products are to be degassed before being mixed. Recently the

group of Professor Matyjaszewski developed methods to perform an ATRP reaction in the presence of small quantity of oxygen by adding a reducing agent like ascorbic acid [41].

Solvents; ATRP is a very versatile reaction and it can be performed in bulk, in solution, or in heterogeneous systems. The solvent is normally added when the growing polymer is not soluble in its own monomer. Particular attention also has to be paid to the effect of the solvent on the structure of catalyst. A variety of solvents have been used like benzene, toluene, anysole, diphenyl ether, ethyl acetate, acetone, dimethyl formamide, ethylene carbonate, alcohol, water, and many others. The use of protic media in the ATRP reaction allows the expansion of the range of polymers that can be synthesized and at the same time increases the solubility of the catalyst and reactions are normally much faster but less controlled. It is necessary to take in account the side reactions involved in the use of protic solvents, for example, in homogeneous conditions [42].

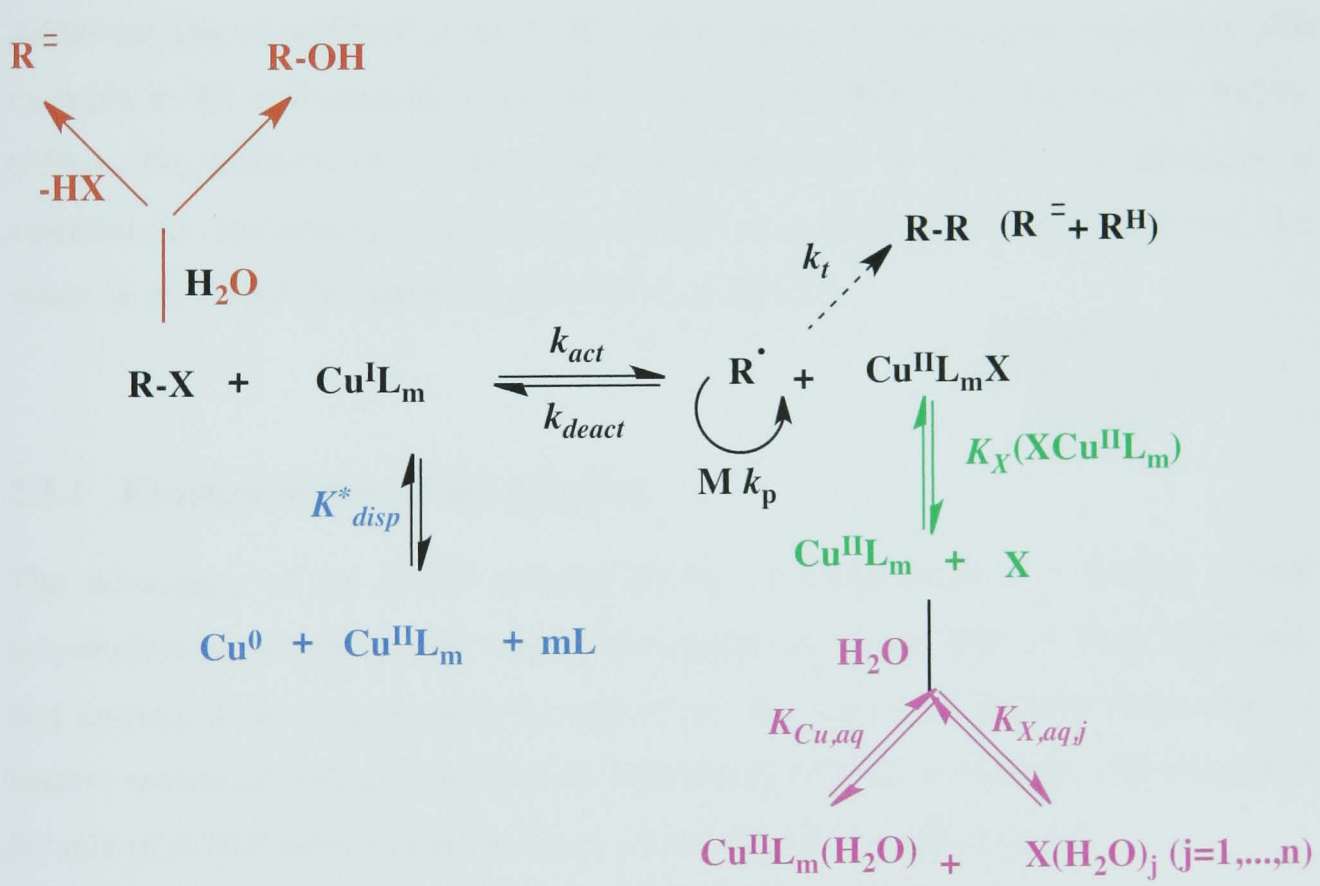

Fig 2.6 Schematic representation of the side reactions in protic solvents. Solvents like alcohol and water lead to disproportionation reactions of the Cu(I) complex; hydrolysis of the initiator or domant species R-X; dissociation of halide from the complex Cu(II)L and consequently complexation with the polar solvent.

The use of a co-solvent, like pyridine, can stabilize the Cu(I) complex, suppressing its disproportion in Cu(0) and Cu(II). To suppress the solvolysis (i.e. where the solvent participates as a reactant in the reaction) of the deactivator Cu(II)LX, an extra halide salt id added to the reaction [43].

It has been demonstrated that the use of higher dielectric constant solvents such as water, methanol and acetone increases the rate of reaction due to an increase of the solubility and activity of the metal/ligand complex [42].

Temperature and reaction time; the optimal temperature for an ATRP reaction depends on the monomer, the catalyst, and the molecular weight that would be achieved. The rate of polymerisation increases with temperature due to an increase of the radical propagation rate constant and the atom transfer equilibrium constant, but, at the same time, side reactions, like chain transfer, become more important. The solubility of the catalyst is favourable at higher temperature but it may cause its decomposition.

Additives; use of additive in an ATRP can be important with some monomers. For example in the polymerisation of MMA, (methylmethacrylate), catalyzed by $RuCl_2$-$(PPh_3)_3$, the addition of a Lewis acid like aluminum, or other metal alkoxides is essential for performing a controlled reaction. The addition of a polar solvent, like water, in an ATRP, increases the speed of the reaction.

2.3.1 Kinetics of the ATRP reaction

The advantage of an ATRP polymerisation in comparison to a normal radical polymerisation is that the rate of polymerisation has a first order kinetics behaviour, and consequently it is possible to pre-define the degree of polymerisation with a narrow molecular weight distribution. Matyjaszewski and coworkers [40] calculated the rate of ATRP polymerisation, v_p, as a function of the CuX/CuX_2 ratio.

Assuming a steady-state kinetics the rate of polymerisation is given by v_p

$$v_p = k_p \frac{k_{act}}{k_{deact}} [R-X][M] \frac{[CuX]}{[CuX_2]}, \qquad \textbf{(2.12)}$$

where k_p is the rate constant for propagation; $[R\text{-}X]$ is the concentration of the growing

ends; $[M]$ is the concentration of the free monomer in the solution; $[CuX]$ and $[CuX_2]$ are the concentrations of CuX and CuX_2, respectively.

The dry thickness of a polymer on the substrate, h, is related to the polymer molecular weight, through

$$h = M_w \frac{\sigma}{\rho N_A} \tag{2.13}$$

where σ is the grafting density of polymer, ρ is the density of the polymer, and N_A is the Avogadro number. Recognizing that $R_p \sim dh/dt$ and neglecting the terms that are constant during the polymerisation, the equation 2.12

$$\frac{dh}{dt} \approx \frac{[CuX]}{[CuX_2]}. \tag{2.14}$$

Equation 2.13 highlights the rate of polymerisation being a function of the ratio of Cu(I) and Cu(II) and not of the total amount of catalyst present in the reaction.

2.4 Hydrogel

A gel can be considered a polymer with a three-dimensional network where the chains are connected through physical or chemical junction points, better defined as cross-links. The cross-linker can have a physical nature if the chains are associated together by hydrogen bonds and van der Waals interactions, or a chemical nature if the polymer chains are linked through covalent bonds. A gel can be considered as having an infinite structure indicating that the linked polymer chains creates a molecule with a high molecular weight [44].

In a polymer gel it is possible to distinguish two parts: sol and gel. The sol is constituted by a suspension of colloidal particles in a liquid. The effect of temperature, for example, is that the colloidal particles start to interact creating junction points that end up in a three-dimensional network [45]. This process is called gelation and the gel point indicates the threshold [26] between the transition from a viscous liquid (sol) to a network with both a liquid and solid-like behaviour (gel).

When the solvent and the gel are thermodynamically compatible, the gel starts to swell. The liquid inside the gel prevents the gel from collapsing and the network traps the liquid, preventing it from flowing away. One common example is gelatin. A few grammes of gelatin powder can hold 100g of water. For this characteristic, a swollen gel presents intermediate properties between a solid and a liquid, it is soft but with a defined three-dimensional structure, and it cannot be dissolved.

If water is the swelling agent the gel is classified as a hydrogel and many find applications in biomedical fields for their compatibility with the human body [45]. For these unique properties, some of the hydrogels can find applications in agriculture, cosmetics.

2.4.1.1 Physical gel (reversible*)*

In this type of gel, the polymer chains are linked through non-covalent interactions such as dipole-dipole (van der Waals) interactions. Normally these links are thermo-reversible in that they can be broken at high temperatures but then can be reformed again at lower temperatures.

As a function of the nature of the monomer, the gel can have some microcrystalline regions linking more than one chain. These gels are thermoreversible and the network breaks if the gel is at a temperature superior to the melting point such gels can be reformed at lower temperatures.

The gel can also microphase separate in certain conditions [11], if the polymer gel is made from a block copolymer with a hydrophilic and a hydrophobic part. One example is gelation via hydrophobic associations of block copolymers in water.

2.4.2 Chemical gel (irreversible).

In this type of gel, the chains are linked through covalent bonds and they form a three-dimensional network. These gels can be formed from the direct reaction of a linear or branched polymer with molecules with di- or multifunctional groups (cross-linking agent). Another method involves a copolymerisation reaction where one of the monomers is added in a smaller quantity and it has a multifunctional group. Common

cross-linkers are poly(ethylene glycol) dimethacrylate (PEGDMA), ethylene glycol dimethacrylate (EGDMA) and bisacrylamide. The cross-linking process can involve chemical reactions such as radical polymerisation; photo polymerisation in the presence of UV light; or radiative cross-linking using electron beams, gamma rays or X-rays [44]. The amount of cross-linker determines the properties of the gel. In reality, the cross linker is not homogeneously distributed within the gel and it forms clusters, the chains can interact through physical entanglements and chain loops, and they can have some non-reacted functional groups remaining. These influence the swelling properties of the gel.

The gel can be classified in respect to its size; if the bulk gel is larger than 100 μm they are known as macrogels and if smaller than 100 μm, as microgels. An advantage of using macrogels is the macroscopic observation of the swelling/deswelling transition, but the disadvantage is the very long time to reach the equilibrium.

2.4.3 Swelling behaviour

After synthesis, the hydrogel can be brought into contact with the solvent until it reaches equilibrium. When the network is thermodynamically compatible with the solvents, it starts to expand in a solvated state. The driving force of the swelling process is mainly entropic because when the volume increases, the chains assume different configurations. This process creates an elastic force due to the stretching of the chains. The latter is accomplished by a decrease in entropy, because there are fewer configurations for extended chains. Equilibrium is reached when the osmotic pressure due to the polymer-solvent interaction balances the elastic contributions due to the stretching energy of the cross-linked polymer chains. The total free energy of the system can be expressed as [23, 26]

$$\Delta G_{tot} = \Delta G_{elastic} + \Delta G_{mix}, \tag{2.15}$$

where $\Delta G_{elastic}$ indicates the contribution of elastic retractive forces and ΔG_{mix} indicates the thermodynamic compatibility of the polymer/solvent system.

Equation 2.14 can be differentiated with respect to the number of water molecules (at constant temperature and pressure) in the system and can be expressed in terms of chemical potentials,

$$\mu_1 - \mu_{1,0} = \Delta\mu_{elastic} + \Delta\mu_{mix}, \tag{2.16}$$

where μ_1 is the chemical potential of the water within the gel and $\mu_{1,0}$ is the chemical potential of pure water. At equilibrium the variation of the chemical potential of the water inside and outside the gel has to be equal to zero, consequently, at equilibrium, the elastic and the mixing contributions have to balance each other.

The thermodynamics of mixing is related to the interaction of the polymer with the solvent, but, in the case of three-dimensional networks, the polymer-solvent interaction is influenced by the concentration of the cross-linker as well.

The classical theory of polymers in solution was described by Flory [26] and Huggins and is based on a lattice model.

The mathematical equation for the $\Delta\mu_{mix}$ is

$$\Delta\mu_{mix} = RT\left[\ln(1-\nu_2) + \nu_2 + \chi\,\nu_2^2\right] \tag{2.17}$$

where ν_2 is the volume fraction of the polymer gel, χ is known as the Flory-Huggins interaction parameter which indicates the mostly enthalpic polymer-solvent interaction, T is the absolute temperature; and R is the gas constant.

The thermodynamic swelling is counterbalanced by the elastic contribution of the network, which can be expressed by

$$\Delta\mu_{elastic} = \frac{RT\varphi_1\, N_c^{gel}}{V_0}\left(\nu_2^{1/3} - \frac{\nu_2}{2}\right), \tag{2.18}$$

where φ_1 is the molar volume of the solvent, N_c^{gel} is the number of monomer between crosslinker, V_0 is the total volume of the relaxed hydrogel. The relaxed state of the polymer is defined as the polymer after cross-linking but before swelling or deswelling. At equilibrium the two contributions are counter balanced. This can be expressed mathematically

$$\mu_1 - \mu_{1,0} = \Delta\mu_{elastic} + \Delta\mu_{mix} = 0 \tag{2.19}$$

and

$$0 = \Delta\mu_{tot} = \frac{RT\varphi_1 N_c^{gel}}{V_0}\left(\nu_{2m}^{1/3} - \frac{\nu_2}{2}\right) + RT\left[\ln(1-\nu_{2m}) + \nu_{2m} + \chi\,\nu_{2m}^2\right], \tag{2.20}$$

yielding

$$\left[\ln(1-\nu_{2m}) + \nu_{2m} + \chi\,\nu_{2m}^2\right] = -\frac{\varphi_1 N_c^{gel}}{V_0}\left(\nu_{2m}^{1/3} - \frac{\nu_{2m}}{2}\right), \tag{2.21}$$

where ν_{2m} indicates the maximum volume fraction of the polymer at equilibrium. The term on the left in equation 2.21 indicates the increase of the mixing chemical potential due to the interaction solvent/polymer. The term on the right indicates the reduction in the chemical potential of the elastic force due to a lowering of the number of chain conformations. Equation 2.21 is valid for ideal networks, without considering physical entaganglements and unreacted functional groups. To take into account these effects, the right hand side can by multiplied by an additional term (1-$2M_c/M$) where M is the molecular weight of the polymer chains prepared in the same conditions but in absence of cross linker [46], M_c is the molecular weight of monomer between crosslinker. If $M = \infty$, the correction term is 1 and the network is ideal.

2.4.4 Determination of structural characteristics

The parameters used to describe a hydrogel are [45]:

M_c is the average molecular weight of the polymer chain between adjacent crosslink points. ρ_c^{gel} is the cross linking density and is inversely proportional to M_c, in agreement with

$$\rho_c^{gel} = \frac{N_c^{gel}}{V_0} = \frac{1}{\tilde{v}M_c}, \tag{2.22}$$

where $\tilde{v}$ is defined as the volume of a unit of mass of material.

Inserting equation 2.22 into equation 2.21 we can mathematically define the crosslinking density as

$$\frac{1}{\tilde{v}M_c} = \rho_c^{gel} = -\frac{RT\left[\ln(1-\nu_{2m}) + \nu_{2m} + \chi\,\nu_{2m}^2\right]}{\varphi_1\left(\nu_{2m}^{1/3} - \frac{\nu_{2m}}{2}\right)}. \tag{2.23}$$

The swelling ratio of a gel is defined as

$$q = \frac{V}{V_0} \tag{2.24}$$

where V is the volume of the swollen gel and V_0 is the volume in the dry state. The maximum swelling ratio q_m can be calculated, using [47]

$$q_m^{3/5} \cong \frac{V_0}{N_c^{gel}}\left(\frac{1}{2} - \chi\right)\frac{1}{\varphi_1} \tag{2.25}$$

The swelling ratio of a polymer network is a function of the quality of the solvent χ, and the density of the cross linking, $V_0/N_c^{gel}=1/p_c^{gel}$.

2.5 Type of hydrogel

In this particular section, we focus on the application of the hydrogel.

The hydrogel can be wet and soft but it conserves its solid structure. Hydrogels can be made from "smart polymers" or "intelligent polymers" [12], so-called because in response to small changes in environmental conditions such as temperature, pH, solvent, electric fields, they are characterized by large changes in chemical and physical properties such as hydrophilicity and hydrophobicity, solubility in a particular solvent or dimensional size. These changes in properties are reversible when the stimulus is reversed [44].

Environmental stimuli are listed in Table 2.2

Physical	Chemical	Biochemical
Temperature	pH	Enzyme substrate
Solvents	Specific ions	Affinity ligands
Radiation (uv-vis)	Chemical agents	Other biological agents
Electric and magnetic field	Ionic strength	

Table 2.2 Environmental stimuli affecting physical, chemical and biochemical properties of smart polymers.

These polymers can be in different states, like in solution, adsorbed or grafted on substrates, cross-linked in the form of hydrogels. Polymers in solution, under an external stimulus, can show a turbidimetric phase that disappears when the stimulus is removed.

2.5.1 pH sensitive hydrogels

These hydrogels respond to changes in the environmental pH; they contain an ionisable side group such as carboxylic acid or an amine group. Examples of these polymers are poly(methacrylic acid), poly(acrylic acid), poly[2-(dimethylamino)ethylmethacrylate], and poly[2-(diethylamino)ethylmethacrylate]. If the hydrogel has an acid side group, it absorbs water in basic conditions and swells, and it releases water in acid conditions assuming a collapsed conformation. This variation in physical properties can be visualized in a macroscopic crosslinked hydrogel by an increase or decrease in size of the gel. In the case of a polyacid grafted on a surface, this transition can be visualized by an increase in hydrophobicity in acid pH and hydrophilicity in basic pH. These phenomena can be explained considering the chemical structure of the acid side group. In basic conditions the acid group is ionized with a negative charge, and to minimise electrostatic repulsions between the chains, the chains stretch away from each other, and the ionisable groups absorb water to screen the charges. For this reason the gel swells in basic conditions. In acid conditions, the acid side groups are not charged anymore, and can release water and

the chains can be close to each other assuming a collapsed conformation. More information about polyelectrolytes will be given in Chapter 3.

2.5.2 Temperature sensitive

Smart polymers can be temperature responsive and they are characterised by a lower critical solution temperature (LCST) [12]. Below a critical temperature (T_c) the polymer is solution has one phase, but above the T_c the polymer is separated in two dehydrated and collapsed phases. With an increase in temperature, the short-range interactions such as hydrogen bonds become weaker and the polymer changes its state from hydrophilic to hydrophobic, precipitating from the solution.

2.6 Applications of the hydrogel

Smart polymers, in the hydrogel state, have been studied for different applications, including drug delivery, actuators and flow control [45].

Contact lenses are a good example of a hydrogel application, due to their good mechanical properties [48], refractive index, and high oxygen permeability.

Hydrogels can be used as a carrier to release drugs in a controlled way and in specific areas of the body. For example hydrogels, based on n-alkyl methacrylate esters, acrylic acid, are swollen in basic condition and collapse in acid condition. The drug encapsulated inside the gel can be specifically release in the small intestine or in the colon where the pH is between 5.0 and 7. An important advantage of polyacid hydrogels for drug delivery is that they resist the acidic environment of the stomach.

Hydrogels have found applications [44] as actuators, because with an appropriate energy stimulus, they can convert chemical energy into mechanical work. When a conducting hydrogel is in an electric field, a redox reaction leads the hydrogel to change conformation and consequently changes in volume are observed.

pH and temperature-responsive hydrogels have found application as valves to regulate flow control. These valves, via reversible swelling and deswelling, prevent or allow the passage of the fluid through the channels.

1. Andreeva, D.V., et al., *Self-healing anticorrosion coatings based on pH-sensitive polyelectrolyte/inhibitor sandwichlike nanostructures.* Adv. Mater., 2008. **20**: p. 2789-2794.
2. Chen, L., P. Degenaar, and D.D.C. Bradley, *Polymer transfer printing: Application to layer coating, pattern definition, and diode dark current blocking.* Adv. Mater., 2008. **20**: p. 1679-1683.
3. Lahann, J., et al., *Reactive polymer coatings: A first step toward surface engineering of microfluidic devices.* Anal. Chem., 2003. **75**: p. 2117-2122.

4. Israelachvili, J.N., *Intermolecular and Surface Forces*. 2nd ed. 1991, London: Academic Press.
5. Lin Q, P.R. and J. Hredrick, *Polymers for Microelectronics and Nanoelectronics*. 2004: Weimar: C.H.I.P.S.
6. Gupta, S.A., H.D. Cochran, and P.T. Cummings, *Shear behaviour of squalene and tetracosane under extreme confinement. 1. Model, simulation method, and interfacial slip.* . J. Chem. Phys., 1997. **107**: p. 10316-10326.
7. Napper, D., *Steric Stabilization of colloidal particles*. 1983, New York: Accademic Press.
8. Leckband, D., S. Sheth, and A. Halperin, *Grafted poly(ethylene oxide) brushes as non fouling surface coatings.* J. Biomater. Sci. Polym. Ed., 1999. **10**: p. 1125-1147.
9. Pinto, J.C., et al., *Organic thin film transistors with polymer brush gate dielectrics synthesized by atom transfer radical polymerisation.* Adv. Funct. Mater., 2008. **18**: p. 36-43.
10. Edmondson, S., V.L. Osborne, and W.T.S. Huck, *Polymer brushes via surface-initiated polymerizations.* Chem. Soc. Rev., 2004. **33**: p. 14-22.
11. Jones, R.A.L., *Soft condensed matter.* Oxford University Press, 2004.
12. Gil, E.S. and S.M. Hudson, *Stimuli-reponsive polymers and their bioconjugates.* Prog. Polym. Sci., 2004. **29**: p. 1173-1222.
13. Nath, N. and A. Chikoti, *Creating "smart" surfaces using stimuli responsive polymers.* Adv. Mater., 2002. **14**: p. 1243-1247.
14. Vyas, M.K., et al., *Switching of friction by binary polymer brushes.* Soft Matter, 2008. **4**: p. 1024-1032.
15. Luo, R., H. Li, and K.Y. Lam, *Coupled chemo-electro-mechanical simulation for smart hydrogels that are responsive to an external electric field.* Smart Mater. Struct., 2007. **16**: p. 1185-1191.
16. Milner, S.T., *Polymer brushes.* Science, 1991. **251**: p. 905-914.
17. Halperin, A., M. Tirrell, and T.P. Lodge, *Tethered chains in polymer microstructures.* Adv. Polym. Sci., 1992. **100**: p. 31-71.
18. Advincula, R.C., et al., *Polymer brushes: Synthesis, Characterization and Applications*. 1st ed. 2004: Wiley.
19. La Spina, R., et al., *Controlling network-brush interactions to achieve switchable adhesion.* Angew. Chem. Int. Ed., 2007. **46**: p. 6460-6463.
20. Raphaël, E. and P.G. de Gennes, *Rubber-rubber adhesion with connector molecules.* J. Phys. Chem., 1992. **96**: p. 4002-4007.
21. Bosker, W.T.E., et al., *Sweet brushes and dirty proteins.* Soft Matter, 2007. **3**: p. 754-762.
22. Motornov, M., et al., *Switchable selectivity for gating ion transport with mixed polyelectrolyte brushes:approaching "smart" drug delivery systems.* Nanotechnology, 2009. **20**: p. 434006-434016.
23. Flory, P.J. and J. Rehner, Jr., *Effect of deformation on the swelling capacity of rubber.* J. Chem. Phys., 1944. **12**: p. 412-414.
24. Alexander, S., *Polymer adsorption on small spheres - scaling approach.* J. Phys. (France), 1977. **38**: p. 977-981.
25. de Gennes, P.G., *Conformations of polymers attached to an interface.* Macromolecules, 1980. **13**: p. 1069-1075.
26. Flory, P.J., *Principles of Polymer Chemistry*. 1953, Ithaca: Cornell University Press.
27. *http://goldbook.iupac.org/E02260.html.* 30-11-2009.

28. de Gennes, P.-G., *Scaling Concepts in Polymer Physics*. 1979, Ithaca: Cornell University Press.
29. Brittain, W.J., et al., *Surface rearrangement of diblock copolymer brushes stimuli responsive films.* Adv. Polym. Sci., 2006. **198**: p. 125-147.
30. Biesalski, M. and J. Rühe, *Scaling laws for the swelling of neutral and charged polymer brushes in good solvents.* Macromolecules, 2002. **35**: p. 499-507.
31. Biesalski, M. and J. Rühe, *Preparation and characterization of a polyelectrolyte monolayer covalently attached to a planar solid surface.* Macromolecules, 1999. **32**: p. 2309-2316.
32. Zhao, B. and W.J. Brittain, *Polymer brushes: surface-immobilized macromolecules.* Prog. Polym. Sci., 2000. **25**: p. 677-710.
33. Zhao, B. and W.J. Brittain, *Polymer brushes: surface immobilized macromolecules.* J. Prog. Polym. Sci., 2000. **25**: p. 677-710.
34. Billmeyer, F.W., *Textbook of Polymer science*. 3nd ed. 1984: Wiley.
35. Patten, T.E. and K. Matyjaszewski, *Atom transfer radical polymerization and the synthesis of polymeric materials.* Adv. Mater., 1998. **10**: p. 901-915.
36. Szwarc, M., *Living polymers.* Nature, 1956. **178**: p. 1168-1169.
37. Kotani, Y., et al., *Living radical polymerization of alkyl methacrylates with ruthenium complex and synthesis of their block copolymers.* Macromolecules, 1996. **29**: p. 6979-6982.
38. Matyjaszewski, K., et al., *Polymers at interfaces: Using atom transfer radical polymerization in the controlled growth of homopolymers and block copolymers from silicon surfaces in the absence of untethered sacrificial initiator.* Macromolecules, 1999. **32**: p. 8716-8724.
39. Fischer, H., *The persistent radical effect: a principle for selective radical reactions and living radical polymerizations.* Chem. Rev., 2001. **101**: p. 3581-3610.
40. Matyjaszewski, K. and J. Xia, *Atom transfer radical polymerization.* Chem. Rev., 2001. **101**: p. 2921-2990.
41. Matyjaszewski, K., et al., *Grafting from surfaces for "everyone": ARGET ATRP in the presence of air.* Langmuir, 2007. **23**: p. 4528-4531.
42. Wang, X.S., R.A. Jackson, and S.P. Armes, *Facile synthesis of acidic copolymers via atom transfer radical polymerization in aqueous media at ambient temperature.* Macromolecules, 2000. **33**: p. 255-257.
43. Tsarevsky, N., T. Pintauer, and K. Matyjaszewski, *Deactivation efficiency and degree of control over polymerization in ATRP in protic solvent.* Macromolecules, 2004. **37**: p. 9768-9778.
44. Galaev, I. and B. Mattiasson, *Smart polymers Applications in Biotechnology and Biomedicine.* CRC Press, 2008.
45. Ratner, B.D., et al., *Biomaterials Science: an introduction to materials in medicine*. 2nd ed. 2004: Elsevier Acad. Press.
46. Mark, J.E., *The use of model polymer networks to elucidate molecular aspects of rubber elasticity.* Adv. Polym. Sci., 1982. **44**: p. 1-26.
47. Flory, P.J. and J. Rehner, Jr., *Statistical mechanics of cross-linked polymer networks. II. Swelling.* J. Chem. Phys., 1943. **11**: p. 521-526.
48. Johnson, B., et al., *Mechanical properties of a pH sensitive hydrogel.* SEM 2002 Annual conference proceedings, 2002.

Chapter 3

Polyelectrolytes

3.1 Introduction

An electrolyte is a compound characterized by having an ionisable group, which can partially or completely dissociate in water forming a cation or anion and an oppositely charged mobile counter-ion [1].

Polyelectrolytes are a class of polymers whose repeating units bear an electrolyte group. The presence of an ionisable group makes the polymer able to be charged and to experience long distance Coulombic interactions. The presence of charges influences the behaviour of this polymer leading to unusual solution properties [2, 3]. The repulsive force developed by close ionisable groups makes the polymer chains stretch and distribute uniformly in the solution as a function of polymer concentration [2].

The presence of charges and mobile counter-ions may influence the swelling behaviour of the brush, because the counter ions can be trapped by the charges on the brush chains creating a higher osmotic pressure than in neutral polymer solutions [4]. When a polyelectrolyte is dissolved in solution, strong attractive forces occur between the ionisable groups and the counter ions. These forces prevent the counter ions from diffusing away and make them partially condense close to the polyion, reducing the effective charge density. The Bjerrum length [2], $l_{i0,}$ is defined as the distance at

which electrostatic interactions between two charges is equal to their thermal motion $\frac{3}{2}k_BT$, where k_B is the Boltzmann constant and T the absolute temperature.

Mathematically this is expressed as:

$$\frac{3}{2}k_BT = \frac{e^2}{4\pi\varepsilon\varepsilon_0 l_{i0}} \tag{3.1}$$

where e represents the single electronic charge (1.6022×10^{-19} C), ε and ε_0 the dielectric constant of the solvent and the permittivity in free space respectively.

In pure water, the Bjerrum length, l_{i0} has a value of 0.7 nm and consequently two charged species, at a distance greater than 0.7 nm, will have substantially reduced electrostatic interactions. When ionisable groups are dissolved in solution they are surrounded or, better said, screened by a shell of counter-ions which reduce the repulsive forces between ionisable groups of the same charge, causing a condensation effect [2].

The Debye length, ζ_B, describes the size of the charge compensation cloud and indicates the distance where the repulsive forces, between ionisable groups and the attractive forces, between ionisable groups and the counter-ions, disappears [5].

In the chapter, shall discuss in more detail the condensation effect, the screening effect and how these properties influence the swelling of polyelectrolytes.

3.1.1 Charge condensation on Rod-like Polyions

The condensation effect of an ionic counter ion on a charged group can be explained by considering a rod-like polymer chain of radius r_0 with a monovalent cation, or an anion, at a distance l_{i0} and with a linear charge density e/l_{i0}. A single monovalent anion is placed at a distance r from the polymer chain with $r > r_0$ [2].

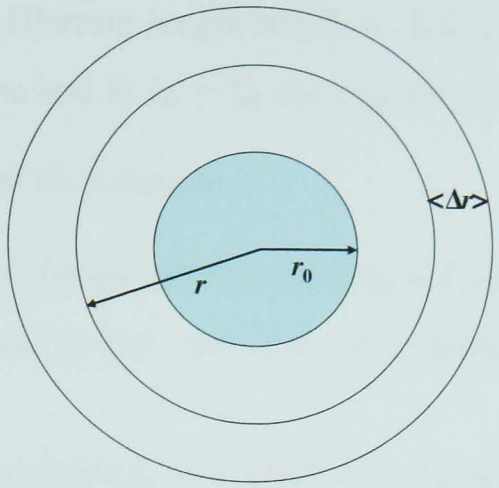

Fig 3.1 Schematic diagram of a rod-like chain cross-section with radius r_0 inside a shell of thickness Δr and radius r.

The potential V of the polymer chain, for a single cation in solution, is given by

$$V(r) = \frac{e}{2\pi\varepsilon\varepsilon_0 l_{i0}} \ln \frac{r}{r_0}. \tag{3.2}$$

It follows that the electrostatic energy of the anion is

$$u_i = -eV(r) \tag{3.3}$$

Considering the free energy associated with the motion of the charges inside the cells, it is possible to recognize the existence of critical distances along the chain l_{i0}, and ζ_B. The latter is the distance between the chain and the counter ion and establishes the condensation of the counter ion on the charged group or its diffusion into solution. Mathematically this value is given by

$$l_{i0} = \frac{e^2}{4\pi\varepsilon\varepsilon_0 kT} = \zeta_B, \tag{3.4}$$

where ζ_B is known as the Bjerrum length which is defined such that, if the distance between the charges on the rod is $l_{i0} > \zeta_B$ the counter ion can diffuse away with a kinetic energy of $\frac{3}{2}k_BT$ into the solution.

If the distance between the charges on the rod is $l_{i0} < \zeta_B$ the counter ion stays in the proximity of the charged group and the phenomena is called counter ion condensation.

The same result has been extended, to a good approximation, considering the more complex situation of a polycation with more than one counter ion.

For $l_{i0} > \zeta_B$ all the counter ions diffuse away into the solution.

For $l_{i0} < \zeta_B$ a fraction of the counter ions remain in proximity of the rod until the effective charge density on the rod amounts to e/ζ_B, the remaining counter-ions diffuse away.

The counter ion can be classified as site-bound if they form a specific ion-pair with the charge on the chain, territorially-bound if they are trapped in the electrostatic potential around the polyion, and as free if they do not have any interaction with the charged group.

The other important parameter in counterion condensation is called the Manning parameter, ξ_M, [6-8] defined as

$$\xi_M = \frac{\zeta_B}{b}, \tag{3.5}$$

where ζ_B is the Bjerrum length and b is the distance between the charges in the chain.

The charge density along the chain in the absence of counter ion condensation is defined as $d_0 = e/b$ but if counter-ions are condensed on the charged groups, the density is reduced to $d_c = \beta d_0$ where β has a value in the range $0 \leq \beta \leq 1$ and represents the fraction of free counter ions.

The Manning parameter [6-8] is related to counter ion condensation through the valence charge of the ions [9]

$$\xi_M < \frac{1}{z_i} \Rightarrow \beta \to 1, \quad d_c = d_0 \text{ and} \tag{3.6}$$

$$\xi_M \geq \frac{1}{z_i} \Rightarrow \beta \to \frac{1}{\xi_M}, \quad d_c = \beta d_0 = \frac{e}{\zeta_B},$$

where z_i is the valence of the i-th ion.

Counter ion condensation is observed for $\zeta_M \geq 1/z_i$, and the threshold condensation decreases with the valence charge of the ions. If multivalent counter ions are present in the solution, they preferentially condense on the charged group and the monovalent ions diffuse away. This phenomenon is favourable because the majority of individual monovalent particles are distributed into solution [10].

3.1.2 The Debye-Hückel theory of charge screening

Charged groups in solution prefer to be surrounded by shells of counter ions to reduce the repulsive force between them [2].

The potential created by an isolated charge in a solution is given by

$$V(r) = \frac{e}{4\pi\varepsilon\varepsilon_0 r}. \tag{3.7}$$

In the presence of multiple ions equation 3.7 becomes

$$V(r) = \frac{e}{4\pi\varepsilon\varepsilon_0 r} \exp - \frac{r}{\zeta_D}, \tag{3.8}$$

where ζ_D represents the Debye screening length [11]. It indicates the length of the counter-ion cloud, i.e. the threshold above which the Coulomb force vanishes.

In the vicinity of the charged group at distance $r << \zeta_D$, the Coulomb potential is active because the charges are not screened, but at distance $r > \zeta_D$ the Coulomb forces vanish rapidly with distance. If salt is added into solution the Debye screening length

decreases and at high salt concentration, the screening effect can be so strong that the polyelectrolyte chains behave as a neutral polymer.

3.1.3 Conformation of a polyelectrolyte chain in solution

The conformation of a neutral polymer in a highly dilute solution is described by the scaling law [12, 13] as:

$R = a_o N^{3/5}$ in good solvent,

$R = a_F N^{1/2}$ in theta solvent.

In the theta solvent, the interaction between the monomer-monomer is the same as the monomer-solvent interaction [14].

The conformation of a polyelectrolyte, in a highly diluted solution is $R \propto N$, assuming that the charged groups are regularly distributed along the chain at a distance l_{i0} with $l_{i0} > \zeta_B$. Under these conditions, the distance between the two ends of the polymer chain (the end-to-end distance), R, is proportional to the degree of polymerisation and in absence of charge screening, the Coulomb forces lead the polymer chains to be stretched [15].

If the concentration of the polyelectrolyte in solution increases, the screening effect starts to show up because of the increased concentration of counter ions and consequently R >> ζ_D >> l_{i0} ($\geq \zeta_B$).

In this condition, the polymer assumes a coiled conformation that depends on the quality of solvent and the concentration of the polymer in solution.

3.2 Osmotic pressure

The osmotic pressure is that which inhibits the flow of liquid (usually water) into a container across a semi permeable membrane. When large molecules are unable to diffuse through the semi permeable membrane, and development of osmotic pressure is observed.

The osmotic pressure of a neutral polymer at low concentrations in the dilute regime is governed by

$$\Pi = kT\frac{c_m}{N}, \tag{3.9}$$

where c_m/N represents the number density of polymer chains.

The situation changes drastically if the polymer is a polyelectrolyte [2]. Assuming that the counter ions are small enough to pass through the semi permeable membrane, the attractive force of the polymer charge groups would not allow their passage in the other compartment for preserving the electro-neutrality of the solution. Consequently, additional osmotic pressure is developed

$$\frac{\Pi}{kT} = \frac{c_m}{N} + \phi_{i0}c_m, \tag{3.10}$$

where ϕ_{i0} is the fraction of charged polymer and c_m the concentration of polymer in solution. The second term, due to presence of the counter ions, is predominant and the following may be assumed

$$\frac{\Pi}{kT} \approx \phi_{i0}c_m. \tag{3.11}$$

If some salt is added to the system, the counter ions start to condense on the charged groups and, when $\zeta_B < l_{i0}$, the free charged ions can pass to the other compartment, until charge neutrality is reached in both sides. At equilibrium, an equal number of positive and negative ions can move in both directions. This well-known phenomenon is called the Donnan effect [2].

3.3 Chemistry of polyelectrolytes

As mentioned at the beginning of this chapter, an electrolyte is defined as any compound that when dissolved in water, is dissociated into ions that conduct electricity [1]. An example is NaCl, which dissociates into Na^+ and Cl^- ions,

$$NaCl \longrightarrow Na^+ + Cl^- . \tag{3.12}$$

Dissociated ions, in solution, are surrounded by water molecules and this process is called hydration. The hydrated ions are able to move in the solution more or less independently and can conduct electricity. A common example of a non-electrolyte is sugar. When dissolved in solution it does not conduct any electricity.
Electrolytes can be divided in two classes:

- Strong electrolytes;
- Weak electrolytes.

Strong electrolytes are compounds that dissociate completely in solution and, consequently, have a high conductivity in solution. All ionic compounds, like salt, are strong electrolytes [3, 16].
Weak electrolytes are compounds with a solute dissociation on the order of 2% in average. An example is the acetic acid that in water is slightly dissociated as

$$CH_3COOH + H_2O \rightleftharpoons CH_3COO^- + H_3O^+ . \tag{3.13}$$

When the solute is dissolved in water, it is dissociated into ions and the reaction 3.12 is shifted to the right. When the concentration of the ions builds up, the ions start to react with each other to form the solute and the reverse reaction occurs. A state of dynamic equilibrium arises when the concentration of the ion is large enough and the rate of the reverse reaction becomes equal to the rate of forward reaction.

In a system under equilibrium, there is a specific relationship between the concentration of the reactants and the products, established by the mass-action expression.

If we have a general chemical reaction at equilibrium:

$$dD + eE \rightleftharpoons fF + gG \tag{3.14}$$

Where D, E, F and G represent the chemical formula and d, e, f and g represent the coefficients, the mass action expression is:

$$\frac{[F]^f[G]^g}{[D]^d[E]^e} = K_c. \tag{3.15}$$

The concentration of the products at equilibrium divided by the concentration of the reactants at the equilibrium, where each concentration is raised to the respective stoichiometric coefficient, gives a constant value called equilibrium constant K_c. The constant K_c is function only of the temperature.

The value of K_c is an important parameter and indicates how far the reaction has proceeded when equilibrium is reached.

The value of K_c also indicates if a compound is a strong or a weak polyelectrolyte. In general if:

- K_c is very large, the reaction proceeds to completion. This is the case for strong polyelectrolytes.
- $K_c \approx 1$ at the equilibrium, the concentration of reactants and products are the same.
- K_c is very small, the reactants are nearly completely non-dissociated. This is the case for weak polyelectrolyte.

3.3.1 Acid and Base

Acid and base compounds are classified as electrolytes because when they are dissolved in water they form ionic species. In the case of acids or bases the reaction with water is an ionization reaction and produces species that conduct electricity. HCl is an example of a strong acid while acetic acid is a weak acid.

Different definitions for acids and bases have been given in the history of chemistry. The first definition was given by Arrhenius, who defined an acid as any substance that, when dissolved in water, releases H_3O^+ ions, while a base was any substance that released OH^- ions when dissolves in water.

$$HCl + H_2O \longrightarrow H_3O^+ + Cl^- \qquad (3.16)$$

when HCl is dissolved in water it releases H^+ ions.

This definition is restrictive because it is relative to the behaviour of the species in aqueous solution. In reality, there are acid-base reactions that occur in solvents other than water or even without solvent, for example, the reaction between the HCl and NH_3 is an acid-base reaction in the gaseous state.

This classification has been changed to a broader one by Brønsted-Lowry, taking in account this exception.

In the Brønsted-Lowry definition, an acid is any species which is a proton donor, and base any species which is a proton acceptor. According with this explanation, the reaction between the HCl and NH_3 in a gas state is an acid-base reaction because HCl is donating a proton to the NH_3 forming the species NH_4Cl.

The Brønsted-Lowry acid-base definition, however, is still not broad enough. There are some other reactions that behave like acid-base reaction but do not involve any proton transfer. An example is the reaction between the NH_3 and BCl_3. The acid/base concept was broadened by Lewis with the definition of an acid is any species that can accept a pair of electrons forming a covalent bond, and base any species able to donate a pair of electrons in the formation of a covalent bond.

3.3.2 A Strong and Weak Acids and Bases

Acids and bases can be classified as weak or strong. Strong acids and strong bases become completely ionized in solution, while weak acids and bases are partially ionized. A way to compare the strength of acids and bases is to introduce the concept of the acid ionization constant and base ionization constant indicated respectively as k_a and k_b.

If we consider the following ionization reaction,

$$HA + H_2O \rightleftharpoons H_3O^+ + A^-, \tag{3.17}$$

at equilibrium the concentration in mol/l of the various species can be related by the mass action law

$$\frac{[H_3O^+][A^-]}{[HA][H_2O]} = K_c. \tag{3.18}$$

For dilute solutions, the concentration of water can be considered constant, and

$$\frac{[H_3O^+][A^-]}{[HA]} = K_c \times [H_2O] = K_a. \tag{3.19}$$

The new constant is called the acid ionization constant, K_a. The same treatment can be done for bases in dilute solution and in this case the constant is defined as the base ionization constant, K_b.

Sometimes the value of K_a or K_b is expressed as pK_a, where $pK_a = -\log K_a$ and pK_b as $pK_b = -\log K_b$.

From the value of the acid ionization constant an acid can be classified:

- $K_a < 10^{-3}$ or $pK_a > 3$ weak acid;
- $K_a = 10^{-1}$ to 10^{-3} or $1 < pK_a < 3$ moderate acid; and
- $K_a > 10^{-1}$ or $pK_a < 1$ strong acid.

We can conclude that the smaller the K_a value or the larger the pK_a value, the weaker the acid. In the case of a base, the smaller the K_b value, the weaker the base.

Another parameter used to compare the strength of acid and base is the percentage of ionization given by

$$percentage\ of\ ionization = \frac{\left[amount\ of\ HA\ ionized\right]}{\left[amount\ of\ HA\ initially\right]} \times 100 \tag{3.20}$$

and is the ratio between the number molecules ionized and the number of original molecules.

This parameter is a function of the dilution of the solution and the temperature.

Another parameter used to compare the strength of an acid or base is the pH.

The pH is defined as

$$pH = -\log\left[H^+\right] \tag{3.21}$$

where $[H^+]$ is the concentration of H^+ ions released from the acid.

In the case of base, $pOH = -\log\left[OH^-\right]$ where $[OH^-]$ is the concentration of OH^- releases from the base when dissolved in water. In general, the pH values are used more often than pOH.

There is a simple relationship that connects the pH with pOH.

$$\left[H^+\right]\left[OH^-\right] = K_w = 1.0 \times 10^{-14} \tag{3.22}$$

Substituting $[H^+]=10^{-pH}$ and $[OH^-]=10^{-pOH}$ and taking the logarithms of both side the relationship becomes

$$pH + pOH = 14, \tag{3.23}$$

which is valid at T=25 °C.

If the $pH < 7$, the solution is acidic; If the $pH = 7$, the solution is neutral; If the $pH > 7$, the solution is basic. The pH is related to the H^+ in that the smaller the pH, the larger the concentration of H^+ ions.

3.4 Polyelectrolyte brushes

The swelling behaviour of polyelectrolyte brushes is more complex than with neutral brushes. The conformation of the chains can be modified by varying the ionic strength, varying the pH, or by applying an external electrical field [17].

In the case of a charged brush, the swelling behaviour is essentially a function of the electrostatic interaction and the osmotic pressure of the counter ions inside the brush.

Polyelectrolyte brushes can be divided into strong or weak polyelectrolyte brushes and they are governed by different swelling models. In the case of strong polyelectrolyte brushes, Pincus [18] presented scaling theories called the osmotic brush regime (OB) in salt-free and in good solvent conditions. In this regime, the height of the brush, h, is calculated by considering the contribution of the repulsive osmotic pressure of the counter ions, tending to swell the chains, and the entropic polymer elasticity, tending to decrease the swelling of the chains. The theory has also been extended to poor solvent conditions and to the quasi-neutral regime, where the excluded volume interaction cannot be neglected. Excluded volume [19] defines the space *effectively* occupied by a macromolecules in dilute solution that cannot be used by another part of the same molecule or other molecule. The excluded volume depends on the energy of mixing of solvent and polymer, and consequently it a function of the quality of the solvent.

3.4.1 Strong polyelectrolyte brushes

The Pincus scaling [18] theory for strong polyelectrolyte brushes is somewhat more simple than the corresponding theory for weak polyelectrolytes but not trivial. So in this section, only the regimes and conclusions will be discussed. Derivations are not therefore included.

In the case of a strong polyelectrolyte, in good solvent conditions and in the absence of salt, the height, h, of the brush is calculated by considering two different situations illustrated in the Fig 3.2.

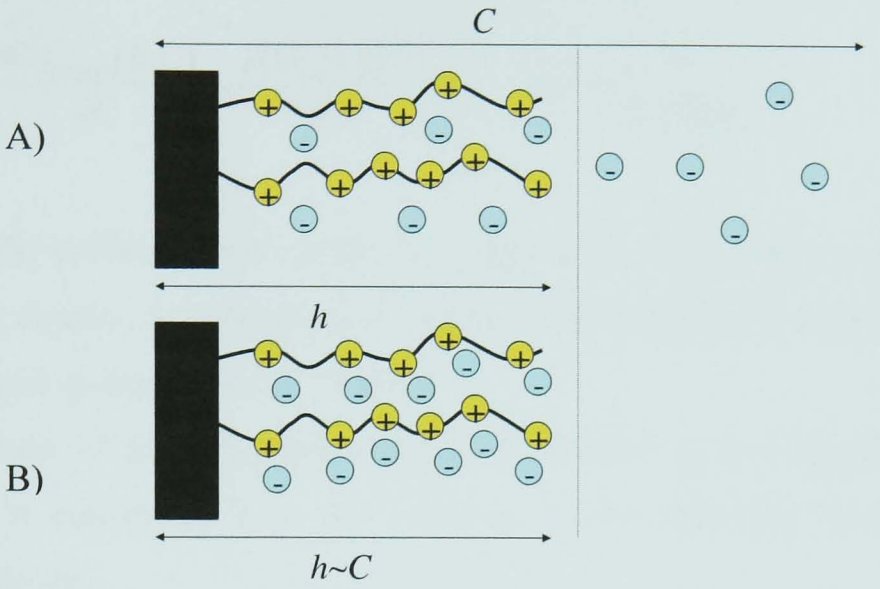

Fig 3.2. Schematic representation of Pincus's model. A strong polycation brush of height h is anchored to a surface. The counter ions inside the container can be at the distance C from the surface where C is defined as the height of the counter ions cloud. A) For $C > h$, a fraction of the counter ions is free to move inside the container. B) For $C \sim h$, the counter ions are trapped by the charge on the brush.

If h represents the height of the brush and C represents the length of the counter ion cloud, then, if $C \approx h$, the counter ions are inside the brush and the system is electro-neutral. If $C > h$ the counter ions are mainly floating in the solution and the brush becomes charged.

a) In the case $C > h$, the total free energy density can be expressed as the contribution of several factors

$$G(h,C) = G_{os} + G^{e} + G_{rep} + G_{st}, \tag{3.24}$$

where G_{os} is the contribution of the osmotic pressure for the counter ions to be a fixed distance C from the surface where the brush chains are attached; G^{e} is the electrostatic contribution due to the charged groups and the counter-ions; G_{rep} represents the repulsion between monomers due to excluded volume and G_{st} is the entropic contribution due to the stretching of the chains.

In order to find the height of the cloud of the counter ions, it is necessary to minimize the free energy with respect to C, which gives [18]

$$\frac{\partial G_{T,brush}(h,C)}{\partial C} = \frac{\partial (G_{os} + G^{e})}{\partial C} = 0 \quad \Rightarrow C \approx \frac{1}{z\zeta_B N f \sigma} \tag{3.25}$$

where the surface charge density is given by $\rho = \sigma N f$, where σ represents the grafting density, N is the number degree of polymerisation and f is the fraction of charged monomers in the brush.

The height of the polyelectrolyte brush, defined as the Pincus height [18], h_{Pincus}, is calculated from the balance of the stretching and electrostatic contributions,

$$\frac{\partial (G_{st} + G^{e})}{\partial h} = 0 \quad \Rightarrow h_{Pincus} \approx N^3 \sigma\, a^2 \zeta_B f^2 . \tag{3.26}$$

An unusual relationship exists between the height of the brush, h, and the degree of polymerisation N where $h \sim N^3$. This means that the brush layer expands faster with the growth of the molecular weight and with the increase of the grafting density σ. The brushes, in this condition, are defined as being in the Pincus brush regime where the major driving force of the system is the attractive energy between charged monomers and counter-ions.

b) If $C \approx h$ the counter-ions are inside the brush and the system can be considered electro-neutral and the electrostatic contribution is not considered in the total free energy of the system. The contribution of the free energy is given by

$$G(h,C) = G_{os} + G_{rep} + G_{st} . \tag{3.27}$$

Two different regimes may be distinguished: the osmotic brush regime and the quasi-neutral brush regime. In the first, the maximum contribution to the

height is given by the balance of the osmotic energy of the counter-ions inside the brush layer and the stretching of the chains.

In this first case, the so-called osmotic brush regime (OB), the minimization of the osmotic and stretching contribution leads to

$$\frac{\partial(G_{os}+G_{st})}{\partial h}=0 \quad \Rightarrow \; h_{osmotic} \approx \frac{Naf^{1/2}}{z^{1/2}} \tag{3.28}$$

where a the Kuhn length and z is the valence of the ion; where the height of the brush is a function of N, the degree of polymerisation, and does not depend on the grafting density.

Another situation whereby $C \approx h$ is known as the quasi-neutral brush regime, where the brushes have a high grafting density which in turn causes a degree of counterions condensation. The height of the brush $h_{q-neutral}$ [20], is due to the balance between the free energy of the excluded volume interactions with the chain stretching energy

$$\frac{\partial(G_{rep}+G_{st})}{\partial h}=0 \quad \Rightarrow h_{q-neutral} \approx Na\left(\frac{\nu\sigma}{a}\right)^{1/3} \tag{3.29}$$

where ν is the excluded volume.

In this quasi neutral regime, the height of the brush has the same dependence on N, ν and σ as a neutral brush.

Pincus theory can be expanded to the case of theta and poor solvents [21]. The dependence of the height of a polyelectrolyte brush is summarised in the table 3.1

Solvent quality	Neutral brush	PE brush
good	$h \approx N\sigma^{1/3}$	$h \approx N$ (OB) $h \approx N^3\sigma$ (PB) $h \approx N\sigma^{1/3}$ (QNB)
theta	$h \approx N\sigma^{1/2}$	$h \approx N\sigma^{1/2}$
poor	$h \approx N\sigma$	$h \approx N\sigma$

Table 3.1 summary of the scaling behaviour of a polymer brush, where (OB) states for osmotic brush, (PB) for Pincus brush, (QNB) for quasi neutral brush.

The Pincus theory, described above, assumes that no salt is added to the system. In general the addition of salt into the system increases the concentration of ions inside the brush, in the species of counter-ions and salts ions. The addition of salt results in more screened charges that results in a decrease in osmotic pressure that leads the brush to de-swell as a function of the concentration of salt in solution. Adding salt to the system changes the profile of a polymer brush from a truncated Gaussian (in the salt free limit), to a truncated parabolic shape, typical for a neutral brush in good solvent conditions [4].

3.5 Weak Polyelectrolyte

The swelling of weak polyelectrolyte brushes is more complex than in the case of strong polyelectrolytes because the number of charges can be varied by external factors like pH and salt concentration and the charges are in dynamic equilibrium with the solution. This means the charges are not fixed but they associate and dissociate with the chain continuously, as mentioned in section 3.3.

The behaviour of a weak polyelectrolyte in a salt solution can be explained in two different regimes: low salt concentration and high salt concentration.

At low salt concentration, the polymer is more charged and the Coulombic forces lead the chain to stretch. In this osmotic regime, the layer thickness $h_{osmotic}$ of the brush is a function of the salt concentration

$$h_{osmotic} \approx N\sigma^{-1/3} n_s^{1/3}. \tag{3.30}$$

Raising the salt concentration leads to the dissociation of further charges, and consequently an increase in the height of the brush.

In the case of high salt concentration, the behaviour of a weak polyelectrolyte is similar to a strong polyelectrolyte. Charges are screened by the ionic particles and the brush layer is collapsed. When the *pH* of the solution is higher than the pK_a, the brush layer behaves like a strong polyelectrolyte. If changing *pH* makes the brush more charged, the thickness of the brush layer increases at any salt concentration.

3.5.1 Polyelectrolyte hydrogels

The most important characteristic of a hydrogel is its ability to change volume, shrinking and swelling under stimuli such as a pH change, change in ionic strength, or the presence of an electric field. Low concentration of monomer, low crosslink density and the presence of charges make this volume transition more pronounced.

In the case of a polyelectrolyte hydrogel in pure water, for each charged group of the polymer there is a counter-ion to keep the system electro-neutral. Thermodynamically, it is favourable that the counter-ions move into the solution to increase the entropy of the entire system but generally few do so because this compromises electro-neutrality of the polymer. The swelling of the hydrogel is dominated by the osmotic pressure due to the counter-ions inside the network and the equilibrium swelling of the hydrogel is reached by the balance between the elastic energy of the network, that decreases, and the osmotic pressure of the ions, which increases [22]. This model is valid in the case of both strong and weak polyelectrolyte hydrogels in salt-free condition.

The swelling behaviour of a hydrogel in salt solution has been described by Flory and is governed by the Donnan effect [23] such that the network behaves as a membrane. The increase in osmotic pressure creates tension inside the network such that it behaves like a series of single chains each with an applied force [24]. Mathematically the free energy of the system is defined as

$$\Delta G_{tot} = \Delta G_{elastic} + \Delta G_{mixing} + \Delta G_{ion}, \tag{3.31}$$

where ΔG_{ion} indicates the free energy charge contribution to the system, in the form of dissociation of the electrolyte group and Coulombic interaction in the system between the free ions inside the network and the dissociated groups in the network. $\Delta G_{elastic}$ is free energy contribution due to the elastic retractive forces acting along the chains and ΔG_{mixing} is the free energy contribution due to the interaction of the polymer chains in contact with the solvent. The repulsive interactions between the charged groups in the polymer chains are neglected because they are assumed to be far apart. ΔG_{ion} is mathematically expressed as [25]

$$\Delta G_{ion} = \Delta G_{dis} + \Delta G_{coul} \tag{3.32}$$

Where ΔG_{dis} is the free energy associated with the dissociation of the charged groups and ΔG_{coul} is the free energy associated with the Coulombic interaction into the system.

The equation can be rewritten in terms of chemical potential

$$\mu_1 - \mu_1^0 = (\Delta\mu)_{elastic} + (\Delta\mu)_{mixing} + (\Delta\mu)_{ion} = 0 \tag{3.33}$$

where μ_1 and $\mu_1{}^0$ are the chemical potential inside and outside the gel respectively and their difference is zero at equilibrium. In the case of a polyelectrolyte hydrogel the solvent inside the network contains ions so we indicate it with μ_1^*. We can substitute the potential as $\mu_1^* = \mu_1$ and so it is required that $\mu_1 - \mu_1^0 = \mu_1^* - \mu_1^0$ and therefore the equation can be rewritten as [23]

$$(\Delta\mu_1^*)_{ion} - (\Delta\mu_1)_{ion} = (\Delta\mu)_{elastic} + (\Delta\mu)_{mixing}. \tag{3.34}$$

Each contribution at the total free energy of the system is given by

$$(\Delta\mu_1^*)_{ion} \approx -\varphi_1 RT\sum_i n_i^* \quad \text{and} \tag{3.35}$$

$$(\Delta\mu_1)_{ion} \approx -\varphi_1 RT\sum_i n_i,$$

where φ_1 is the molar volume of solvent in polymer networks, and $\sum_i n_i^*$ and $\sum_i n_i$ are the concentration of all ionic solutes in the solution and inside the network respectively.

The contribution of the elasticity of the chains to the total free energy of the system is mathematically expressed as

$$(\Delta\mu)_{elastic} = RT\varphi_1\frac{N_c^{gel}}{V_o}\left(\upsilon_2^{1/3} - \frac{\upsilon_2}{2}\right) \tag{3.36}$$

and υ_2 is the volume fraction of polymer in a swollen network, N_c^{gel} is the average number of monomers between crosslinks in a polymer network, and V_0 is the total volume for a relaxed polymer network; this expression is also valid for neutral networks as it contains no charge dependence as shown in equation 2.18.

The changing in chemical potential from the mixing is

$$(\Delta\mu)_{mixing} = RT\left[\ln(1-\upsilon_2) + \upsilon_2 + \chi\upsilon_2^2\right], \tag{3.37}$$

where υ_2 is the volume fraction of polymer, χ is the Flory-Huggins parameter which characterises segment-solvent interactions.

Substitution of these definitions into equation 3.34 in a equilibrium system, (denoted by a subscript *m*), gives

$$RT\sum_i (n_i - n_i^*) = \frac{RT}{\varphi_1}\left[\ln(1-\upsilon_{2m}) + \upsilon_{2m} + \chi\upsilon_{2m}^2 + \varphi_1\frac{N_c^{gel}}{V_o}\left(\upsilon_{2m}^{1/3} - \frac{\upsilon_{2m}}{2}\right)\right] \tag{3.38}$$

where

$$RT\sum_i (n_i - n_i^*) = RT(n_+ + n_- - n_+^* - n_-^*) \tag{3.39}$$

and n_+, n_-, n_+^*, n_-^*, are the concentrations of positive and negative ions inside and outside the network.

If a salt $M_{\nu_+}Y_{\nu-}$ of concentration n_s is added to the solution it will dissociate forming $\nu^+ M^{z+}$ cations and $\nu^- Y^{z-}$ anions; ν^+ and ν^- are the stoichiometric coefficients in the reaction of dissociation of the salt.

For Donnan equilibrium, the concentration of solute in the gel and in the external solution has to be the same, i.e.

$$\frac{n_{neutral}}{n_{neutral}^*} = 1, \tag{3.40}$$

where $n_{neutral}$ and $n_{neutral}^*$ represent the concentration of non-dissociated salt inside and outside the network.

If we consider that weak polyacid network then it dissociates in solution in agreement with

$$\frac{n_{A^-} n_{H^+}}{n_{HA}} = K_a = \frac{[A^-][H^+]}{[HA]}. \tag{3.41}$$

n_+, the concentration of cations inside the network, is given by the product of the concentration of the salt inside the solution and the stoichiometric coefficient for the cation,

$$n_+ = \nu_+ n_{neutral} \tag{3.42}$$

The concentration of anions inside the network is given by

$$n_{-} = \nu_{-} n_{neutral} + \alpha \frac{n_{HA}}{z_{-}}, \tag{3.43}$$

where α is the degree of dissociation of the charged group in the polymer chains and $\alpha\, n_{HA}$ represents the concentration of the ions on the polymer chains.

The expression 3.42 can be combined with 3.43 to give

$$n_{+} + n_{-} = \left(\nu_{+} + \nu_{-}\right)\, n_{neutral} + \alpha \frac{n_{HA}}{z_{-}} = \bar{\nu} n_{neutral} + \alpha \frac{n_{HA}}{z_{-}}, \tag{3.44}$$

where $\bar{\nu}$ is the sum of the stoichiometric coefficients of the dissociation of the salts. The concentration of ions outside the network is given by

$$n_{+}^{*} = \nu_{+} n_{neutral}^{*} \tag{3.45}$$

and

$$n_{-}^{*} = \nu_{-} n_{neutral}^{*}. \tag{3.46}$$

Adding equations 3.45 and 3.46 together follows

$$n_{+}^{*} + n_{-}^{*} = \left(\nu_{+} + \nu_{-}\right) n_{neutral}^{*} = \bar{\nu} n_{neutral}^{*}. \tag{3.47}$$

Introducing the expression 3.44 and 3.47 into the equation 3.39 gives

$$RT \sum_{i} (n_i - n_i^{*}) = RT(n_{+} + n_{-} - n_{+}^{*} - n_{-}^{*}) = RT\left[\frac{\alpha n_{HA}}{z_{-}} - \bar{\nu}\left(n_{neutral} - n_{neutral}^{*}\right)\right], \tag{3.48}$$

which we can then combine with equation (3.38) to obtain

$$\frac{\alpha n_{HA}}{z_-} - \bar{\nu}\left(n_{neutral} - n^*_{neutral}\right) = \frac{RT}{\varphi_1}\left[\ln(1-\upsilon_{2m}) + \upsilon_{2m} + \chi\upsilon_{2m}^2 + \varphi_1 \frac{N_c^{gel}}{V_o}\left(\upsilon_{2m}^{1/3} - \frac{\upsilon_{2m}}{2}\right)\right]. \quad \textbf{(3.49)}$$

To solve this equation we need to apply some approximations. We first consider that the gel has a very small amount of crosslinker and consequently a higher amount of swelling at the equilibrium so $\upsilon_{2m}^{1/3} >> \upsilon_{2m}$ and we can omit the term $\upsilon_{2m}/2$ and the term in the expansion of $\ln(1-\upsilon_{2m})$. The concentration of salt dissolved in solution is small in comparison with the dissociation of the charged groups in the polymer chains $n^*_{neutral} << \alpha n_2/z$ and we can neglect $\bar{\nu}(n_{neutral} - n^*_{neutral})$ where α is the degree of dissociation of the polymer network and n_2 can be defined as $\upsilon_{2m}/V_{monomer}$ where $V_{monomer}$ is the molar volume of the monomer. This approximation leads the equation of the swelling of the hydrogel at equilibrium q_m and is equal to $q_m = 1/\upsilon_{2m}$ given by

$$\frac{\alpha}{q_m z_- V_{monomer}} = \frac{1}{\varphi_1}\left(\chi - \frac{1}{2}\right)\left(\frac{1}{q_m}\right)^2 + \frac{N_c^{gel}}{V_0}\left(\frac{1}{q_m}\right)^{1/3}. \quad \textbf{(3.50)}$$

This equation shows that the degree of dissociation has a strong dependence on q_m [23]

$$\alpha = z_- V_{monomer} q_m \left[\frac{1}{\varphi_1}\left(\chi - \frac{1}{2}\right)\left(\frac{1}{q_m}\right)^2 + \frac{N_c^{gel}}{V_0}\left(\frac{1}{q_m}\right)^{1/3}\right] \quad \textbf{(3.51)}$$

$$= z_- V_{monomer}\left[\frac{1}{\varphi_1}\left(\chi - \frac{1}{2}\right)\frac{1}{q_m} + \frac{N_c^{gel}}{V_0} q_m^{2/3}\right]$$

1. Lewis, R. and W. Evans, *Chemistry.* Palgrave Foundations, 2006.
2. Strobl, G., *The Physics of Polymers.* Springer, 2007.
3. O'Shaughnessy, B. and Q. Yang, *Manning-Oosawa counterion condensation.* Phys. Rev. Lett., 2005. **94**: p. 048302.
4. Galaev, I. and B. Mattiasson, *Smart polymers Applications in Biotechnology and Biomedicine.* CRC Press, 2008.
5. Hinderberger, D., *Polyelectrolytes and their counterions studied by EPR spectroscopy.* PhD Dissertation, 2004, Mainz, Germany.
6. Manning, G.S., *Limiting laws and counterion condensation in polyelectrolyte solutions I. Colligative properties.* J. Chem. Phys., 1969. **51**: p. 924-933.
7. Manning, G.S., *Limiting laws and counterion condensation in polyelectrolyte solutions II. Self-diffusion of the small ions.* J. Chem. Phys., 1969. **51**: p. 934-938.
8. Manning, G.S., *Limiting laws and counterion condensation in polyelectrolyte solutions. III. An analysis based on the Mayer ionic solution theory.* J. Chem. Phys., 1969. **51**: p. 3249-3252.
9. Oosawa, F., *Polyelectrolytes.* Marcel Dekker, NY, 1971.
10. Hinderberger, D., et al., *Electrostatic site attachment of divalent counterions to rodlike Ruthenium (II) Coordination polymers characterized by EPR spectroscopy.* Angew. Chem. Int. Ed., 2004. **43**: p. 4616-4621.
11. Debye, P. and E. Huckel, *On the theory of electrolytes. I. Freezing point depression and related phenomena.* Phys. Z., 1923. **24**: p. 185-206.
12. de Gennes, P.G., *Conformations of polymers attached to an interface.* Macromolecules, 1980. **13**: p. 1069-1075.
13. de Gennes, P.-G., *Scaling Concepts in Polymer Physics*. 1979, Ithaca: Cornell University Press.
14. Jones, R.A.L., *Soft condensed matter.* Oxford University Press, 2004.
15. Volk, N., et al., *Conformation and phase diagrams of flexible polyelectrolytes.* Adv. Polym. Sci., 2004. **166**: p. 29-65.
16. Mansky, P., et al., *Controlling polymer-surface interactions with random copolymer brushes.* Science, 1997. **275**: p. 1458-1460.
17. Barbey, R., et al., *Polymer brush via surface-initiated controlled radical polymerization, synthesis, Characterization, properties, and application.* Chem. Rev., 2009. **109**: p. 5437-5527.
18. Pincus, P., *Colloid stabilization with grafted polyelectrolytes.* Macromolecules, 1991. **24**: p. 2912-2919.
19. Rubinstein, M. and R.H. Colby, *Polymer Physics*. 2003, Oxford: Oxford University Press.
20. Borisov, O.V., T.M. Birshtein, and E.B. Zhulina, *Collapse of grafted polyelectrolyte layer.* J. Physique II, 1991. **1**: p. 521-526.
21. Ross, R.S. and P.A. Pincus, *The polyelectrolyte brush: poor solvent.* Macromolecules, 1992. **25**: p. 2177-2183.
22. Flory, P.J. and J. Rehner, Jr., *Effect of deformation on the swelling capacity of rubber.* J. Chem. Phys., 1944. **12**: p. 412-414.
23. Flory, P.J., *Principles of Polymer Chemistry*. 1953, Ithaca: Cornell University Press.
24. Skouri, R., et al., *Swelling and elastic properties of polyelectrolyte gels.* Macromolecules, 1995. **28**: p. 197-210.
25. Riska, J. and T. Tanaka, *Swelling of ionic gels-quantitative performance on the Donnan theory.* Macromolecules, 1984. **17**: p. 2916-2921.

Chapter 4

Experimental techniques

4.1 Introduction

Material preparation and experimental techniques are presented in this chapter. The chapter is divided into two main parts: material preparation, which concerns the synthesis of the brush, the thin hydrogel film, and the polyacid hydrogel; and the experimental techniques, used to characterize the individual components and the adhesion of the hydrogel in contact with the brush/hydrogel thin film.

4.2 Sample preparation

ATRP (atom transfer radical polymerisation), presented in the previous chapter, has been used for the synthesis of the poly[2-(dimethylamino)ethyl methacrylate] (PDMAEMA) brush on silicon wafers and for the synthesis of the random copolymer of 2-(dimethylamino)ethyl methacrylate and benzophenone methacrylate, poly(DMAEMA-*ran*-BPMA); and the random copolymer of 2-(hydroxyethyl methacrylate) and benzophenone methacrylate, poly(HEMA-*ran*-BPMA) polymers. The latter are spin coated on the functionalized silicon wafers and then photo-cross-linked using a UV lamp (Omnicure 1000, 18 W/cm^2).

The polymer brush synthesis by the "grafting from" method constitutes the initiator deposition on the silicon wafer and the growth of the brush on the surface.

The poly(methacrylic acid) (PMAA) hydrogel was synthesised by free radical polymerisation.

4.2.1 ATRP initiator deposition on a silicon wafer

The silicon wafers, purchased from Prolog Semicor and used as substrates, have the following characteristics: diameter 50 mm, type dopant p-type boron, orientation (100) ± 1 degree, thickness 4000 ± 50 μm.

The deposition of the initiator layer takes place on a clean hydrophilic surface. For this purpose, the silicon wafers are firstly washed with acetone and toluene. Afterwards, the wafers are exposed for 1 hour to a UV ozone lamp to render the surface hydrophilic.

The initiator is (11-(2-bromo-2-methyl)propionyloxy)undecyl trichlorosilane [1] and is deposited on the hydrophilic silicon surface by the mechanism shown in Fig 4.1

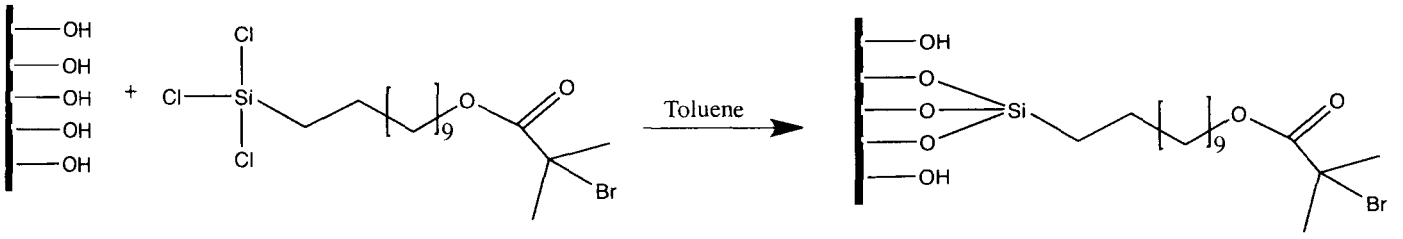

Fig 4.1 Mechanism of the initiator deposition on a hydrophilic silicon wafer.

For performing the deposition, the silicon wafer is placed into a glass vial onto which a lid is tightly sealed. A solution of 1.5 μl ml^{-1} trichlorosilane, in dry toluene is added into the vial and left in the freezer for 6 hours. After the time of reaction, the silicon wafer is removed from the vial and washed with copious toluene and successively dried under nitrogen.

4.2.2 Brush synthesis

The PDMAEMA brush is synthesised using the ATRP reaction by the "grafting from" method. The final brush has a controlled degree of polymerisation and low polydispersity as a consequence of the linear rate of polymerisation. The ATRP reaction includes the use of an initiator with a transferable halogen that, in the grafting from method, is deposited on the silicon surface; a catalyst, composed of an activator metal M^+ with two states of oxidation separated by one electron; a ligand, able to complex the metal; the solvent; and the monomer. In this case, the metal M^{2+} is added in the reaction solution to directly establish an equilibrium between the dormant species, the inactive polymer, and the active species, the living polymer form, and also to reduce the fraction of low molecular weight generated by the termination reaction. The reaction was performed in a tightly sealed 200 ml flask and degassed under nitrogen for 20 min. The reagents are added into the flask in the following order: firstly the species in the solid state, such as catalysts and ligand, and after the liquid products such as the solvent and the monomer.

The solid species, inside the flask, are stirred and degassed for 10 min. Each liquid species is purged for at least 20 min under nitrogen using a spurger and then is added into the flask using a syringe previously purged as well. The monomer is the last product added because, in the absence of oxygen, it can start to homopolymerise. The solution is then left for one hour at room temperature in a nitrogen environment to allow equilibrium formation between the catalyst and the ligand. Afterwards the reaction solution is added to an airtight glass cell, containing the silicon wafer functionalized with the initiator layer. The cell was first degassed for 1 hour and then left to equilibrate at the reaction temperature in a thermal bath. The cell, filled with the solution, is then replaced inside the bath at the right temperature for the reaction time. In an ATRP reaction preparation, the purging process is key and has to be done carefully at all stages.

4.2.3 PDMAEMA brush synthesis

For the preparation of the PDMAEMA brush [2], we used the reagents and quantities shown in Table 1

Reagents	Quantities	
$CuCl_{(s)}$	0.0208 g	0.210 mmol
$CuBr_{2\ (s)}$	0.00137 g	0.0062 mmol
$BPY_{(s)}$	0.075 g	0.4802 mmol
$Acetone_{(l)}$	5.3 ml	0.0722 mol
$Water_{(l)}$	0.5 ml	0.0278 mol
$DMAEMA_{(l)}$	3.6 ml	0.0213 mol

Table 4.1 Reagents used for the synthesis of PDMAEMA brush; Solid and liquid compounds are identified by (s) and (l) respectively.

The copper chloride, CuCl, (Aldrich, 99%), is purified before use. It is stirred overnight in glacial acetic acid, filtered and washed with ethanol and diethyl ether a few times and then dried under vacuum. The copper bromide, $CuBr_2$, (Aldrich, 97%), the 2,2[1]-Bipyridine, (BPY), (Aldrich, 99%), the solvent and DMAEMA (Aldrich, 98%) are used as received. The reaction is performed at 35 °C, which yields a growth rate of 0.27 Å/min. Fig 4.2 illustrates the reaction process,

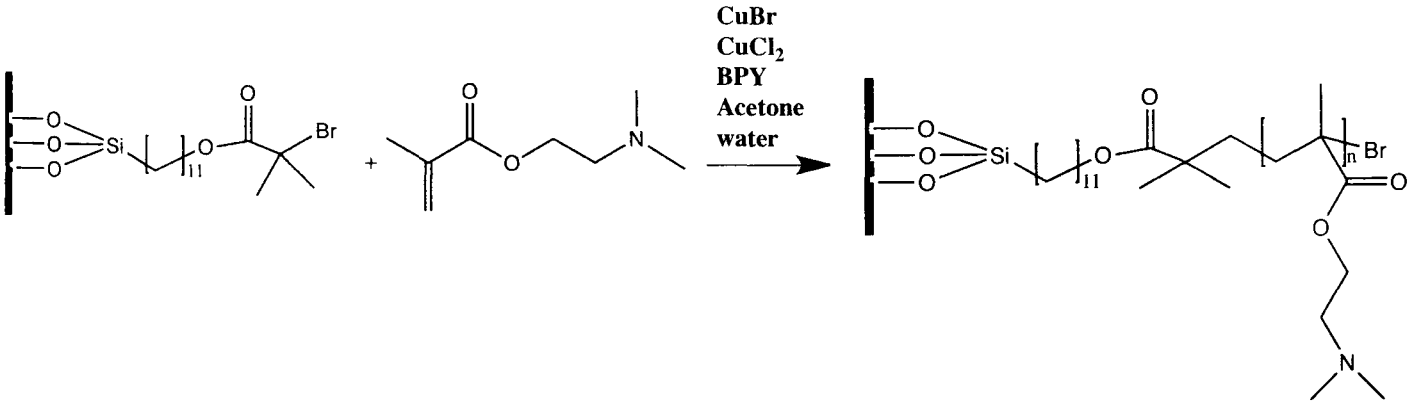

Fig 4.2 Synthetic pathway for the preparation of the PDMAEMA brush [3].

4.3 Synthesis of thin polymer gel films.

Poly(DMAEMA-*ran*-BPMA) and poly(HEMA-*ran*-BPMA) are synthesised using an ATRP reaction. BPMA is a photo-cross-linker agent which, under UV exposure, reacts with the alkyl halide group of the living polymer. In our case, the alkyl halide is the (11-(2-bromo-2-methyl)propionyloxy)undecyl trichlorosilane initiator, that is deposited on the silicon wafer using the procedure explained in section 4.2.1. The poly(DMAEMA-*ran*-BPMA) is dissolved in $CHCl_3$ at a concentration of 6.4 mg ml^{-1} and then spin coated on the modified silicon wafer at a speed of 2000 rpm. The resultant film is cured for 7.5 min by exposing to UV light and is then washed with copious $CHCl_3$.

The poly(HEMA-*ran*-BPMA) is dissolved in methanol at a concentration of 6.4 mg/ml and spin coated on a initiator-coated silicon wafer under the same conditions as the poly(DMAEMA-*ran*-BPMA). After curing, the polymer layer, washed with copious methanol and dried under nitrogen, has a final thickness of 300 Å.

The photo-cross-linker and the poly(DMAEMA-*ran*-BPMA) are synthesised using the procedure described by Huang et al [4].

4.3.1 Synthesis of the BPMA photo cross-linker

For the synthesis of BPMA [4] we used the reagents and quantities, tabulated in Table 4.2:

Reagents	**Quantities**	
4-hydroxybenzophenone$_{(s)}$	20 g	0.1009 mol
triethylamine$_{(l)}$	20 ml	0.1426 mol
Dichloromethane$_{(l)}$ (DCM)	200 ml	3.1202 mol
Methacryloyl chloride$_{(l)}$	11.7 ml	0.1209 mol

Table 4.2 Reagents used for the synthesis of the PBMA photo cross-linker: (s) and (l) indicate solid and liquid compounds respectively.

The reagents were used as supplied.

In a flask, the 4-hydroxybenzophenone (Fluka, 99%) and the triethylamine (Aldrich, 99%) are dissolved in DCM. The methacryloyl chloride (Fluka, 97%) is added drop by drop at 0°C at the concentration of 23% v/v in DCM to the solution which is then left overnight to stir at room temperature. The final mixture is washed with water, a saturated solution of $NaHCO_3$ and NaCl to eliminate any residue of the starting materials. The DCM solution is dehydrated with $MgSO_4$, filtered and then evaporated. The final product is purified by crystallization from n-hexane, dried in vacuum and then characterized by ^1H NMR (300 MHz) in $CDCl_3$ where δ is the chemical shift associated with each peak. The single peak at $\delta = 2.11$ ppm is due to the 3 equivalent protons in the $CH_2=C(CH_3)$ part of molecules while the single peak at $\delta = 5.84$ ppm is associate to the 2 equivalent protons in the $CH_2=C(CH_3)$ part of the molecule. The multiple peaks between δ (7.29-7.92) ppm are due to the 9 protons in the phenyl part of the molecule.

4.3.2 Synthesis of poly(DMAEMA-*ran*-BPMA)

The random copolymer, poly(DMAEMA-*ran*-BPMA), is synthesised using the procedure of Huang et al [4]. The reagents used for this synthesis and their quantities are listed in Table 4. 3

Reagents	**Quantities**	
$CuCl_{(s)}$	0.016 g	0.1616 mmol
$CuCl_{2\ (s)}$	0.004 g	0.0297 mmol
BPMA $_{(s)}$	0.19 g	0.7089 mmol
HMTETA $_{(l)}$	44 µl	0.1617 mmol
Acetone $_{(l)}$	2 ml	0.0272 mol
DMAEMA $_{(l)}$	4.7 ml	0.0278 mol
EBriBu $_{(l)}$	12 µl	0.0818 mmol

Table 4.3 Reagents used for the synthesis of poly (DMAEMA-*ran*-BPMA), indicated with (s) for solid and (l) for liquid compounds.

CuCl is purified as described in section 4.2.3 and $CuCl_2$, DMAEMA, the ligand 1,1,4,7,10,10-hexamethyltriethylenetetramine (HMTETA), (Aldrich, 97%), and the initiator ethyl 2-bromoisobutyrate (EBriBu), (Fluka, 97%), are used as received. BPMA is synthesised as described in section 4.3.1. For the preparation of the reaction solution, the addition of the reagents follows the general method; solid CuCl, $CuCl_2$ and BPMA are added first and following this, in sequence, HMTETA, acetone and DMAEMA are added. The initiator EBriBu is the final compound to be added. The reaction is performed under stirring for 24 h at 50°C. The polymer is dissolved in acetone and then the solution is passed through a neutral alumina column to remove the Cu. The final polymer was obtained by precipitation in n-hexane and dried in vacuum. The ratio of DMAEMA to BPMA in the random copolymer was determined using ^1H NMR in $CDCl_3$ by dividing the area due to the single peak at a chemical shift δ = 4.15 ppm, associated to the two protons of the CO-O-CH_2- part of the PDMAEMA, by the area of the multiple peak at δ between 7.29 and 7.92 due to the 9 protons associated with the phenyl groups of the BPMA. The molecular weight distribution of the poly(DMEAMA-*ran*-BPMA) copolymer was examined using a PL-GPC50 integrated GPC system from Polymer Laboratories. The copolymer was characterized at 30°C using the following GPC set-up: THF eluent containing 2 % v/v triethylamine at a flow rate of 1.0 mL min^{-1}; two 5 μm (30 cm) mixed C columns (sensitive for value of M_W between 200-2,000,000 g mol^{-1}); a WellChrom K-2301 refractive index detector operating at 950 ± 30 nm. Molecular weights were determined using PL Cirrus GPC online software (version 2.0). A series of 10 near-monodisperse linear poly(methyl methacrylate) calibration standards (M_p from 1,280 to 330,000 g mol^{-1}) were purchased from Polymer Labs. The copolymer poly(DMEAMA-*ran*-BPMA) has M_n (average number molecular weight) of 67,300 g mol^{-1} and a M_w (weight average molecular weight) of 82,800 g mol^{-1} and a PDI (polydispersity index) of 1.23. The reaction scheme for the synthesis of poly(DMEAMA-*ran*-BPMA) is shown in Fig 4.3.

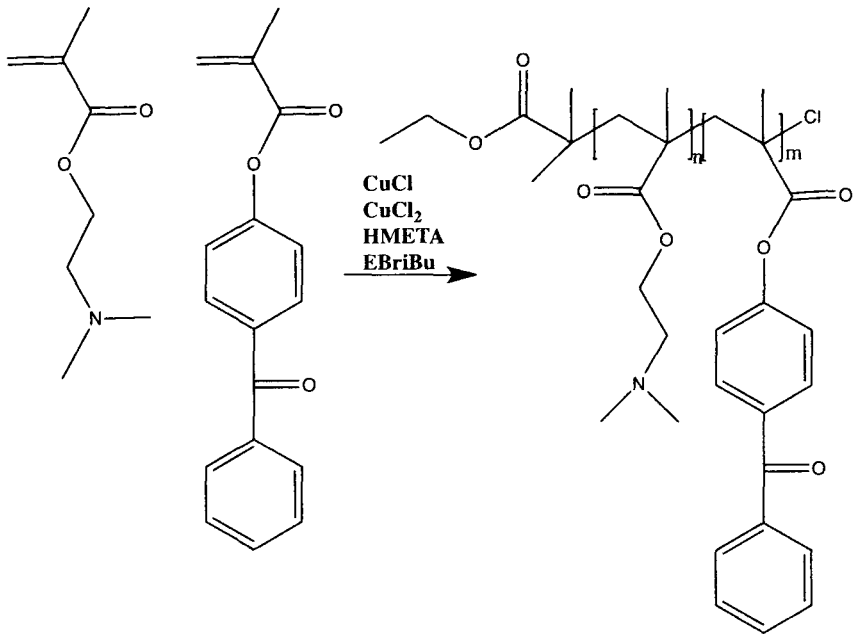

Fig 4.3 Synthetic pathway for the preparation of the poly(DMAEMA-*ran*-BPMA).

4.3.3 Synthesis of poly(HEMA-*ran*-BPMA)

The random copolymer, poly(HEMA-*ran*-BPMA), is synthesised using a modification of the procedure of Huang et al [4, 5]. The reagents and the quantities are listed in Table 4.4

Reagents	Quantities	
CuCl (s)	0.048 g	0.0485 mmol
$CuCl_2$ (s)	0.012 g	0.0892 mmol
BPMA (s)	1.14 g	0.0042 mol
HMTETA (l)	132 µl	0.0485 mmol
Methanol (l)	30 ml	0.7406 mol
HEMA (l)	10.168 ml	0.0488 mol
EBriBu (l)	36 µl	0.2453 mmol

Table 4.4 Reagents used for the synthesis poly(HEMA-*ran*-BPMA) indicating with (s) solid and (l) liquid compounds.

CuCl is purified as explained in section 4.2.3 and $CuCl_2$, the ligand 1,1,4,7,10,10-hexamethyltriethylenetetramine (HMTETA), (Aldrich, 97%), and the initiator ethyl 2-bromoisobutyrate (EBriBu), (Fluka, 97%), are used as received. The monomer HEMA is passed through a neutral alumina column before use. The BPMA is

synthesised as described in section 4.3.1. For preparing the reaction solution, the addition of the reagents follows the general method. The solid CuCl, $CuCl_2$ and BPMA are added at the beginning, thereafter the liquids HMTETA, acetone and HEMA, and finally the initiatior EBriBu are introduced. The reaction is performed under stirring for 48 h at 50°C. The polymer is dissolved in methanol and then to remove the Cu, the solution is passed through a silica gel column. The final polymer was obtained by precipitation in diethyl ether, and dried in vacuum. The ratio of HEMA to BPMA in the random copolymer was determined using ^1H NMR in CD_3OD by dividing the area due to single peak at chemical shift δ = 2.49 ppm, associated to the two protons of the CO-O-CH_2- part of the PHEMA, by the area of the multiple peak at δ between 5.70-6.50 due to the 9 protons associated with the phenyl groups of the BPMA.

The reaction scheme is shown in Fig 4.4

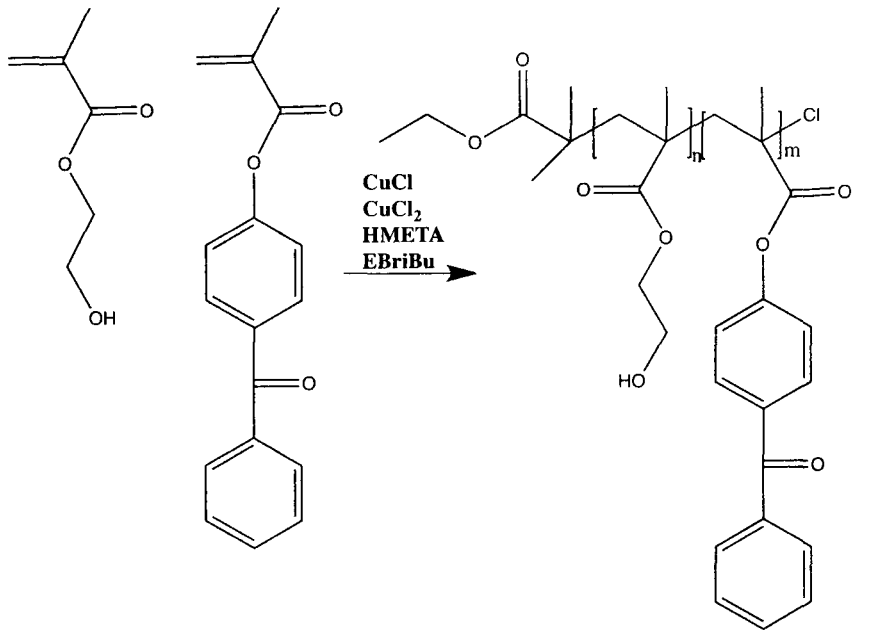

Fig 4.4 Synthetic pathway for the preparation of the poly(HEMA-*ran*-BPMA).

4.3.4 Synthesis of the poly(methacrylic) acid hydrogel

The poly(methacrylic) acid hydrogel, PMAA [6], is synthesised via a free radical mechanism. The reaction is performed in water using 2,2'-azobis(2-methylpropionamide) dihydrochloride (AMPA) (Aldrich, 98%), as initiator and N,N`-methylene bisacrylamide (MBA) (Aldrich, 98%), as cross-linking agent. MAA, (Aldrich, 98%), is distilled under vacuum before use.

The quantities used are listed in Table 4.5.

Reagents	Quantities	
$Water_{(l)}$	144 ml	8 mol
$MAA_{(l)}$	67.7248 ml	0.7985 mol
$AMPA_{(s)}$	1.2913 g	4.7614 mmol
$MBA_{(s)}$	0.9792 g	6.3514 mmol

Table 4.5 Reagents used for the synthesis of PMAA hydrogel indicated with (s) for solid and (l) for liquid compounds.

The reaction solution is prepared by mixing MAA with MBA and water with AMPA. When the two solutions are completely dissolved, they are stirred together for 20 min under nitrogen. After the compounds are dissolved, the solution is transferred to an airtight glass mould and degassed for 1 hour. The reaction is performed for 45 min in a preheated oven at 90 °C. After the reaction is completed, the hydrogels are placed in water and then washed in acid and then under basic conditions to remove any residual starting materials, and finally equilibrated to the required pH.

The PMAA hydrogels are synthesised in two different shapes depending upon the experiments to be performed. For the adhesion experiments, discussed in section 4.4, the hydrogels need to have a hemispherical shape. For this reason, they are synthesised from a glass mould containing 12 hemispherical holes with a radius of 3 mm.

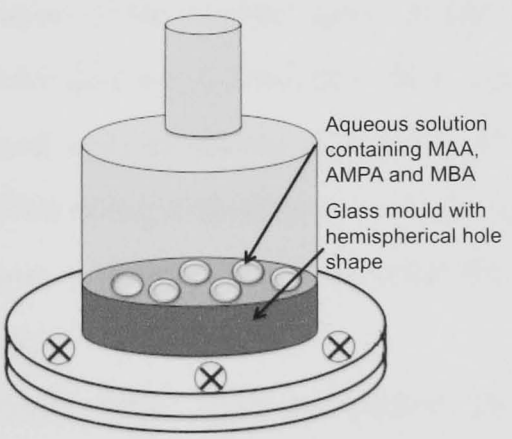

Fig 4.5 Scheme of the mould used to prepare the hemispherical gel shape gels. The aqueous solution of monomer MAA, the crosslinker MBA and the initiator AMPA is added inside the mould. The synthesized hydrogel lenses have a hemispherical shape .

For the neutron reflectivity experiments, the hydrogels are required to have a flat sheet shape. The synthesis is performed on a glass Petri dish of 7 cm radius, and afterwards the gel is divided into disks of 3.5 cm diameter using a metallic cutter. The glass moulds are placed inside a glass bottle sealed with a rubber septum. Fig 4.6 illustrates the reagents for the reaction.

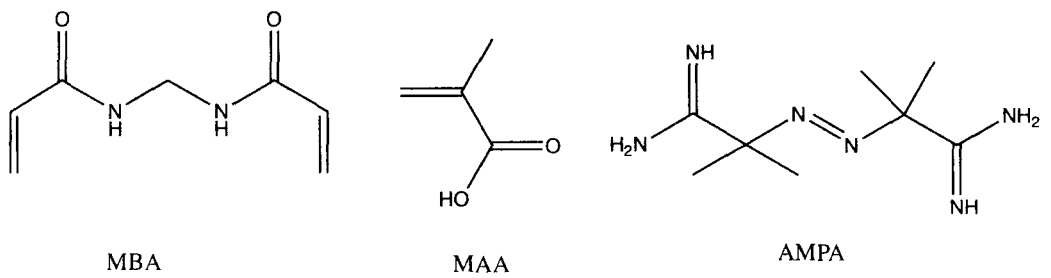

Fig 4.6 Chemical formula of the reagents for the preparation of the PMAA hydrogel.

4.4 Adhesion experiments

To measure the strength of interaction between the polybase or the neutral polymer film in contact with the polyacid hydrogel in aqueous solution, we used a modified JKR set-up. To perform these experiments, the thin films are synthesised on 5 cm diameter silicon wafers and the hydrogel lenses are cast from a glass mould in a hemispherical shape with a diameter of 3 mm. This interaction is quantified using the JKR equation, where the work of adhesion is a function of the radius of the lens, the elastic modulus, the force applied and the radius of contact between the hydrogel and the silicon wafer. The variation of the contact radius is the main measured parameter. These experiments are performed on a modified JKR set up formed using a light source, a camera and a liquid cell, as shown in Fig 4.7. The variation of the contact radius in solution is monitored using a camera and a light source placed either side of the gel. This geometry allows a good contrast between the gel and the water, which have a similar refractive index.

Further adhesion experiments have been performed in the laboratory of Prof. Stanislav Gorb in the Evolutionary Biomaterials Group, Max-Planck-Institut für Metallforschung, Stuttgart. These further experiments consist of the quantification of the total energy necessary to detach the PMAA gel lens from the polymer coated

silicon wafer under aqueous conditions. The experimental set-up will be discussed in section 4.4.2.

4.4.1 JKR set-up

The main set-up consists of a light source, a high resolution Watec CCD camera, (WAT-902 B model), and a liquid cell in which the adhesion experiments are performed. This set-up has been used for measuring the adhesion between the brush and the hydrogel and also for monitoring switchable adhesion as the pH is lowered to 1.The light and the camera are positioned in front of each other either side of the gel so that the variation in contact radius of the gel can be observed.

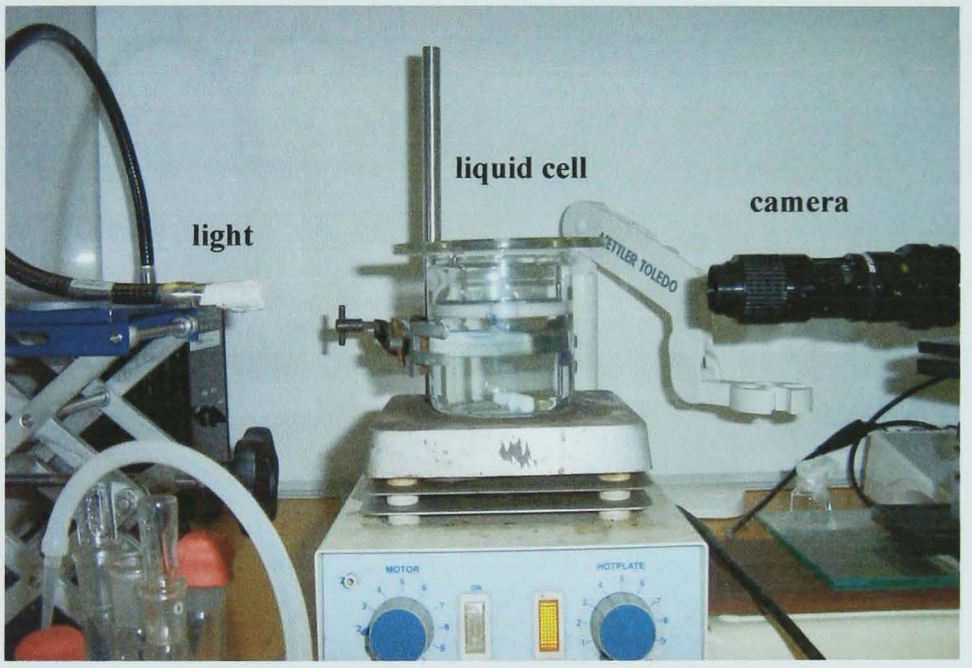

Fig 4.7 Photograph of the set up used to measure the variation of contact diameter between the hydrogel and the polymeric silicon wafer in different pH solutions.

The software Capture Studio Professional v.4.05 is used to collect pictures with the maximum frequency of one frame per second and videos with a frequency of 25 frames per second. The adhesion experiments are performed inside a 300 ml volume glass beaker, placed on a magnetic stirrer.

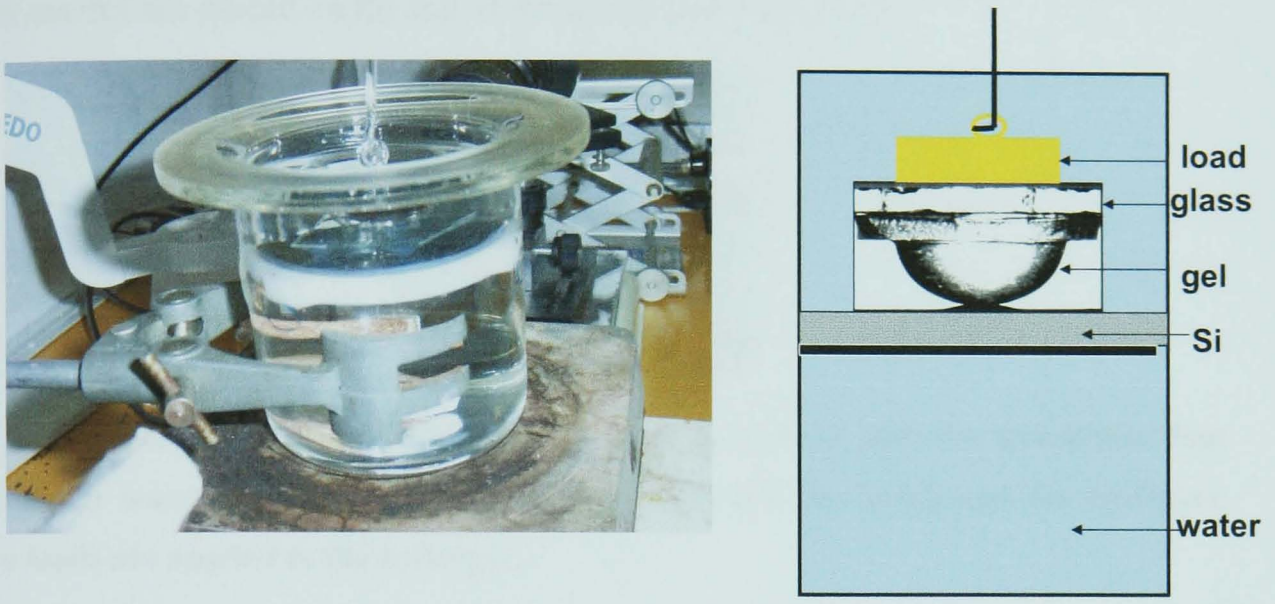

Fig 4.8 Photograph and schematic representation of the liquid cell where the adhesion experiments are performed. The liquid cell has a diamter of 8 cm and a height of 25 cm.

The silicon wafer holder is composed of a PTFE ring pressed against the glass wall of a container at 15 cm from the top. The wafer is placed inside the ring in a way that the centre of the silicon disk corresponds to the centre of the beaker. The container is filled with solution of known pH and the wafer is left to equilibrate for at least 2 hours.

Afterwards, three hydrogel lenses are positioned on a 3 × 3 cm square glass slide, forming a triangle where the total centre of mass of the gels corresponds to the centre of the glass slide (Fig 4.9).

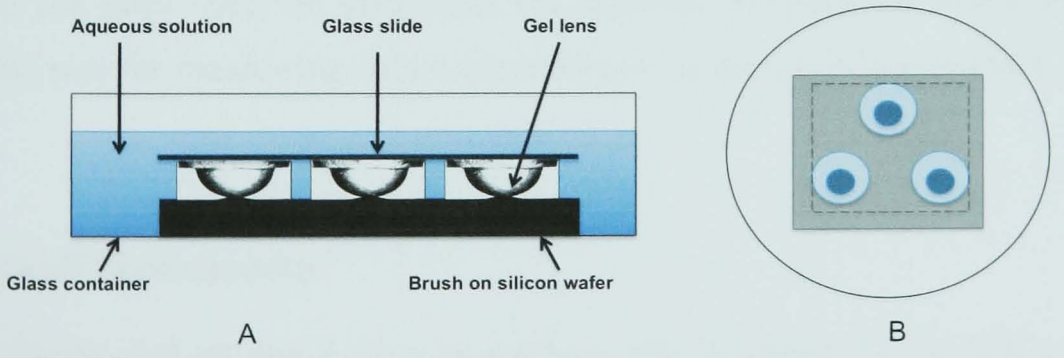

Fig 4.9 Diagram of the liquid cell used to study the adhesion for the brush-gel system. (A) View from the side and (B) view from above.

Using a PTFE frame as a guide, the three lenses, supported by the glass slide, are placed in contact with the silicon wafer in a such way that the glass slide is in the

centre of the beaker. To increase the contact between the hydrogel and the brush, known masses are placed on the top of the glass slide (Fig 4.10).

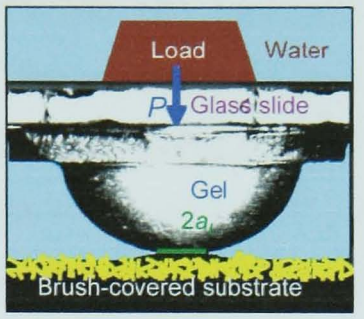

Fig 4.10 Representation of a single hydrogel lens in contact with the brush/thin film layers under water. To increase the interaction between the brush and the hydrogel, known loads are applied to the hydrogel.

The loads are cylindrical PTFE shape with the same diameter of 2.5 cm but different heights from 0.3 cm to 3.9 cm. The loads are added under water and the real force applied (i.e. to correct for buoyancy), is of the order of 20-250 mN, as measured using a dynamometer when the loads are suspended in a water solution. Each load is added on the centre of the glass slide through a Perspex stick connected to the load using the hook – eye system, where the eye is on the top of the load. The load is located on the centre of the glass slide using a passage in the lid of the beaker. This ensures that the load is always in the same place and it yields equally distributed forces on the three gels. The load is applied for 15 min before being removed using the same stick.

The variation of the gel contact radius is monitored with the camera at each stage of the experiment: at the beginning, before the load is applied; then after it is removed. This set-up has been used for measuring the adhesion between the brush and the hydrogel and also for monitoring switchable adhesion as the pH is lowered to 1.

4.4.2 Pull-off experiments

The set-up for the pull off experiments is similar to that described for the JKR work of adhesion experiments. The liquid cell, in which the experiments are performed, is situated between the light and a high resolution camera (Leica M125) and the gel is observed from the side. The liquid cell consists of a 300 ml glass square container where the silicon disk is placed to equilibrate under known pH solution. The disk is placed onto a glass cell of 7 cm diameter and screwed at the side via two glass clamps

to ensure that the wafer is stable during the hydrogel pull-off process. The hydrogel lens is brought in contact to the disk and pulled off by a micromalipulator (World Precision Instruments Model DC300 1R) connected to a 100 g force transducer (World Precision Instruments). The micrometer is set to a velocity of 20 μm/s in both the loading and unloading stages. The hydrogel is mechanically attached to the force tester using a Perspex support to avoid any use of glue that can pollute the samples. The experimental procedure consists of clamping the disk in the glass support and leaving the solution to equilibrate for two hours; after which the hemispherical gel is clamped on the Perspex support and brought into contact with the wafer until the required force, 20 mN, is reached. The gel and the wafer are left in contact for 15 min and then the gel is pulled until it is detached from the surface. These experiments have been performed using different hydrogel cross-linker densities; both brush and polymer gel films.

4.5 Neutron reflectivity measurement: theory, analysis and instrumention.

Neutron reflectometry (NR) is a technique that provides detailed information in the order of molecular dimensions about the structure of the surface, interface and composition of thin films. It can be used to provide information on the thickness, the density and roughness of any layer. Being a non-destructive technique, NR allows the investigation of the behaviour of layers in complex environments such as in liquid cells, cryostats and pressure cells. It is suitable for biological membranes, polymers, proteins, surfactants and is often used as a complementary technique to X-ray reflectivity and ellipsometry, which are more restrictive in their applicability [7]. Important neutron properties are listed in Table 4.6.

Properties	Value
Mass	$1.67\ 10^{-27}$ kg
Charge	0
Spin	1/2

Table 4.6 List of the principle properties of a neutron.

Neutrons have a half life of 1000 seconds as a free particle before decaying into a proton and electron. They scatter via an interaction with the nucleus of the target particle. In a collision process, the elastic scattering occurs when the kinetic energy before the scattering event is the same as that after it, inelastic scattering occurs if the energy is not conserved before and after the scattering event.

As well as treating the neutrons like particles, they should be also be considered as waves obeying the de Broglie law $\frac{h}{\lambda} = mv$, h is the Planck's constant, λ is the wavelength, m is the mass of the particle moving at a velocity v. In a complex system with more scattering centres, the scattering is coherent if the phase of the reemitted signal is correlated to the incident wave, and incoherent if they are not correlated. The process of scattering can be described in quantum mechanics by considering neutron and nucleus wavelength [8]. The wavelength of the neutron is larger than the nucleus that acts as the "scatter point".

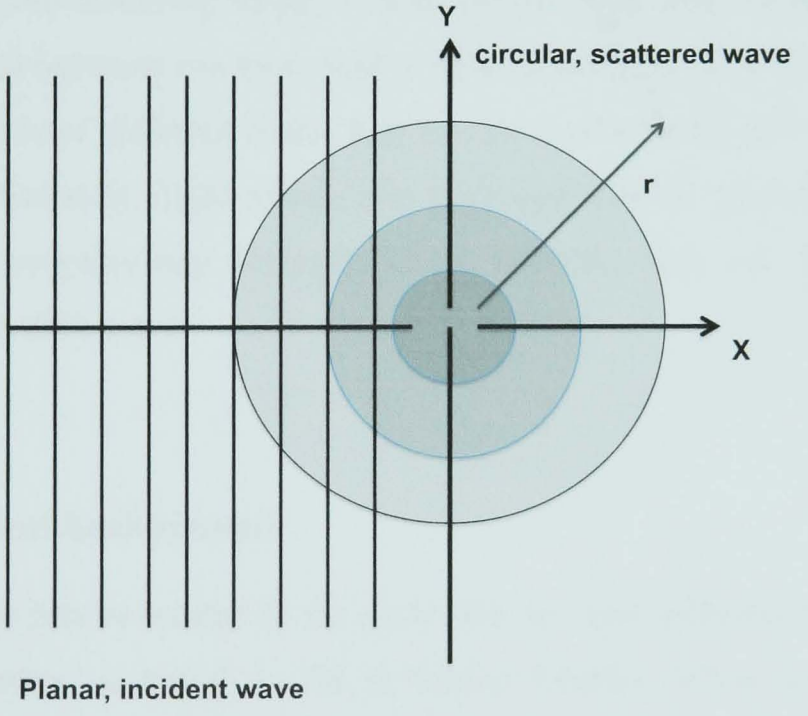

Fig 4.11 Schematic representation of a scattering event.

The scattering between the neutron and the nucleus is a spherically symmetric process and, mathematically, the wave function of the scattered neutron at distance r from the nucleus is described by

$$\Psi_{sc} = -\frac{b}{r}\exp(ikr), \tag{4.1}$$

where k is the wavevector of the incident neutron, b is the scattering length and represents the amplitude of the scattered wave function [9]. The amplitude of the scattered wave depends on the strength of the interaction between the neutron and the nucleus.

The scattering process of a neutron with a single nucleus is related to the cross section of the nucleus, σ, which is the apparent area that the nucleus presents to the neutrons. The scattering length and the cross section are related by

$$\sigma = 4\pi b^2. \tag{4.2}$$

In the case of neutrons, the scattering strength is not related to atomic number, unlike for X rays, but to the scattering length b, that changes apparently randomly across the periodic Table and between isotopes, with several advantages [10]. Firstly isotopes of the same element have different b and they can be used to label part of molecules or different layers. Secondly, light atoms, like hydrogen, can be identified by selective deuteration, and neighbouring elements in the periodic table can be distinguished because they have different b.

4.5.1 Theoretical background

Neutron reflection can be treated in the same way as light reflection but for neutrons "the refractive index" is based on the scattering lengths. When the neutron beam interacts with a surface, part of the beam is reflected and part refracted as a function of the scattering length of the medium and surface. The refracted radiation can interfere in a constructive and destructive manner as a function of the wavelength of the incident beam, incident angle, thickness of the layer and refractive index of the neutron in agreement with Bragg's law,

$$m\lambda = 2dn\sin\theta, \tag{4.3}$$

where m is an integer number with $m \geq 1$, λ is the neutron wavelength, d is the film thickness, θ is the grazing angle, and n is the refractive index of the medium.
In general the refractive index of the material is defined as

$$n = 1 - \delta + i\beta, \tag{4.4}$$

where δ represents the effect of the scattering and β the effect of absorption of the incident beam due to the incoherent scattering. β is normally two orders of magnitude smaller than δ and in most cases it is negligible. δ is defined by

$$\delta = \frac{\lambda^2}{2\pi} N_A \sum_i \frac{\rho_i}{A_i} b_i, \tag{4.5}$$

where ρ represents the density of the component i, with atomic mass A and scattering length b. The term $N_A \sum_i \frac{\rho_i}{A_i} b_i$ represents the scattering length density N_b for the component i. It is defined as the ratio of the coherent scattering length and the specific volume.
In the case of a molecule of density ρ with scattering length b_i and atomic mass A_i for component atom i, we have

$$\delta = \frac{\lambda^2 N_A \rho}{2\pi} \sum_i \frac{b_i}{A_i}. \tag{4.6}$$

Substituting equation 4.6 into equation 4.4, the refractive index is expressed as a function of the scattering length density, neglecting the absorption effect,

$$n = 1 - \frac{\lambda^2 N b}{2\pi} \tag{4.7}$$

The neutron refractive index for most materials is usually slightly less than one because δ is normally in the order of 10^{-6}. Some materials, especially those rich in hydrogen (with $b_i < 0$) have values of $n > 1$. A common example is polyethylene.

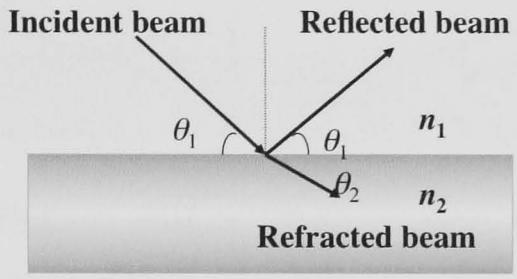

Fig 4.12 Diagram illustrating a beam of incident angle θ_1 that interacts between two media of refractive index n_1 and n_2. Reflection and refraction occur respectively at angles θ_1 and θ_2 .

Considering an interface separated by two media with refractive index n_1 and n_2 and a neutron beam that hits the surface at an angle θ_1,

the refracted angle θ_2 is related to the refractive index of the two media and to the incident angle in accordance with Snell's law

$$n_1 \cos\theta_1 = n_2 \cos\theta_2 . \tag{4.8}$$

This equation gives a real value of angle of refraction if $n_2 > 1$ so that $\cos\theta_2 < \cos\theta_1$ and consequently $\theta_2 > \theta_1$.

If $n_2 < 1$ then $\cos\theta_2 > \cos\theta_1$, and $\theta_2 < \theta_1$; Snell's law gives a real solution only until a critical value of the incident angle θ_c is reached and the incident beam is all reflected at the surface and only an evanescent wave propagates into medium 2.

The value of this critical angle can be approximated as

$$\theta_c = \lambda\sqrt{\frac{Nb}{\pi}} . \tag{4.9}$$

Equation 4.9 shows that the value of critical angle is a function of wavelength of the incident radiation and the scattering length density of the medium through which it passes.

The amount of radiation scattered, when the incident beam hits the surface, is quantified as the difference in the wavevector between the scattered and the incident vector [11].

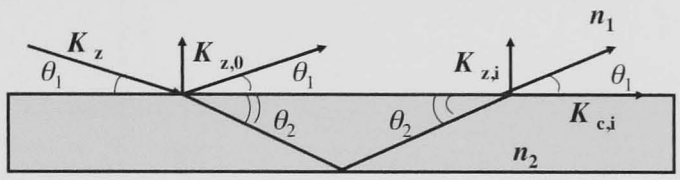

Fig 4.13 Diagram illustrating the incident vector K_z at an angle θ_1 that interacts with media of refractive indexes n_1 and n_2. $K_{z,i}$ represents the projection of the reflected vector from the medium n_2 and $K_{c,i}$ is the total external reflection vector.

In a medium i where, the reflected and incident angles are equal, the final wavevector or final momentum transfer is perpendicular to the surface and is given by

$$k_{z,i} = \sqrt{k_{z,0}^2 - k_{c,i}^2}, \tag{4.10}$$

where $k_{c,i}$ represent the critical value for $k_{z,i}$ below which the total reflection occurs. When total reflection occurs $k_{z,I} = 0$.

In vacuum the wavevector normal to the surface is equal to,

$$k_{z,0} = \frac{2\pi}{\lambda}\sin\theta_1 \tag{4.11}$$

and the momentum transfer is given by

$$\hbar Q_{z,0} = \frac{4\pi\hbar}{\lambda}\sin\theta_1. \tag{4.12}$$

In what follows we shall ignore the $\hbar$ prefactor and refer to $Q_{z,0}$ simply as the momentum transfer, in keeping with common practice in the neutron science community. These equations show that the condition of total reflection can be reached by fixing the value of incident angle θ and changing the value of wavelength λ, or by varying the wavelength λ and keeping θ fixed.

A general neutron reflectivity curve for an interface between two media is shown in Fig 4.14

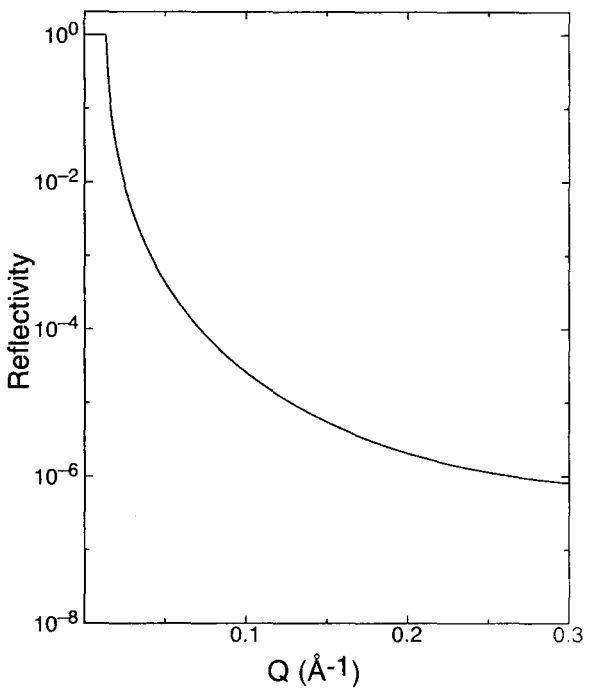

Fig 4.14 Simulated reflectivity as a function of the momentum transfer *Q* for a smooth silicon wafer of roughness 0 Å in contact with D_2O.

The reflectivity is the ratio of the number of reflected neutrons and the total number of neutrons incident on the sample and is generally a function of Q. For $\theta_1 < \theta_c$ the reflectivity has a plateau due to total reflection of the incident radiation, for constant λ. For values of $\theta_1 > \theta_c$, the reflectivity decreases because part of the radiation is refracted inside the second medium. The Fresnel equations define the propagation of the radiation inside media with different refractive indices.

The reflectance or the reflection coefficient of an interface between two media i and $i+1$ is defined by

$$r_{i,i+1} = \frac{k_{z,i} - k_{z,i+1}}{k_{z,i} + k_{z,i+1}}, \tag{4.13}$$

where k_z indicates the z component of the wavevector for the component i and $i+1$.

In the case of a polymer layer in air or in vacuum, $i = 0$ for air and $i = 1$ for polymer layer, the reflectance is

$$r_{0,1} = \frac{k_{z,0} - k_{z,1}}{k_{z,0} + k_{z,1}}. \tag{4.14}$$

The reflectivity R is defined as

$$R = r_{0,1} r_{0,1}^{*}, \tag{4.15}$$

where the asterisk denotes the complex conjugate.

Substituting the equation 4.14 into 4.15 and expressing R as a function of wavevector, then in the case of a sharp interface in contact with air or vacuum, R is given by

$$R_F(k_{z,0}) = \left| \frac{1 - \left[1 - \left(\frac{k_{c,1}}{k_{z,0}}\right)^2\right]^{1/2}}{1 + \left[1 - \left(\frac{k_{c,1}}{k_{z,0}}\right)^2\right]^{1/2}} \right|^2. \tag{4.16}$$

In the limit $k_{z,0} \gg k_{c,1}$,

$$R_F(k_{z,0}) \propto \left(\frac{k_{c,1}}{k_{z,0}}\right)^4. \tag{4.17}$$

Therefore, for a sharp interface, $R_F(k_{z,0})^4$ = constant at high values of $k_{z,0}$. This is known as Porod's law, which is illustrated in the graph shown in Fig 4.15.

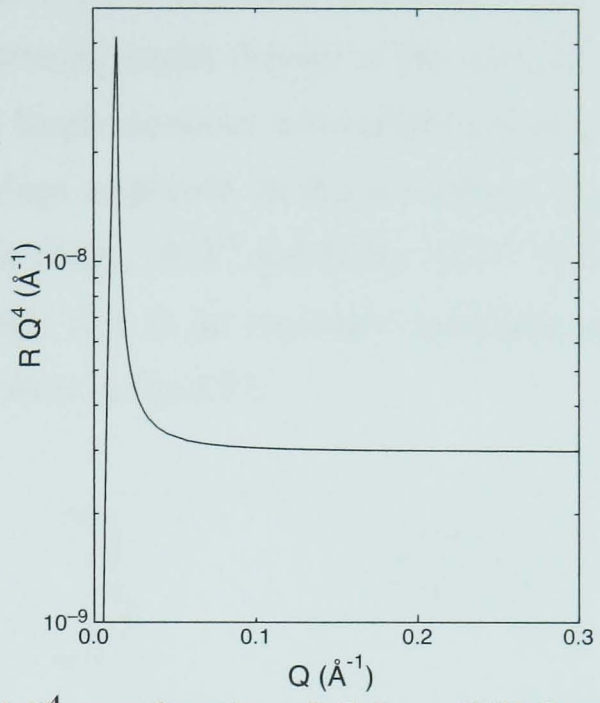

Fig 4.15 The trend of $R\ Q^4$ as a function of Q for a Si/D_2O system; the neutrons are travelling through the silicon so in this case $k_{z,0}$ would refer to the neutron wavevector in silicon and $k_{z,1}$ that for D_20.

The reflectivity of a single polymer film depends on the scattering length density of the polymer and its substrate, the thickness of the layer and the roughness of the layer. The influence of these parameters is illustrated in Fig 4.16, Fig 4.17 and Fig 4.18.

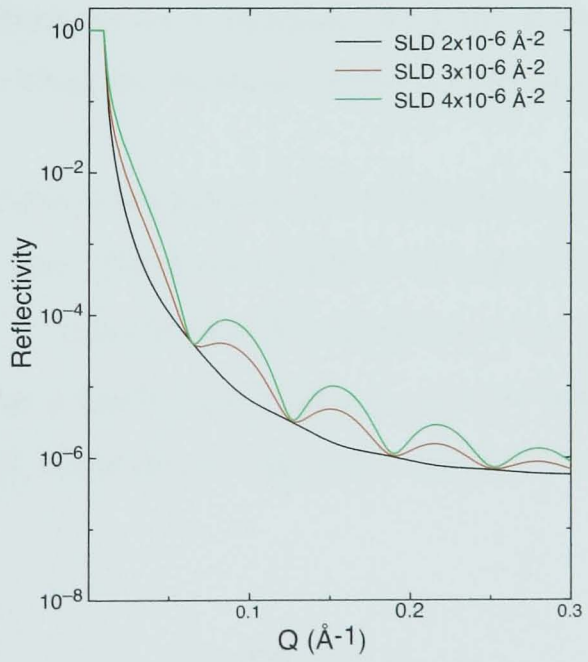

Fig 4.16 Simulated reflectivity for a dry smooth polymer layer of 100 Å covering a silicon wafer, when the scattering length density (SLD) of the polymer is varied. Here the neutrons are propagate through air and are reflected at the silicon wafer.

The reflectivity, of a 100 Å layer deposited on a silicon wafer in a dry state, changes as a function of the scattering length density of the polymer layer because a greater difference in scattering length densities between the polymer film and silicon wafer causes an increase in fringe amplitude. In this simulation, the value of the roughness is taken as to 0 Å and the SLD_{air} =0 $Å^{-2}$ and $SLD_{Si} = 2.07 \times 10^{-6}$ $Å^{-2}$.

The thickness of polymer film is an important parameter, and can also affect the fringe amplitude as we show in Fig 4.17.

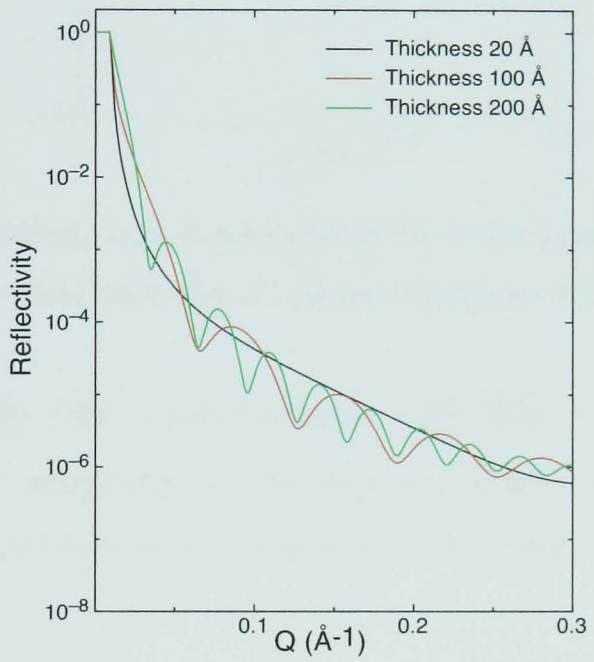

Fig 4.17 Simulated reflectivity as a function of Q for a dry smooth polymer layer covering a silicon wafer, when the thickness of the polymer layer is varied.

Fig 4.17 shows the calculated reflectivity of a deuterated polymer film deposited on a silicon wafer in a dry state. The polymer film is assumed to have no roughness and $SLD_{polymer} = 4 \times 10^{-6} Å^{-2}$. Changing the film thickness causes a variation in the fringe wavelength. In particular a thicker layer has a shorter wavelength then a thinner one. The difference in Q, ΔQ, between two successive minima is related to the thickness of the layer by,

$$d = \frac{2\pi}{\Delta Q}. \qquad \textbf{(4.18)}$$

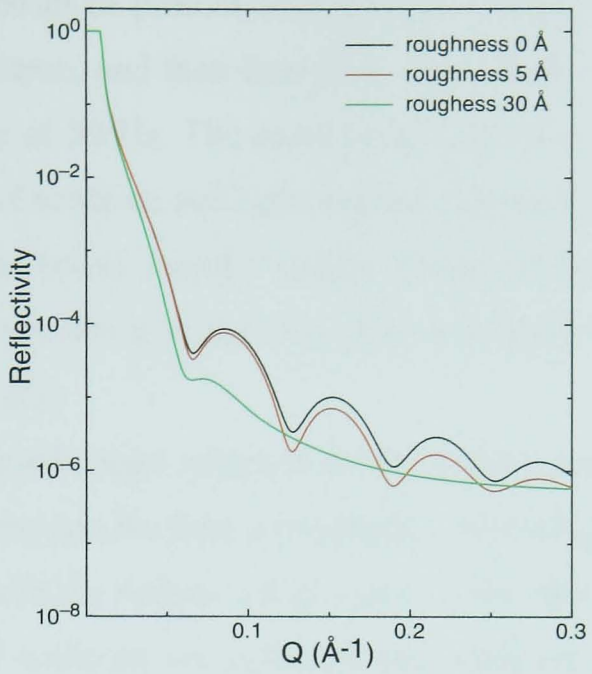

Fig 4.18 Simulated reflectivity as a function of *Q* for a deuterated dry smooth polymer layer covering a silicon wafer, for different values of polymer film roughness.

Fig 4.18 illustrates a dry 100 Å polymer layer with SLD = 4×10^{-6}Å^{-2} on silicon wafer. The increase in roughness of the polymer layer results in a decrease in reflectivity as well as a decrease in the amplitude of the fringe.

4.5.2 Instrumentation

In a reflectometer, it is possible to identify 4 main parts: source, neutron optics, sample holder (goniometer), and detectors.

The neutron source is in general of two types [9]: reactor and pulsed sources. In the reactor source, the neutrons are produced by the fission reaction of ^{235}U nuclei and they have a range of energy of the order of MeV. To slow down their energy, the neutrons are lead inside a moderator filled with liquid H_2, but other moderators are also used. The neutrons interact with the nuclei through inelastic scattering and they equilibrate with a thermal energy equal to the temperature of the moderator. For example, a moderator at the temperature of 290 K slows down the neutrons to a mean energy value of 25 meV and a corresponding neutron wavelength of 1.8 Å. In the case the moderator is filled with liquid H_2, at its temperature of 20 K, the neutrons have a wavelength of 5.3 Å.

In a pulsed source, a beam of protons is accelerated at high energy using a particle accelerator and synchrotron, and then fired to a target made of a heavy metal such as tantalum at a frequency of 50 Hz. The neutrons are produced by a spallation process, which is the emission of neutrons and light nuclear fragments from the violent impact of the protons with the heavy metal nucleus. These neutrons then pass through a moderator that slows them down so that they have a range of wavelengths suitable for the scattering experiments.

To produce the wavelength range required for the experiments, neutrons are selected using filters and choppers and the flux is drastically reduced in this stage.

The neutrons interact with the sample which can be either dry or inside a liquid cell or cryostat. The scattered neutrons are collected and analysed inside a detector which records neutron counts as a function of time. The incident beam is analysed through the use of a detector placed just before the sample, as a reference to normalize the signal that is reflected by the sample. In the time of flight spectrometer, the intensity is measured as a function of the time taken to reach the detector with the chopper triggering the start of the time pulse. The de Broglie equation relates the wavelength of the neutrons with their velocity

$$v = \frac{h}{\lambda m}. \tag{4.19}$$

Neutrons of greater velocity therefore have a shorter wavelength than those at a lower velocity. The velocity is a function of the energy that the neutrons gained in the previous stages. The velocity can be expressed as $L/\Delta t$ where L is the known chopper-detector distance. Rearranging equation (4.19) the time, t, taken from the neutron to traverse a distance L, can be expressed as a function of λ,

$$t = \frac{m}{h} L\lambda. \tag{4.20}$$

4.5.3 Beamlines and set-up

The neutron reflectivity experiments presented in this thesis were performed at the Laboratoire Léon Brillouin (LLB) at Saclay in France and at the Rutherford-Appleton Laboratory, ISIS Chilton, Didcot, in the United Kindom.

The LLB has a neutron reactor source (Orphée reactor), and the experiments have been performed using the EROS time of flight neutron reflectometer, that is presented schematically in Fig 4.19.

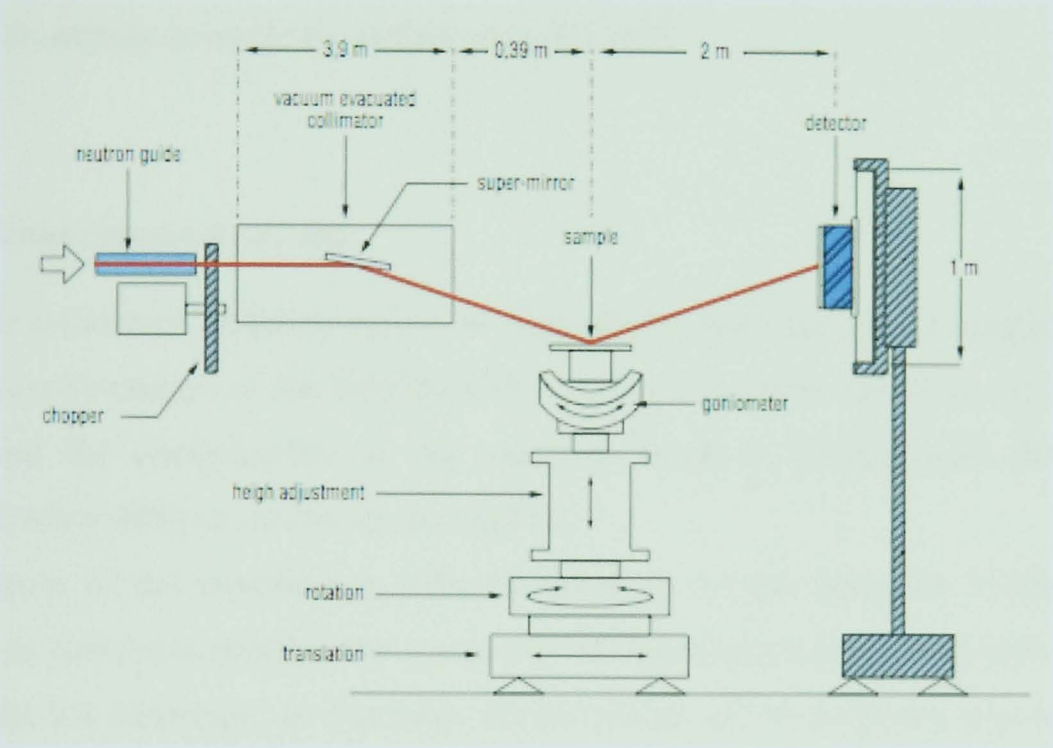

Fig 4.19 Schematic representation of the Eros spectrometer in Saclay, taken from http://www-llb.cea.fr/spectros/pdf/eros-llb.pdf retrieved on 13-12-09.

The neutron beam, coming from the moderator, is passed through a chopper to make the range of neutron wavelengths narrow and is then conveyed to a vacuum collimator of 3.9 m. Inside the collimator, the supermirror reflects efficiently low energy (high wavelength) neutrons. In this way fast unmoderated neutrons will be removed from the beam. The narrow neutron beam passes through slits for further collimation and then hits the sample. The sample is placed on a goniometer which can be adjusted to align the sample for the reflectivity measurements. The sample interface has to be at the right value of height and angle to ensure the specular reflection of the beam where the incident angle and the reflected angle are the same. In this particular reflectometer, the beam has a range of wavelength between 3 and 25 Å and angular

range from 0.1° to 6°, an energy in the range of 0.021 and 1.41 zJ and it can illuminate an area of 2 cm^2, depending on the incident angle.

In ISIS, pulsed neutrons are produced by spallation process between protons and a heavy metal target. The final collimated neutron beam, a "white beam", has a range of wavelength that is measured with a time-of-flight detector. The experiments are performed at a fixed angle and the wavelengths are selected by the chopper. The experiments were performed at the CRISP [12] station that covers a range of wavelength between 1 and 7 Å, the beam has an energy in the range of 1.07-26.29 zJ, and can illuminate an angle dependent area of 2 cm^2.

4.5.4 Experimental set-up.

We have performed different series of experiments with the goal of understanding both the conformation of the PDMAEMA brush and gel film on silicon substrates in water, and the conformation of the polybase brush in contact with the PMAA hydrogel when different pressures are applied.

The purpose of the experiments with the brush in contact with the hydrogel is to emulate as closely as possible the same type of experiments performed with the JKR equipment but observing, in this case, the behaviour of the polybase film instead of the polyacid hydrogel.

All the experiments are performed in an inverted (upside-down) geometry with the interface film/water face down and the neutron beam incident through the sample before being incident on the interface, Fig 4.20.

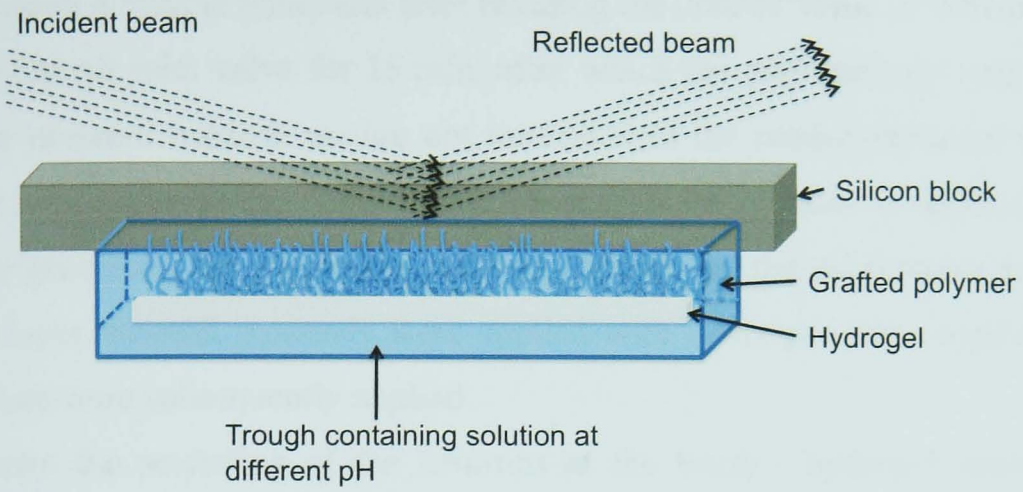

Fig 4.20 Schematic diagram of the liquid cell used to perform the neutron reflectivity experiments .

Each sample is clamped through a rubber ring on a Perspex™ cell. We use Perspex™ because it is a transparent material, which allows us to check the presence of air bubbles on the surface. The polymer/aqueous solution interface requires a large difference in scattering length density to maximize the scattering of the neutrons and increase the signal resolution. For this purpose we take advantage of the difference in scattering length density between H and D, which have essentially the same chemical behaviour. To study the conformation of the brush in different pH environments, D_2O is used for contrast with the hydrogenated polymer on the Si surface. When the brushes are in a collapsed conformation at the interface, the neutrons scatter more than when the brushes are in a swollen state. In the latter situation, D_2O can diffuse into the hydrogenated polymer and the SLD difference decreases at the interface. The experiments are performed starting from a neutral pH solution and, afterwards, in a more acidic pH down to pH 2. After each experiment the Si wafer was removed from the cell, washed, clamped again and equilibrated in the new pH solution for at least 2 hours before performing the next experiment. We checked for equilibration of the samples, by verifying that the neutron reflectivity data did not change with time.

Another set of experiments was performed to study the effect of pressure when the PDMAEMA brushes are in contact with the PMAA hydrogel in pH solution. These experiments were performed in an inverted geometry and the brush sample is clamped via a rubber ring to a Perspex cell and the hydrogel is placed inside that cell on a support connected on its base to an inflatable membrane. The membrane is connected to a pressure scale in the range of 0-500 mBar that measures the force applied at the interface between the hydrogel and the polymer-coated silicon wafer. The pressure is

increased using a bicycle pump and after reaching the desired value, it is held constant by closing the air inlet valve for 15 min, after which the pressure was removed. We release the pressure because we are not interested in the conformation of the brush during the application of the pressure but rather after the pressure is applied. Despite the inverse geometry, the interaction is strong enough that the gel remains attached to the brush layer. Several pressures were applied with lower pressures applied before higher values were subsequently applied.

To maximize the scattering of the neutrons at the brush / hydrogel interface, the brushes are deuterated, while the hydrogel and the water are hydrogenated. This system does not give any total reflection plateau because the neutron pass through the silicon, which have SLD 2.07×10^{-6} Å^{-2}, to the polymer-water mixture, with a SLD of a value less than that of the silicon. Although the polymer is deuterated and hydrated so has in total a neutron refractive index higher than the silicon. In agreement to Snell's law, the refracted angle is always bigger than the grazing one and the condition of total reflection is not reached. For this reason reflectivity data cannot be normalized to a total reflection edge and so require normalization to a sample set with such an edge, like silicon/D_2O.

4.5.5 Analysis

The variation of reflectivity $R(Q)$ derives from the variation of scattering length density at the interface as a function of the distance from the surface. In this project, we study the behaviour of the brush in solution at different pH values and in contact with the hydrogel at different applied pressure. The conformation of the brush is obtained by fitting the neutron reflectivity data using the slab fit program written by Dr Devinderjit S. Sivia (Rutherford Applenton Laboratory) [13]. Slab fit is an *ab initio* program and that searches for a scattering length density profile as a function of the distance from the surface in agreement with the reflectivity data. The density profile is obtained by considering the total polymer film as the sum of uniform layers of material (i.e. slabs) with a constant Gaussian roughness for all the internal layers, and a separate outer and innermost interfacial roughness. The initial parameters are the surface and interfacial roughness, the thickness of the dry layer, and the total thickness of the layer in solution with a tolerance of 10 %. For the first iteration, the

program considers the total film as a single layer and it gives the density profile curve that comes from the fitting of the neutron reflectivity curve. The quality of the fitting of the neutron reflectivity curve is established by the χ^2 parameter, which needs to be minimized. If this condition is not satisfactory (usually $\chi^2 < 1$), the program considers the film to be the sum of two uniform layers with the same total thickness as for the single layer and it varies the thickness of the two slabs with a tolerance of 10 % to improve the fitting quality. If this condition is still not satisfactory, the number of layers is increased up to a maximum of 20 in order to reduce the number of parameters. The interlayer roughness ensures that the volume fraction profile is smooth. It is constant between layers in order to reduce the number of integral fitting parameters. The increase of the number of slabs corresponds to an increase in the number of interfaces inside the polymer layer. The brush density profile also has to have mass conserved. This means that the integral of the brush volume fraction with respect to depth of the layer has to be equal to the thickness of the dry film. If this condition is not valid the fit is discarded. This procedure ensures the best quality fit and a more realistic profile. The profile that best describes the brush conformation, is chosen from the high quality fits that are mass conserved and is taken as the one generally with the fewest slabs.

1. Beers, K.L., et al., *The synthesis of densely grafted copolymers by atom transfer radical polymerization.* Macromolecules, 1998. **31**: p. 9413-9415.
2. Topham, P.D., et al., *Controlled growth of poly(2-(diethylamino)ethyl methacrylate) brushes via atom transfer radical polymerization on planar silicon surfaces.* Polym. Int., 2006. **55**: p. 808-815.
3. Ryan, A.J., et al., *Responsive brushes and gels as components of soft nanotechnology.* Faraday Discuss., 2005. **128**: p. 55-74.
4. Huang, J., et al., *Synthesis and in situ atomic force microscopy characterization of temperature-responsive hydrogels based on poly(2-(dimethylamino)ethyl methacrylate) prepared by atom transfer radical polymerization.* Langmuir, 2007. **23**: p. 241-249.
5. Huang, W.X., *Functionalization of surfaces by water-accelerated atom-transfer radical polymerization.* Macromolecules, 2002. **35**: p. 1175-1179.
6. Crook, C.J., et al., *Chemically induced oscillations in a pH-responsive hydrogel.* Phys. Chem. Chem. Phys., 2002. **4**: p. 1367-1369.
7. Russell, T.P., *X-ray and neutron reflectivity for the investigation of polymers.* Mater. Sci. Rep., 1990. **5**: p. 171-271.
8. Hubbard, A.T., *Encyclopedia of surface and colloid science.* CRC.
9. Squires, G.L., *Introduction to the theory of thermal neutron scattering.* Dover publications, Inc, 1996.
10. *Neutron Training course.* Course Booklet CCLRC, 2006.
11. Russell, T.P., Mater. Sci. Rep. **5**: p. 171-271.
12. Penfold, J., R.C. Ward, and W.G. Williams, *A time-of-flight neutron reflectometer for surface and interfacial studies.* J. Phys. E: Sci. Instrum., 1987. **20**: p. 1411-1417.
13. Geoghegan, M., et al., *The pH-induced swelling and collapse of a polybase brush synthesized by atom transfer radical polymerization.* Soft Matter, 2006. **2**: p. 1076-1080.

Chapter 5

Network-brush interaction

5.1 Introduction

Tuning the interactions between surfaces is an important area of research with technological benefits. Polyelectrolytes are good candidates for this kind of study for their remarkable behaviour [1]. By altering environmental pH, ionic strength, temperature, electric and magnetic fields, polyelectrolytes can undergo conformational transitions, which, if controlled, enable a wide range of applications in such fields of nanotechnology as microfluidics, targeted drug delivery and controlled wetting and adhesion [2, 3].

In our case we are interested in the interaction between a responsive brush polymer grafted on an inorganic substrate and an external medium. In particular, the class of polymer brush that we are studying is a pH responsive polyelectrolyte that can change its conformation as a function of pH and is also characterised by a wettability transition as a function of the pH [4].

The external media that we are considering is a crosslinked polyelectrolyte hydrogel. This kind of gel is elastic and pliable when hydrated and is capable of large deformations in some pH environments. Also, an environmental change from basic to acidic pH induces a physical transition from hydrophobic to hydrophilic behaviour and vice versa in the gel [5].

In the present study we investigate the interaction between poly[2-(dimethyl amino)ethyl methacrylate] (PDMAEMA) brushes, chemically grafted to planar silicon substrates by atom transfer radical polymerisation, with a hydrogel of poly(methacrylic acid) (PMAA) [6]. The polyacid and polybase have similar but opposite behaviour regarding pH responsiveness. In particular, the polyacid hydrogel is in a collapsed state at pH value lower than 5 and in a swollen state at a pH value above 5. The polybase brush, made by the PDMAEMA polymer [7], is stretched at a value of pH below 6 and collapsed at a pH value above 6.

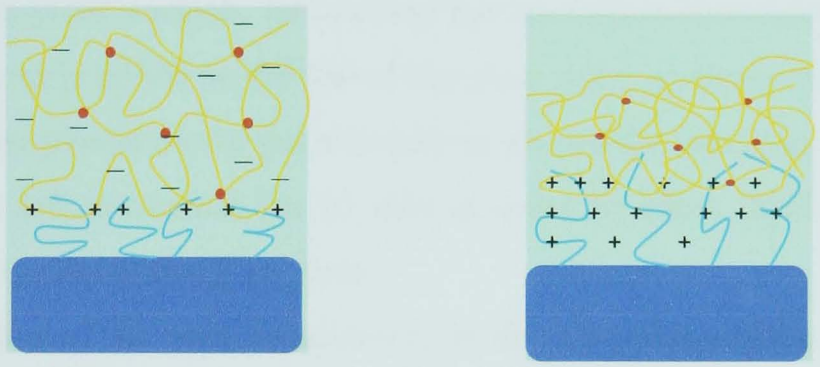

Fig 5.1 Schematic representation of the brush layer in contact with the hydrogel. The brush and the hydrogel adopt opposite conformations in extreme pH environments. In neutral/basic condition, Fig 5.1 A), the brushes assume a collapsed conformation and they are partially charged, while, in the same pH range, the polyacid network mainly is charged. In acid conditions, B), the brush is mainly charged and adopts a stretched conformation. Here the hydrogel is collapsed and is likely to be uncharged or at least weakly charged.

Upon examining the contact between brush and hydrogel at different pH, we recognize a pH region where the brush and gel do not interact with each other, and a region where they interact strongly and it is difficult to remove the gel from the brush without any damage to either or both components.

As a second step we investigated whether the process is switchable, that is whetever, after changing the pH, the brush and gel would come apart without damaging either of the components.

The experimentally observed phenomena that we shall describe in this chapter are:

- at pH less than 2, there is no significant interaction between the brush and hydrogel, whereas above pH 3, there is a strong adhesion which is comparable to that of an epoxy with a silanated glass [8] ;
- the adhesive interaction between the brush and gel above pH 3 can be reversed if immersed in a solution at pH 1 [6].

The silicon wafer covered by a polymer brush film is left to equilibrate for 2 hours in a glass container filled with a known pH solution. Afterwards, three PMAA hydrogel lenses, with a radius of curvature of 3.5 mm, held by a glass slide, are brought into contact with the brush surface. To increase the interaction between the brush and the gel, a known load is added on the top of the glass slide, as shown in Fig 5.9. A lamp and a camera are placed on the gel side and we record the variation of contact radius, *a*. The load is left in contact for 15 min in order to allow equilibration and then removed from the top of the glass slide.

The quantification of the work of adhesion, in the unloading regime, is obtained from the JKR equation [9],

$$W_{adh} = \frac{\left(P - Ka^3/R\right)^2}{6\pi K a^3}, \tag{5.1}$$

where W_{adh} is the work of adhesion, R is radius of the lens, P is the load applied and K is the elastic constant of the system.

We performed the experiments by applying different loads on the gel-brush system and then quantified the work of adhesion in the unloading regime, after removing the load from the top of the glass. The interaction between the brush and the gel has a "pressure effect" that the adhesion energy increases as larger loads are applied and removed. This suggests that probably more than one mechanism is involved in the adhesion process. We therefore hypothesize that the interaction between the brush and hydrogel could be pressure sensitive due to interfacial (e.g. electrostatic) or interdigitation effects. We consider these in turn.

- Interfacial (surface) effect

  The force applied produces an increase in the contact area between the brush and hydrogel, creating more surface available for electrostatic or hydrogen bond

interactions between the amino and carboxylic groups of the polybase and polyacid respectively.

- Interdigitation effect

The Velcro™ [10] effect could be another mechanism involved where the increase in the applied load generates an interdigitation of the brush into the hydrogel.

The actual mechanism could be a mixture of both interfacial and interdigitation effects whose contributions may vary over a range of applied pressures.

To study the pressure sensitive effect between the brush and the hydrogel, we performed some experiments using the JKR set-up and neutron reflectometry. Experimental evidence, explained in this chapter, suggests a larger contribution of the surface effect due to electrostatic and/or polar bonds between proton donor and proton acceptor over the interdigitation mechanism of the brush chains inside the hydrogel.

We discuss in the following order:

- the behaviour of weak polybase brush and PMAA hydrogels in different pH environments;
- the study and quantification of the adhesion between polybase brushes and polyacid hydrogels; and
- the investigation of the mechanism of the interaction.

5.2 Behaviour of the polyacid hydrogel

The polyacid hydrogel is synthesised as explained in chapter 4 in section 4.3.4 and has carboxylic acid as the reactive side group (Fig 5.2).

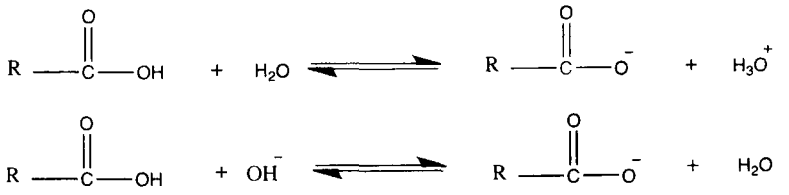

Fig 5.2 Acid/base reaction of the carboxylic acid in water, in acid and in basic conditions

The carboxylic group is a weak acid whose equilibrium between changed and uncharged forms is a function of pH. In acid conditions, the carboxylic group is protonated and the chains are in a "collapsed state" due to the absence of repulsive

forces between the charges. In basic conditions, the carboxylic group becomes more charged as the pH increases; the chains are in a "swollen state" because they absorb water to screen the electrostatic repulsion between the charged groups with the counterions. The swelling behaviour of the polyacid hydrogel is influenced by different parameters such as the pH, the percentage of crosslinker and the ionic strength [5].

In order to quantify the pH dependent swelling of the hydrogels, we performed swelling experiments of a PMAA hydrogel disk, 2 cm in diameter and 5 mm thick, which was allowed to equilibrate at different pH between 2 and 11. The swelling is monitored by the change of hydrogel weight, as a function of pH.

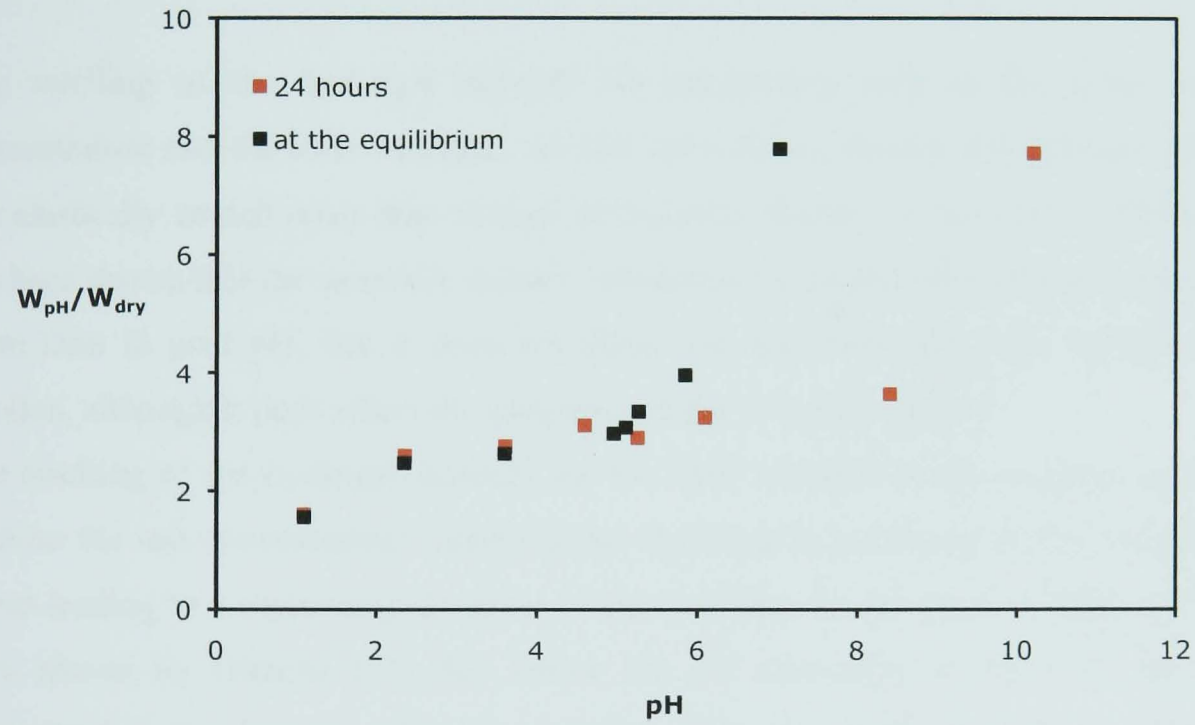

Fig 5.3 The swelling of the gel in pH solution from 2 to 11. When the equilibrium is reached, the PMAA hydrogel shows a sharp transition at pH 5.8 between the collapsed and the swollen state, which is the pH swelling transition.

In acid conditions, the carboxylic groups are mainly uncharged and the swelling of the hydrogel is not drastically influenced by the pH environment; above pH 5.8 the gel starts to swell in increasing amounts with increasing pH. At a pH of 5.8 the swelling transition is observed [4], which characterizes the sharp transition between hydrophobic to more hydrophilic behaviour of the PMAA hydrogel. This phenomenon may be explained considering the reaction of the carboxylic group with

the OH^- ions (Fig 5.2), producing COO^- ions, which create repulsive forces between the chains.

One also has to be aware that the pH is also influenced by side reactions of atmospheric CO_2, dissolved into the water as H_2CO_3 (carbonic acid), which is an acid that reacts with NaOH contributing to lower the pH as shown in Fig 5.4.

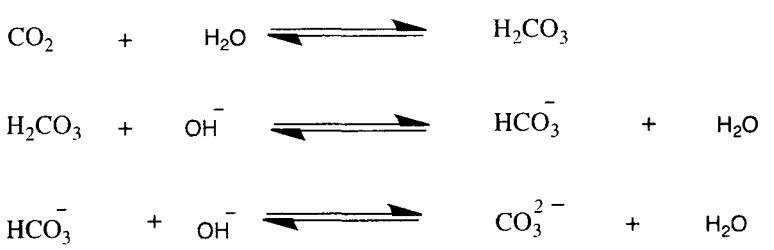

Fig 5.4 Reaction of the CO_2 dissolved in water and in air in basic environments.

The swelling of the hydrogel depends on parameters such as the cross linker concentration and the ionic strength. At low cross linker density the polymer chains can elastically stretch more than at high cross linker density. In the case of PMAA it has been shown that the crosslink density influences the degree of swelling at high pH more than in acid pH, but it does not affect the transition pH from collapsed to swollen, although it does effect the sharpness of the transition [11].

The swelling of the hydrogel depends on the ionic strength of the solution as well, because the salt concentration increases the electrostatic screening of the carboxylic group leading to a monotonic decrease of the swelling. In the case of PMAA, it has been shown by Ostroha [11] that below the pH transition, at pH = 5, for low concentration, the does not effect the swelling. Close to the pH transition, at pH 5.6, the swelling increases with a salt concentration and then decreases. This trend shows that at pH values greater than that of the swelling transition, the electrostatic repulsion between the charged carboxylic groups is more important than the screening of the charges by the salts.

5.3 Behaviour of the polybase brush

The PDMAEMA brush, covering the silicon wafers, was synthesised as described in the previous chapter in section 4.2.2. The amino group, located on the polymer brush side chains, is charged in acid conditions and uncharged in basic conditions [12].

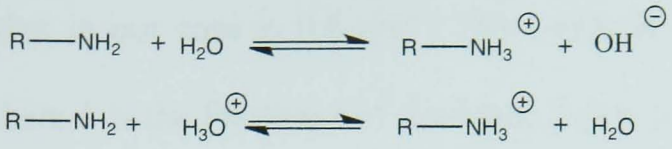

Fig 5.5 Acid/base reaction of the amino group in water, in acid condition and in basic conditions.

This pH transition is macroscopically represented by the hydrophilic to less hydrophilic behaviour of the silicon wafer covered by the PDMAEMA brush in acid and basic conditions; in acid condition the brush assumes a swollen conformation because of the effect of the charge repulsion between the polymer side chains. In basic conditions, the amino group is uncharged and the brush chains are closer to each other, assuming a less swollen conformation. The swelling of the PDMAEMA brush was studied in known pH solution using AFM in contact mode in a liquid cell.

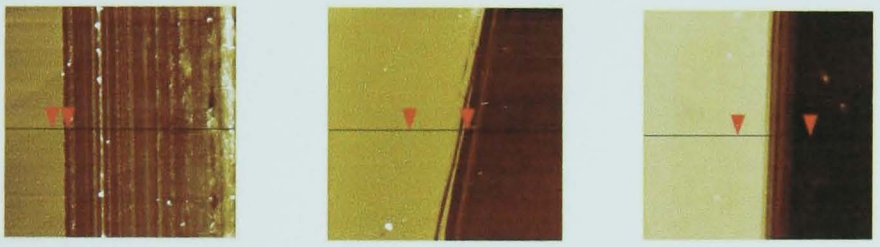

pH	Vertical distance (Å)
dry	230
5.8	414
2	660

Fig 5.6 Section images of a PDMAEMA brush on a silicon wafer A) in the dry state, B) at pH=5.8, and C) at pH 2. The brush surface is scratched using a blade to allow the measurement of the height of the brush relative to the substrate. The red marks are the points where the difference in height between the brush and the silicon wafer is calculated.

The threshold between swollen and collapsed states depends primarily on the grafting density of the brush that in our case is 0.8 nm^{-1}. This value is calculated using the formula $\sigma = \frac{h\rho N_A}{M_w}$ where h is the thickness of the brush layer, ρ is the density, N_A is the Avogadro's number and M_w is the molecular weight of the polymer. To calculate the molecular weight, we added a known amount of the external initiator (ethyl 2-bromoisobutyrate) inside the reaction solution where the silicon wafer covered with the initiator layer is placed to react. We assume that the rate of growth of the brush on the silicon wafer is the same as for the external initiator. The polymer formed was then washed with acetone for the GPC analysis.

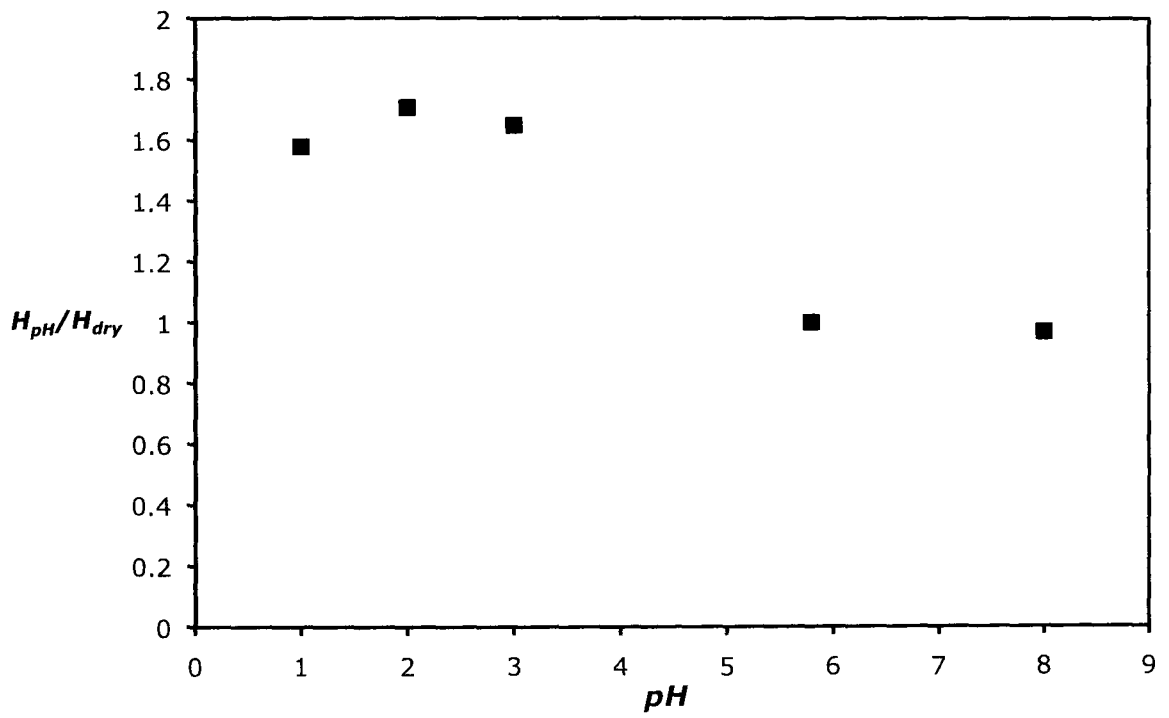

Fig 5.7 The graph shows the swelling of the PDMAEMA brush as a function of pH. The swelling of the brush is calculated as the ratio between the thickness of the polymer layer at the known pH solution, H_{pH} divided by the dry thickness, H_{dry}.

AFM measurements were performed to measure the thickness of the brush in different pH environment (Fig 5.6) and the swelling is calculated as the ratio of the swollen thickness to that in the dry state (Fig 5.7). The PDMAEMA brush is less swollen in basic pH such as pH 5.8 and 8 but it is swollen is acid pH. In acid pH such as pH 1 it is possible to observe a slightly deswelling of the brush layer possibly due to screening of the charges on the brush by the counter ions.

5.4 Thermodynamic work of adhesion

In sections 5.2, we described the behaviour of the brush and the gel by themselves. In this section we shall explain how we quantified the adhesion when the PMAA hydrogel is brought into contact with the PDMAEMA brush.

The work of adhesion has been calculated using a modified JKR set-up described in section 4.4.1. The polybase brushes are equilibrated for two hours in a known pH solution and then three polyacid hemispherical hydrogels, held in place by a glass slide, were added on the brush-coated silicon wafer. The hydrogel is pressed against the brush by adding known loads on the top of the glass and the variation of the contact radius is recorded at the beginning, during and after the loading stage. Specifically, we observe the variation of the contact diameter ($2a$) of the gel with the brush under different loads. We first measure the contact radius when the gel is placed in contact with the brush without any pressure applied. When the load is applied, the contact diameter between the gel and the brush increases, but this decreases again after the load is removed. If the value of the contact diameter after the load is removed is larger than that before the load was applied, we conclude that there is adhesion between the brush and gel. If the value of the contact diameter is the same as at the beginning, there is no adhesion between the brush and the hydrogel.

Upon examining the contact between brush and hydrogel as a function of pH, we observed a region of pH where the brush and gel do not interact, and a region where they interact strongly, which make it very difficult to remove the gel from the brush without damaging the brush or the gel. Fig 5.8 shows the results of a kinetic experiment with the PMAA gel in contact with the brush before, during, and after the application of a load under different pH conditions.

A)

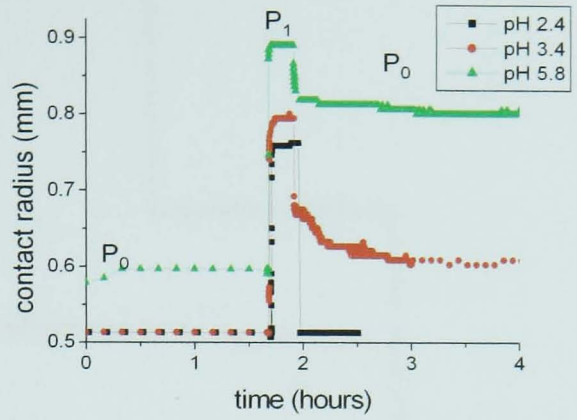

B)

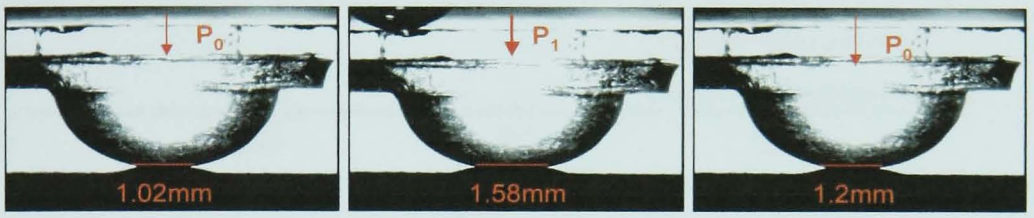

Fig 5.8 A) The variation of the contact radius when the gel is brought into contact with the brush surface and no load is applied (P_0 stage, left), when the load P_1 is added on the top of the glass, when the load P_1 is removed (P_0 stage again, right). B) The variation of the contact diameter in the three situations is shown in the gel pictures. The experiments are performed when the brush and the hydrogel are allowed to equilibrate at pH 2.4, 3.4, 5.8. In B) we show the results for pH 3.4.

If the gel and the brush are equilibrated at pH 2 they do not adhere, i.e. the value of the contact diameter after the load is removed is the same as that before it was applied, showing no adhesion between the brush and the hydrogel. If they are equilibrated at pH 5.8 they adhere very strongly, marked by a large increase in contact diameter after the load is removed than before it was applied; the only way to separate the two components is to tear the brush off the surface, or to rupture the gel. If they are equilibrated at pH 3.4 the final value of contact diameter, after the unloading, is larger than at the beginning but smaller than at pH 5.8. If the two components initially in contact at pH 5.8 (strong adhesion) are equilibrated at pH 1 the gel detaches from the brush without damaging either and the system may be used again.

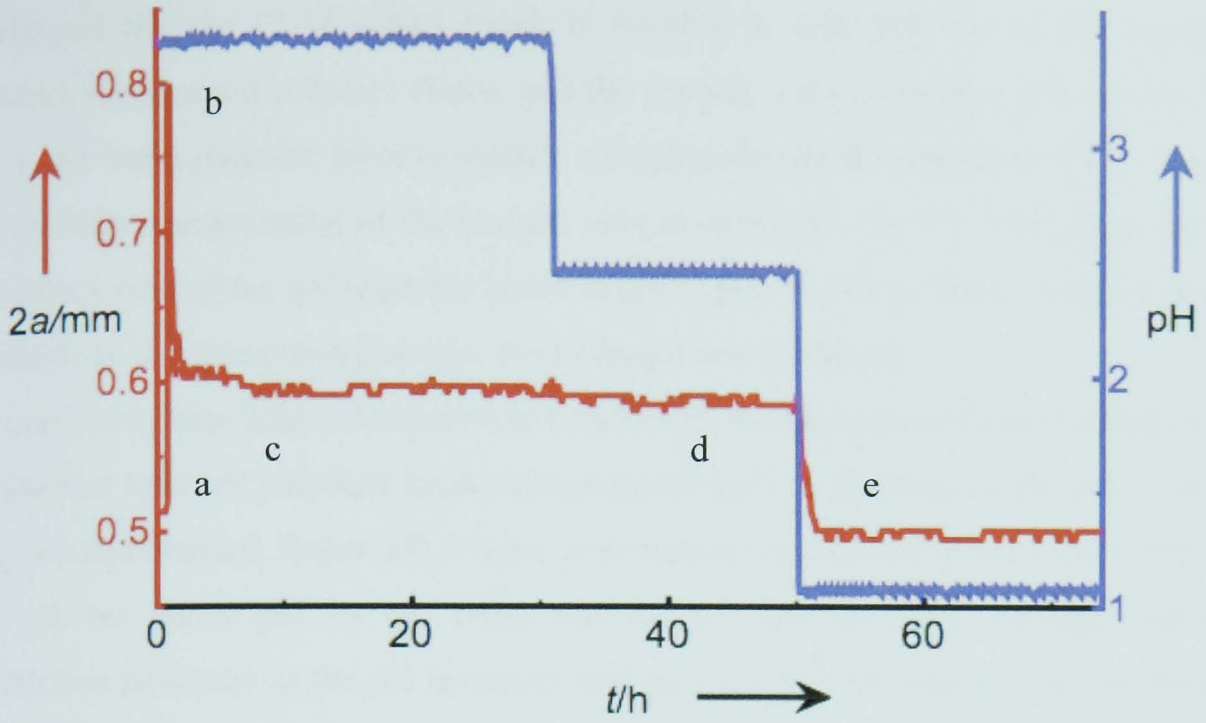

Fig 5.9 Kinetics of the brush and the hydrogel when the pH is lowered. Contact diameter is shown in red and pH in blue. The brush and hydrogel are first equilibrated at pH 3.4; the change in contact diameter is recorded when the brush and hydrogel are brought in contact (a), when the load is applied (b), and successively removed (c). After removing the load, the value of the contact diameter is greater than at the beginning of the experiment but lower than when the load is applied and it is constant after 24 hours. When the pH is reduced from pH 3.4 (c) to pH 2.4 (d), no significant change in the contact diameter is recorded. Then the pH is lowered from pH 2.4 to pH 1 (e), and we observe a decrease in the contact diameter until it becomes comparable to the value of the contact diameter at the beginning. In this situation the brush and the hydrogel can be taken apart without damaging either of the two parts.

Fig 5.9 shows the results of a kinetics experiment of the PMAA gel in contact with the brush after equilibration at pH 3.4. After the load is removed (c), the value of the contact diameter is greater than at the beginning of the experiment (a). Lowering the pH at 2.4 (d) does not change the contact diameter, after 24 hours, even though we know that they do not adhere when applied together at this pH. Detachment of the gel from the brush does however occur at a pH of ~1 (e). In this condition, the brush and the gel can be taken apart without ripping them off and, if they are equilibrated in water, they may be shown to adhere again. To explain the detachment of the gel from the brush at pH 1, we can consider the behaviour of the brush and gel separately in acid pH. The experiments of the swelling of the hydrogel and brush show that the PMAA hydrogel is collapsed in acid pH because the carboxylic group is mainly

uncharged and the PDMAEMA brush is swollen in acid pH, due to the repulsion between the charged polymer chains and the osmotic pressure of the counter-ions. At pH 1, the brush polymer layer is slightly collapsed due to the screening of the charges for the high concentration of the counter ions as shown in Fig 5.7. This suggests that the detachment of the gel from the brush at pH 1 may be due to fewer charged groups available in the interaction between the hydrogel and the brush.

To conclude; these kinetics experiments show that the phenomenological effect of the interaction between polybase brush and polyacid gel is a function of the pH at which they are equilibrated. Below pH 2 there is no strong interaction between the brush and the gel, but above pH 3.4 the brush and the gel interact really strongly and this interaction increases as the pH increases and the only way to separate the two parts is to rip them off. If after the contact, the system is immersed in a solution of acid pH such as pH 1, the brush and the gel can separate without any damage of the two parts, making the adhesion switchable. The brush and the gel sample can be re-equilibrated in solution above pH 2 and they adhere again.

5.5 Quantitative studies of the adhesion

The degree of adhesion in the unloading stage can be measured using the JKR equation, provided we know the contact diameter, the radius of the (gel) lens and the elastic constant of the system. The value of the contact radius in the unloading stage is recorded by a camera while the radius of curvature of the lens is calculated by fitting an image of the gel to the equation for a semi-circle $x^2 + y^2 = R^2$ where x and y are the coordinates of each point and R is its radius (Fig 5.10).

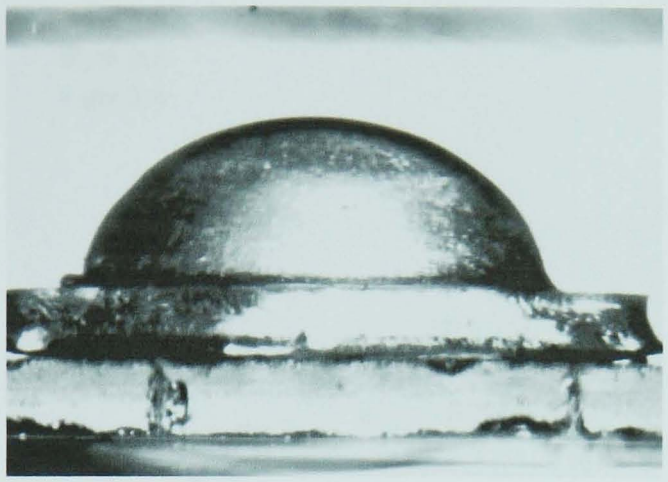

Fig 5.10 Photograph of the gel. The coordinates (in pixels) are fitted to the equation for a semi-circle using Lab view software in order to obtain the radius of the gel. A known reference (3 mm PTFE cylinder) is used for calibration.

The modulus of the gel is a bulk property which depends on its degree of swelling. For this reason, for each pH value studied, the modulus of the hydrogel is calculated by performing the same experiment as for the brush substrate; the hydrogel is brought into contact with an uncoated silicon substrate and the variation of contact diameter a is measured as the applied load P increases. The adhesion between the hydrogel with radius of curvature R and the silicon wafer is negligible and the Hertz equation ($PR = Ka^3$) may used to estimate K in the loading regime (Fig 5.11).

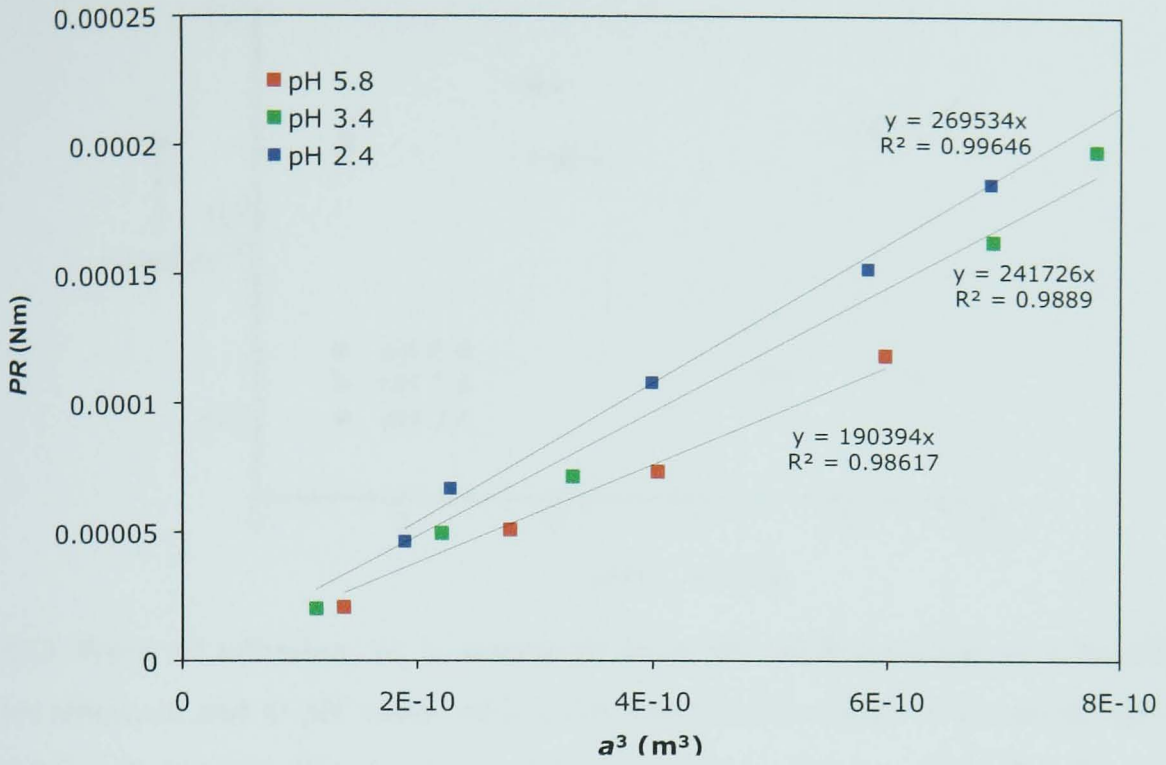

Fig 5.11 Variation of *PR* as a function of a^3 in solutions of pH 2.4, 3.4 and 5.8. The modulus *K* is calculated from the gradient of the linear fits to the data.

The work of adhesion between the brush and the hydrogel is calculated in the unloading regime; when the load is removed, the hydrogel releases parts of the elastic energy, gained from the applied load. Using the JKR equation (equation 5.1), the thermodynamic work of adhesion between the brush and hydrogel is estimated as a function of the pH and the stress applied (related to the load applied). In each case the brushes have a thickness of 200 Å. The PMAA hydrogel is equilibrated in the relevant pH solution before being used for the experiments.

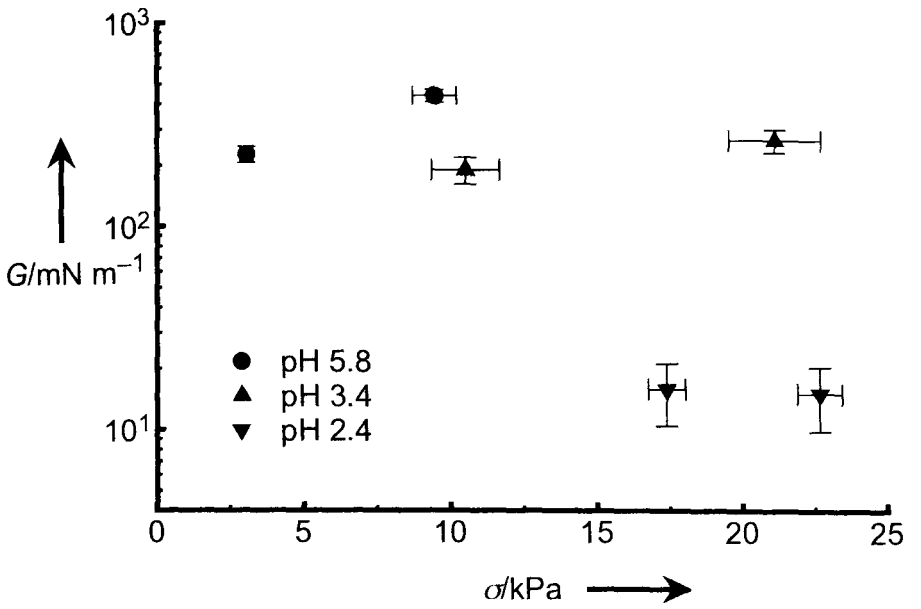

Fig 5.12 Work of adhesion, *G*, is measured from the JKR equation as a function of surface stress, σ, and at pH values of 2.4, 3.4, and 5.8 after loads of 32 and 62 mN were applied for 15 minutes. The dry brush thickness is here ~20 nm, except for the smallest stress (applied at pH 5.8), where the brush is ~16 nm thick.

These experiments show (Fig 5.12) that if a load of 32 mN (the smaller stress point measured at each pH) is applied to the gel/brush system, the calculated adhesion energy increases from 15.9 mJ/m^2 at pH 2 to 170 mJ/m^2 at pH 3 and 226 mJ/m^2 at pH 7. If a load of 62 mN (the larger stress datum measured at each pH) is applied, the adhesion energy increases from 15.2 mJ/m^2 at pH = 2 to 442 mJ/m^2 at pH = 7, varying by a factor of 30. The interaction between the brush and gel at pH 7 and 3 increases with larger loads, although at pH 2 there is no dependence on the applied load because there is no adhesion under that condition. The load dependence means that the adhesion is pressure sensitive; the energy of adhesion increases with load until it is expected to saturate. The data in Fig 5.12 are plotted as work of adhesion as a function of the stress at the maximum contact radius a_{max} given by [13]

$$\sigma(r) = \left(\frac{3KW_l}{2\pi a_{\max}}\right)^{1/2} \frac{1}{\left(1-\frac{r^2}{a_{\max}^2}\right)^{1/2}} - \frac{3Ka_{\max}}{2\pi R}\left(1-\frac{r^2}{a_{\max}^2}\right)^{1/2} \qquad \textbf{(5.2)}$$

This equation is the sum of the tensile stress applied at the edge of the hydrogel and compressive stress applied at the centre of the hydrogel and it has been explained in the chapter 1 in section 1.3.1.

This pressure sensitive behaviour involved the work of adhesion is not constant along the contact area but rather decreases from its centre toward its edges as it has been shown by Silberzan [13]. It is possible therefore that a different mechanism from the interfacial interaction could be involved when a load is applied to the system.

We hypothesize that the pressure sensitive interaction between brush and hydrogel is due to either a surface and/or an interdigitation effect.

- Interfacial (surface) effect

  The applied force produces an increase in the contact area between the brush and hydrogel, creating more surface available for electrostatic or hydrogen bonds between the amino and carboxylic groups of the polybase and polyacid respectively.

- Interdigitation effect

  The Velcro^{TM} [10] effect could be another mechanism involved where the increasing of the applied load generates an interdigitation of the brush into the hydrogel.

The actual mechanism could be a mixture of both an interfacial and interdigitation contribution. We therefore performed some experiments to understand if there is any dominant mechanism in the interaction between the brush and the hydrogel, and we discuss this in the remainder of this chapter.

5.5.1 Kinetics of the gel release

In Fig 5.13 we compare the kinetics of detachment of the brush/hydrogel system equilibrated at pH 3.4, when loads of different magnitude are applied.

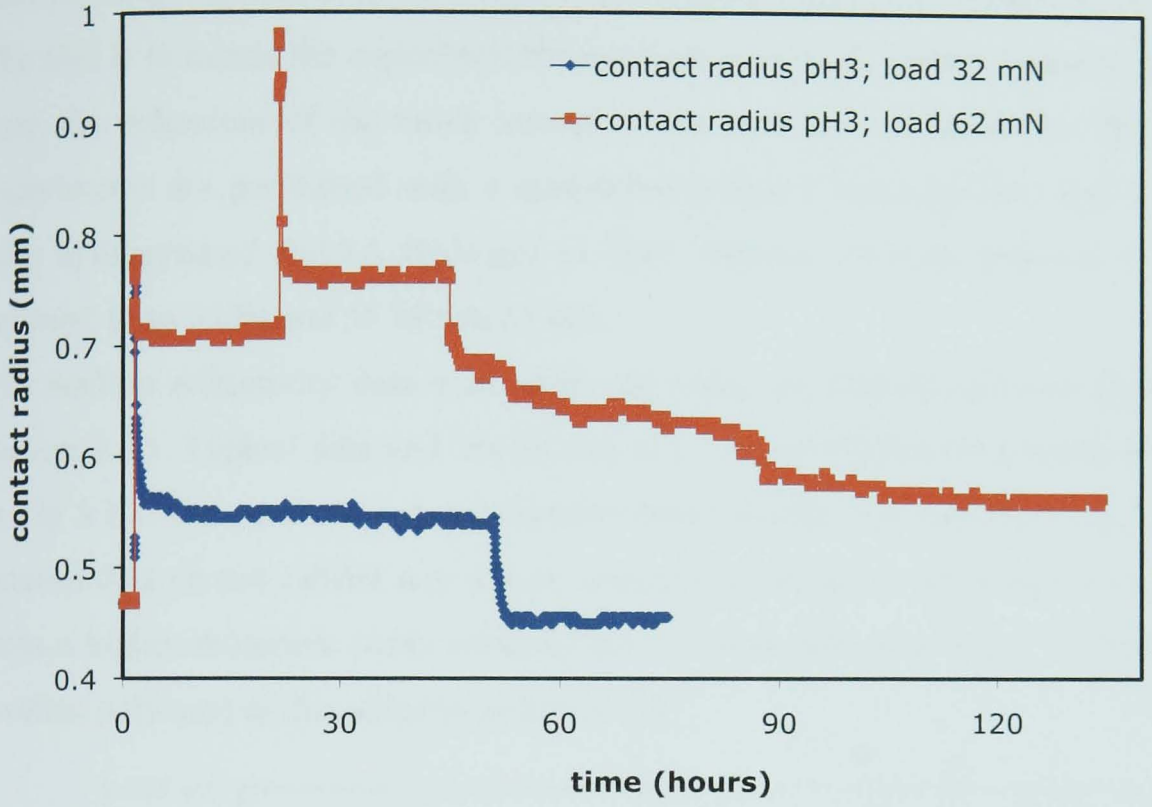

Fig. 5.13 Kinetics experiments were performed to compare the release time of the hydrogel from the surface when a load of 32 mN is applied and when a load of 62 mN are applied on the glass top.

Fig 5.13 shows the variation of contact radius for a gel/brush equilibrated at pH 3.4 when a load of 32 mN and 62 mN are applied to the system. The applied load influences the detachment of the gel from the brush; when a load of 32 mN load is applied, the release time is around 7 hours but, for the 62 mN load, it becomes of the order of days. This behaviour points out that the pressure sensitive effect may influence the gel release time but it does not suggest any preferable mechanism involved. The increase in the release time with the larger load could be due, to the larger contact area between the brush and the hydrogel which influences the diffusion of the HCl at the interface, or to an increase in interdigitation of the brush into the gel when the larger load is applied.

5.5.2 Conformation of the brush in contact with the hydrogel

To observe the behaviour of the brush in contact with the hydrogel we performed neutron reflectivity experiments in which the applied pressure at the interface brush/hydrogel is controlled with the aid of the cell described in section 4.5.4.

The idea is to mimic the experimental conditions for the JKR set-up observing, in this case, the behaviour of the brush instead of the hydrogel. In particular, the neutron experiments are performed with a deuterated polymer brush in H_2O and in contact with hydrogenated PMAA hydrogel in H_2O solution, with an increase in applied pressure from 3 kPa and 15 kPa to 35 kPa.

The neutron reflectivity data were analysed using the slab-fit program described in section 4.5.5. Typical data and fits for the 111 Å thick PDMAEMA brush are shown in Fig 5.14. The resultant volume fraction depth profiles are shown in Fig 5.15. The neutron data do not exhibit any silicon critical edge because the neutrons are passing from a higher refractive index (silicon) into a lower refractive index medium (water swollen polymer) as discussed in section 4.5.4.

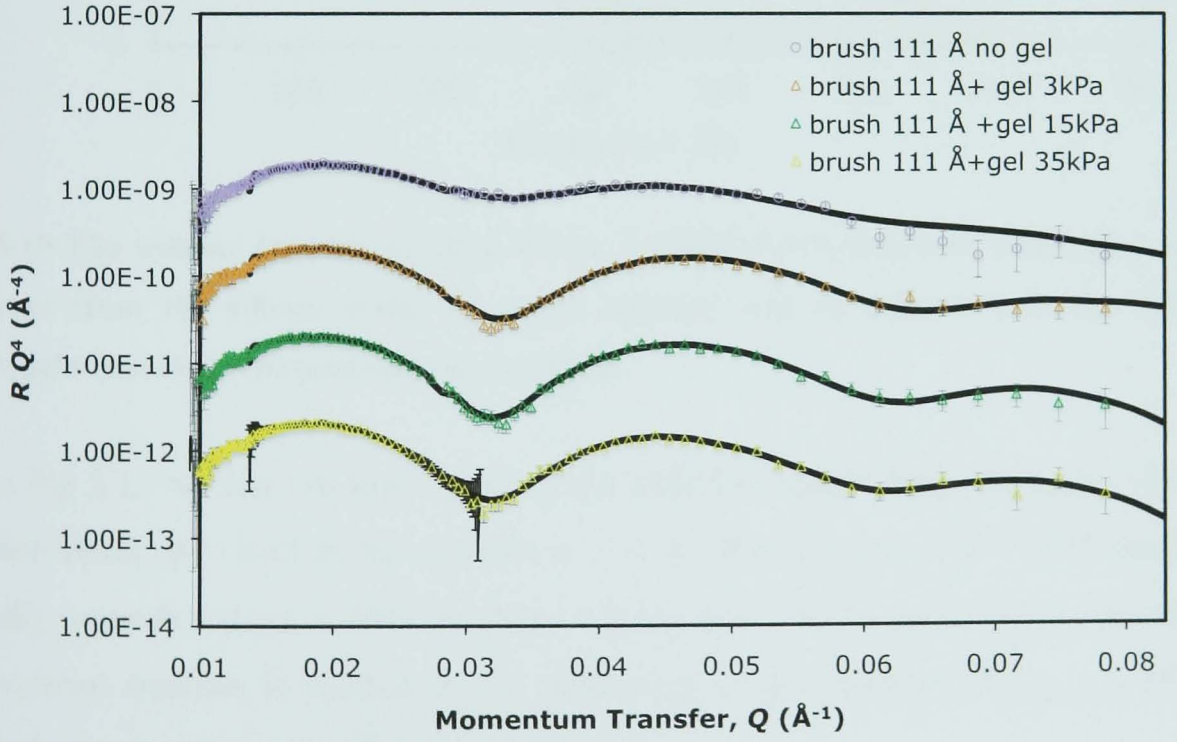

Fig. 5.14 Neutron reflectivity data for the 111 Å PDMAEMA brush in water solution and in contact with the PMAA hydrogel when increasing pressures are applied and released. The data are shown in the Porod form, RQ^4 where Q is the neutron momentum transfer on reflection and R is the reflectivity. Each data set are shifted down by increasing factors of 10. The data for the brush without the gel is not shifted.

The sample cell contains the PDMAEMA brush in solution at pH 5.8 and the PDMAEMA brush in contact with the PMAA hydrogel after that a known pressure is applied for 15 min. It is important to highlight that the neutron data are collected after each applied pressure is released; we observe how the gel brought into contact with the brush at an applied pressure modifies the conformation of the brush.

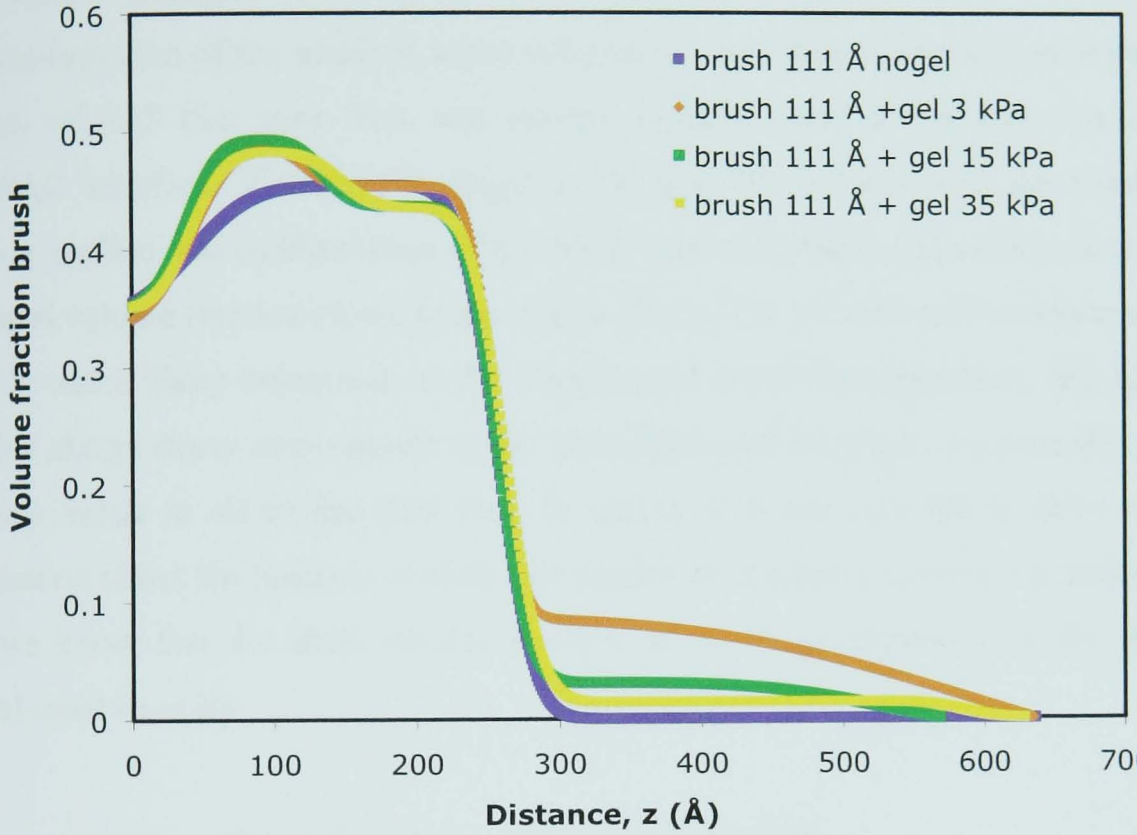

Fig 5.15 The volume fraction profiles of 111 Å PDMAEMA brush as a function of the distance from the silicon wafer in water solution and in contact with the PMAA hydrogel when different pressures are applied.

From Fig 5.15 we can see that for all of the different experiments the brush volume fraction starts, $\phi = 0.45$ at the distance $z = 0$ Å. The volume of $\phi = 0.45$ does not actually mean that there is 45% brush by volume at $z = 0$. As we demonstrate below, the volume fraction is related to the scattering length density $Nb_{(component)}$ of the studied components by the following equations:

$$Nb(z=0) = (Nb_{H_20})\phi_{H_2O} + (Nb_{brush})\phi_{brush}, \tag{5.3}$$

with

$$\phi_{H_20} + \phi_{brush} = 1, \tag{5.4}$$

where $Nb(z=0)=Nb_{silicon}$. The value of ϕ = 0.45 gives a scattering length density of 2.07×10^{-6} Å^{-2}, which is that of silicon. The volume fraction at z = 0 therefore refers to the silicon substrate.

The conformation of the brush in water solution shows, close to the silicon, a volume fraction of 0.45 that rises first, and decays abruptly later in the direction of the brush/H_20 interface. When the hydrogel is brought into contact with the brush and 3 kPa is applied, the conformation of the brush does not change drastically; a slightly increased volume fraction closer to the silicon (from 0.45 to 0.49) can be observed but with the same sharp behaviour in the direction of brush/H_2O interface. We believe that this abrupt decay corresponds to the brush/hydrogel interface, because this sharp interface exists in all of the data sets. In reality it is not possible to have all the information about the position of each component for a ternary system. To understand this, we know that the total volume fraction of all the components in the system studied must be unity

$$\phi_{D_20} + \phi_{brush} + \phi_{Hydrogel} = 1, \text{ and also that} \tag{5.5}$$

$$Nb(z=0) = (Nb_{H_20})\phi_{H_2O} + (Nb_{brush})\phi_{brush} + (Nb_{Hydrogel})\phi_{Hydrogel}. \tag{5.6}$$

We have therefore three unknowns (the three volume fractions) and only two equations, so there can be no unique solution.

The brush conformation is consistent at all applied pressures, suggesting that the slight change in conformation close to the silicon is probably dominated by the effect of the applied pressure more than for the presence of the hydrogel; the applied pressure pushes the brush close to the silicon wafer while at the interface brush/hydrogel the pressure does not produce any change in conformation. From these experiments, we can say that the brush and hydrogel may interact at their interface but this does not exclude any interpenetration because we cannot establish the position of the hydrogel.

We performed another set of experiments where the hydrogenated PMAA hydrogel is brought into contact with a 200 Å thick deuterated PDMAEMA brush. These experiments were performed because we expect that the interdigitation mechanism of the brush chains into the hydrogel would favour longer brush chains. The experiments are performed using the same procedure as for the 111 Å brush. Each set of experiments is recorded after the pressure is released.

A)

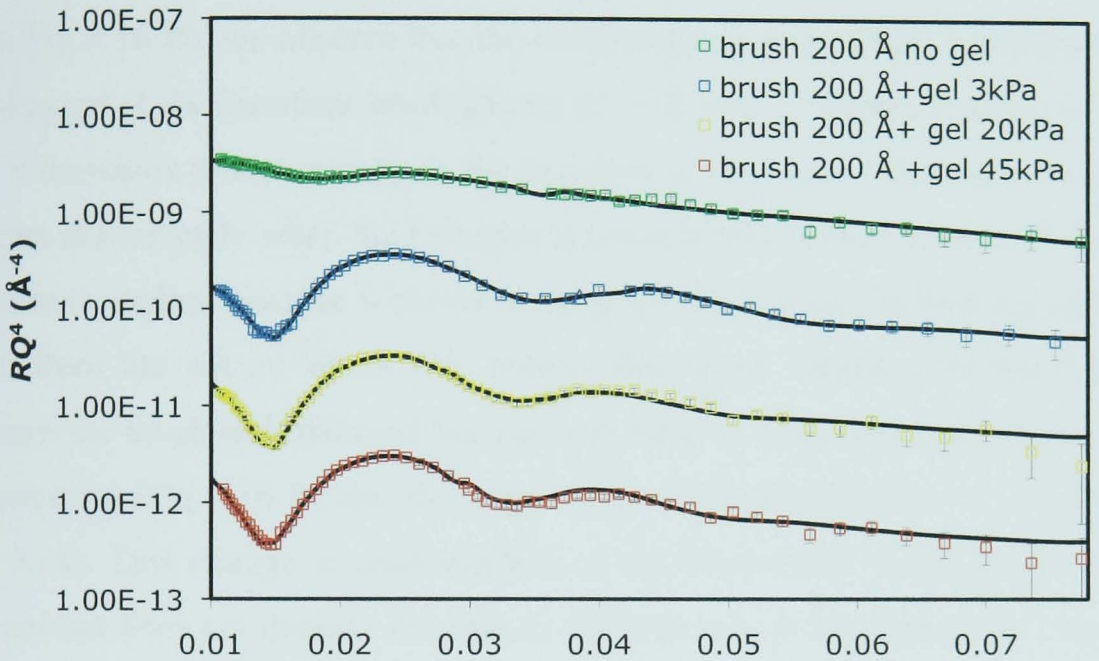

B)

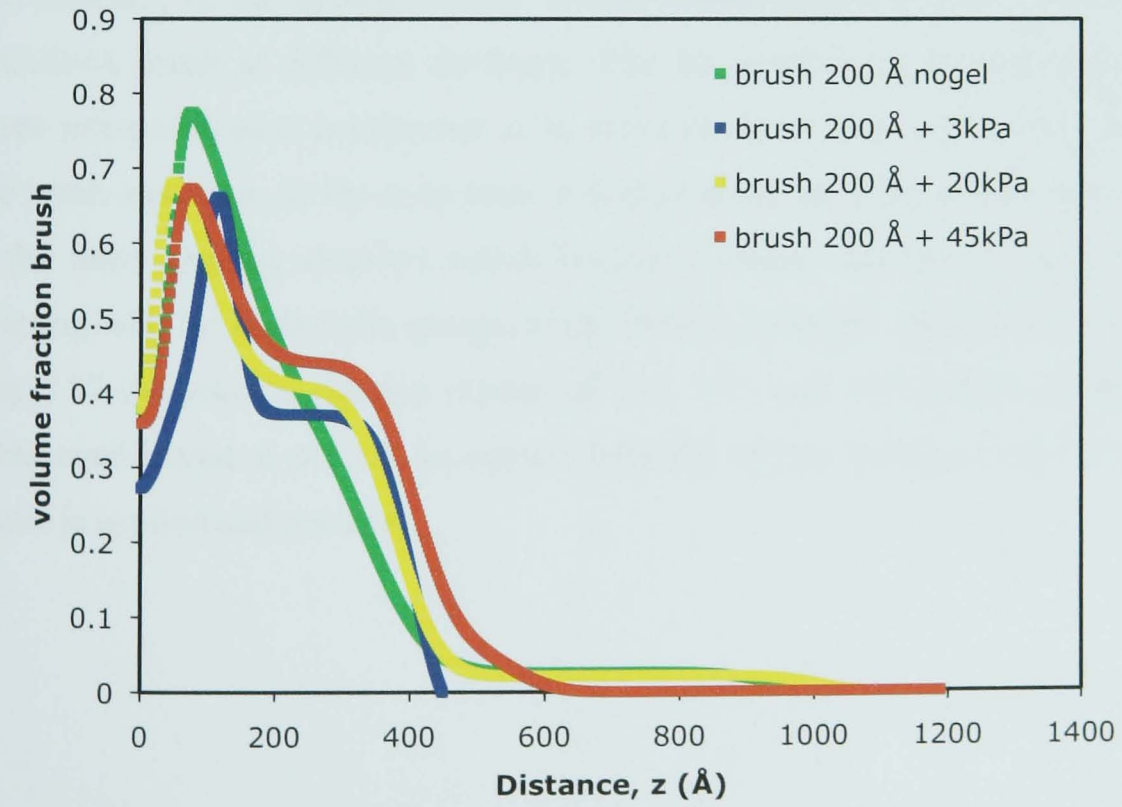

Fig 5.16 A) Neutron reflectivity data for the 200 Å PDMAEMA brush in water and in contact with the PMAA hydrogel when different pressures are applied and released. The

data are shown in the Porod form, RQ^4 where Q is the neutron momentum transfer on reflection and R is the reflectivity value. Each set of data are shifted down by increasing factors of 10 for clarity. The data for the sample with no gel are not shifted. B) Volume fraction profiles of the polymer as a function of the distance from the silicon wafer for a 200 Å PDMAEMA brush in water and in contact with the PMAA hydrogel when different pressures are applied.

From Fig 5.16 B), we observe that the conformation of the brush equilibrated in H_20 is collapsed at the interface brush/silicon ($z = 0$) with a volume fraction of 0.78 and then it decreases monotonically in the direction of the water. The brush conformation changes dramatically when the hydrogel is brought into contact with the brush and the pressure is applied because it shows a sharp interface at the furthest extremity of the brush from the silicon wafer. We believe this sharp interface corresponds to that between the brush and hydrogel because the trend is consistent with all the rest from the same set (Fig 5.16 B) and the same effect is observed for the 111 Å thick brush (Fig 5.15). This change in conformation of the brush when the hydrogel is brought into contact does not directly confirm to the presence of interpenetration but it could suggest a possible contribution. To have a better idea of the role of the sharp interface in the direction of the hydrogel/water system we compare the conformation of the PDMAEMA brush at different thickness. The thickness is an important parameter because interpenetration is expected to be more likely to have place as the thickness of the brush increases. At the same time, a thicker brush has a larger molecular weight (for the same grafting density) which implies a larger number of amino groups interacting with the carboxylic groups of the PMAA hydrogel. We therefore compare in Fig 5.17 the volume fraction profile of 111, 147 and 200 Å thick PDMAEMA brushes equilibrated at pH 5.8, in contact with the PMAA hydrogel after 15-20 kPa pressure is applied and released.

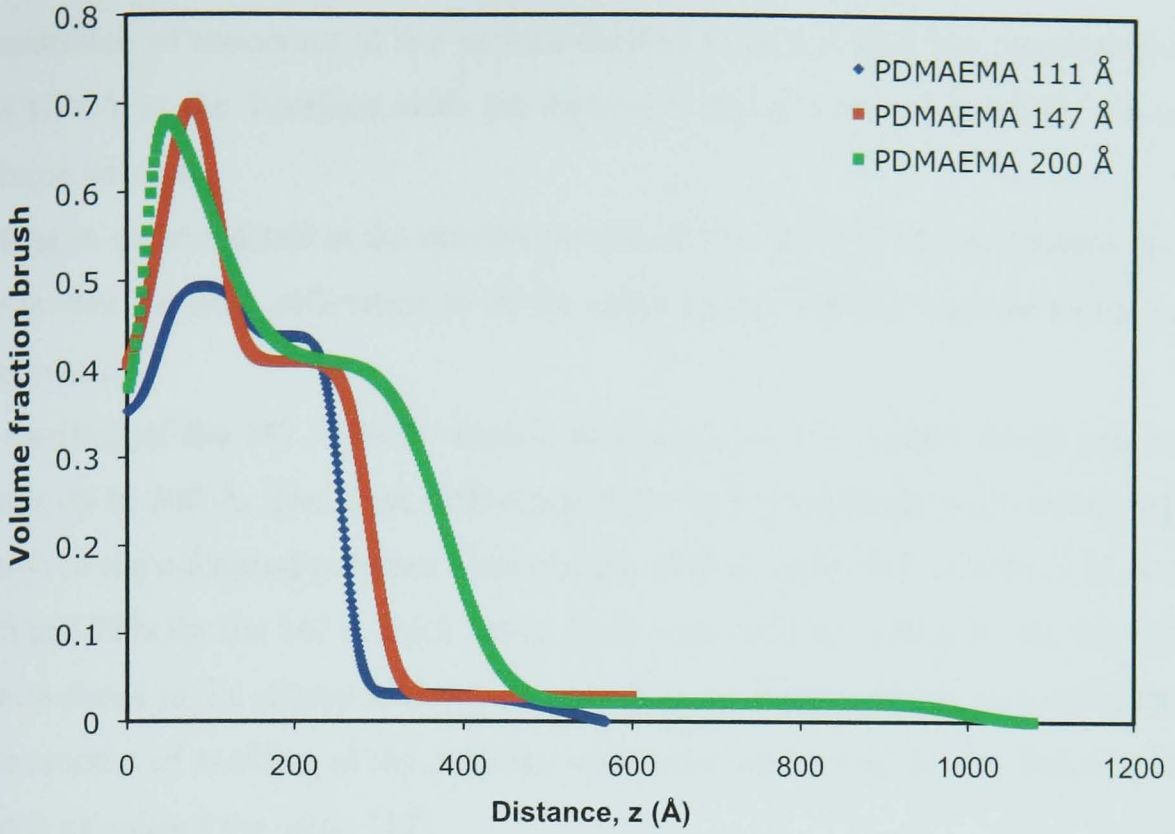

Fig 5.17 The conformation of brushes of thickness 111, 147 and 200 Å in contact with the hydrogel, in water environment, after a pressure of 15 kPa was applied for 15 min before being released.

The 111 Å thick brush, close to the silicon, has a volume fraction of 50% due to the water and 50% due to the polymer, and shows a sharp interface close to the hydrogel. The 147 Å thick brush assumes a more collapsed conformation close to the silicon wafer, with 30% water and 70% polymer, and a sharp interface close to the hydrogel; a similar trend is observed for the 200 Å thick brush. The sharp interface, in the direction of the hydrogel, presents the same volume fraction value of 50% of polymer and 50% of water for all the analyzed thicknesses. This is important because it shows that the concentration of polymer and consequently the degree of ionization at the interface is the same and is independent of the brush thickness. This consideration supports the claim that the sharp interface corresponds to the brush/hydrogel interface. We emphasize again that we cannot prove the location of the hydrogel at the extremity of the brush, but we believe this to be a reasonable conclusion from the data. A similar effect is reported by Kusumo [14], studying the absorption of bovine serum albumin (BSA), as a function of the PDMAEMA brush grafting density. They describe a linear increase in the concentration of BSA adsorbed as a function of the increasing of the grafting density of the PDMAEMA at the surface. They observed the average number of DMAEMA monomers per BSA bond remains constant as the

concentration of monomer at the surface increases; in our case the concentration of PDMAEMA at the interface with the hydrogel remains the same when the brush thickness changes.

Looking in greater detail at the conformations of 111 and 147 Å thick brush, we can observe that the only difference is in the value of the volume fraction closer to the silicon wafer.

The swelling of the 147 Å thick brush is similar to the 111 Å thick brush and it only extends up to 300 Å. The main difference in the two conformations is in the volume fraction of the collapsed polymer closer to the silicon wafer, 50% for the 111 Å thick brush and 75% for the 147 Å thick brush. In the case of 200 Å thick brush, the volume fraction closer to the silicon is similar to 147 Å thick brush and the main difference is in the amount of swelling of the polymer which extends to 422 Å. The height h of the brush is calculated the using [15]

$$h = 2\frac{\int_0^\infty z\,\phi(z)\,dz}{\int_0^\infty \phi(z)\,dz}, \tag{5.7}$$

The collapsed layer, close to the substrate, is not expected to play any role in the adhesion process because it is considered too far from the interface. For the 200 Å thick brush, the volume fraction of the polymer close to the substrate is similar to that of the 147 Å thick brush, but the amount of polymer swollen is much larger, as shown in Fig 5.17, suggesting that the brush with the larger thickness presents a larger number of amino groups available to form long-range interactions with the carboxylic groups of the hydrogel.

In conclusion the neutron reflectivity experiments of the brush in contact with the hydrogel when the pressure is applied and released suggest that the main mechanism of interaction between the brush and hydrogel is due to the electrostatic interaction between the amino group of the brush and the carboxylic group of the hydrogel at the interface. From the resulting volume fraction-depth profiles, there is no evidence of any interpenetration of the brush chains into the hydrogel, because each set of data shows a sharp profile close to where we expected the hydrogel to be located. The comparison of the brush profile at different brush thickness shows that the

composition of the polymer at the interface is the same and is independent of the brush thickness. The amount of polymer swollen is larger for thicker brushes suggesting a larger contribution of long-range interactions between the amino group of the brush chains and the carboxylic group of the PMAA hydrogel as the thickness of the brush increases.

5.5.3 Thermodynamic work of adhesion between PDMAEMA brush of different thickness.

The neutron reflectivity experiments suggest that the dominant mechanism of interaction between the brush and the hydrogel is an interfacial effect. The brush and the hydrogel are both polyelectrolytes and they can interact electrostatically between the amino group of the brush and the carboxylic group of the hydrogel, or through hydrogen bonds. The comparison of brush thicknesses of 111, 147 and 200 Å, in the same range of applied and released pressure and in contact with the PMAA hydrogel, shows that the amount of polymer at the hydrogel/brush interface is the same, 50% polymer and 50% water, and is independent of the brush thickness. At the same time, an increase in brush thickness, from 147 Å to 200 Å, leads to a larger amount of swollen polymer, suggesting an increase in long-range interactions with the hydrogel. We performed adhesion experiments to understand if the thermodynamic work of adhesion between the brush and the hydrogel is a function of the brush thickness. The experiments are performed using the same experimental procedure as that described above; we compare the thermodynamic work of adhesion for a 200 and 90 Å thick brush in contact with the hydrogel.

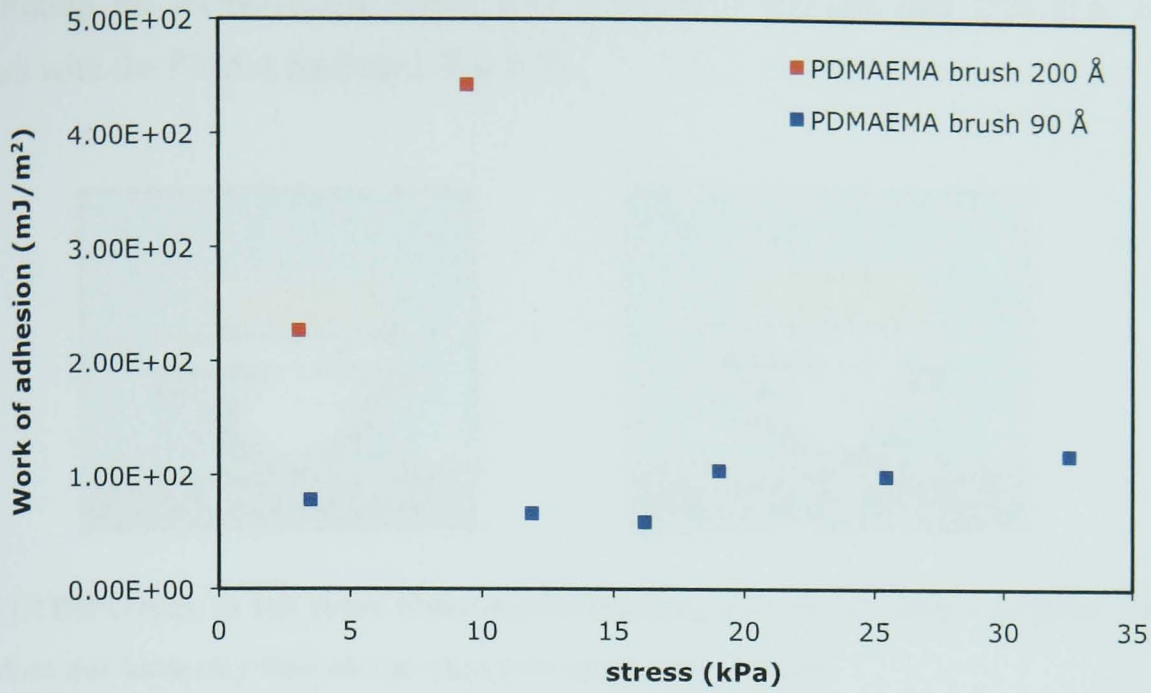

Fig 5.18 Themodynamic work of adhesion of the brush/hydrogel system for a 200 Å thick brush and the 90 Å thick brush.

The thermodynamic work of adhesion between the brush and the hydrogel is a clear function of the brush thickness. In the case of the thinner brush, 90 Å, the thermodynamic work of adhesion is almost half than the thicker brush, 200 Å, and is less dependent on the applied pressure. This difference in the thermodynamic work of adhesion could suggest a mechanism of interpenetration of the brush chains into the hydrogel as the brush thickness increases. As discussed in section 5.5.2, the volume fraction profiles of the brush, in the same range of thickness, (Fig 5.17), allows us to discard this mechanism of interaction. This difference in the thermodynamic work of adhesion as a function of the brush thickness could be justified by considering that a thicker brush has a larger number of available amino groups that can interact with the carboxylic groups of the PMAA hydrogel than the brush of smaller thickness. This is in agreement with the conclusions that we drew from the volume fraction profiles of the brush over the same thickness range.

5.5.4 Replacing PDMAEMA brush with a PDMAEMA gel film

For a better understanding of the role of the interpenetration mechanism of the brush chains into the hydrogel, we performed some experiments with the JKR set-up by

substituting the PDMAEMA brush with a PDMAEMA gel thin film [16, 17] in contact with the PMAA hydrogel, Fig 5.19.

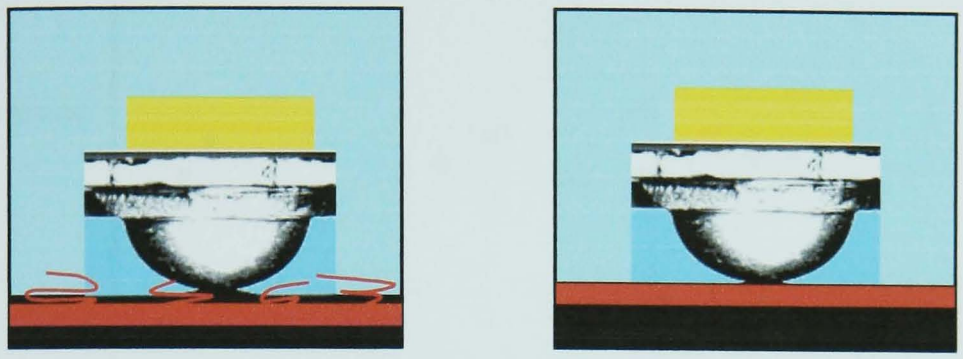

Fig 5.19 Difference in the three dimensional topology of a brush with a gel film. The gel film does not have any free chains that interpenetrate the gel.

The idea behind these experiments is to compare the value of adhesion energy between two substrates coated with the same PDMAEMA but with the polymer having a different three-dimensional structure. The brushes, with extended chains in the *z* direction, are likely to interpenetrate the hydrogel. The gel film is photo-crosslinked with the PBMA on an initiator coated silicon surface and will respond to changes in pH but, in contrast with the brush, it has a very low probability of significant interpenetration due to the small quantity of free dangling ends. The synthesis and the deposition of the PDMAEMA gel film have been described in detailed in section 4.3.

Fig 5.20 shows a plot of thermodynamic work of adhesion calculated in the unloading regime as a function of the stress for a PMAA hydrogel in contact the 110 Å thick PDMAEMA gel film, and in contact with a 90 Å thick PDMAEMA brush.

All the experiments have been performed in water solution at pH 5.8.

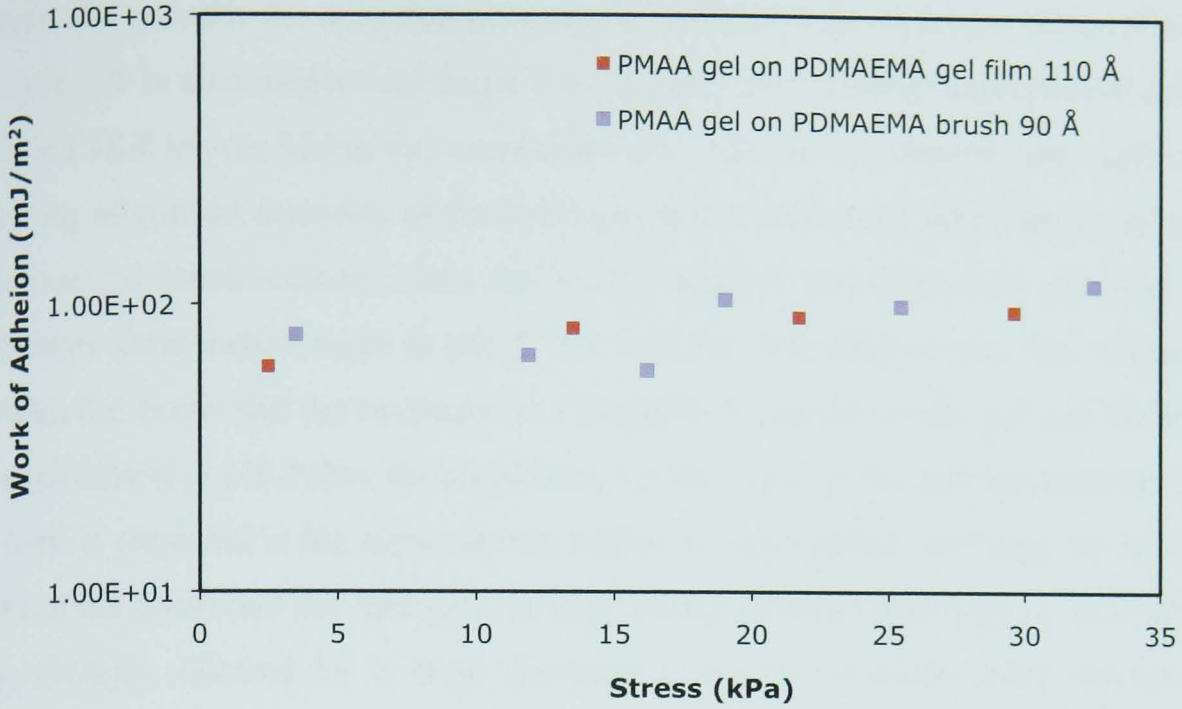

Fig 5.20 Thermodynamic work of adhesion of a brush/hydrogel system and hydrogel/gel film system. The brush and the gel films have similar thicknesses.

The thermodynamic work of adhesion in the case of the PDMAEMA brush and gel film with similar thicknesses, 90 and 110 Å respectively, has the same order of magnitude. The brush is rather thin for studying the interpenetration effect but, in any case, we see from the neutron reflectivity experiments no dramatic change in the conformation of the brush as a function of the thickness is observed. The comparison of the thermodynamic work of adhesion for the brush and the gel film surface in the same range of thickness suggests that the interpenetration mechanism is unlikely to happen and confirms that the surface effect is the main mechanism of interaction.

5.6 Conclusion

In this chapter, we studied the interaction between oppositely charged polyelectrolytes. In particular we focus on the interaction between a weak base brush, PDMAEMA, grafted from a silicon surface and a weak polyacid hydrogel, synthesised from the MAA monomer. The brush and gel are both pH responsive. The weak polybase brush is positively charged in acid pH and uncharged in base pH while the weak polyacid hydrogel is charged in basic conditions and uncharged in acid pH. The amount of charges on both polymers causes the swelling of the polymer chains because the polymers uptake water to minimize the repulsion forces between the

charges. To quantify the adhesion between the brush and the hydrogel we synthesised the hydrogel in a hemispherical shape and we performed kinetics experiments using a modified JKR set-up. Using the camera and the light we can observe and collect the changing of contact diameter of the hydrogel at the beginning, when the hydrogel is added on the brush surface, when the load is applied and when it is removed. We performed these experiments at pH 2, 3.4 and 5.8. We observe that the interaction between the brush and the hydrogel is a function of the pH. If the gel and the brush are equilibrated at pH 2 they do not adhere, i.e. the value of the contact diameter after the load is removed is the same as that before it was applied, showing no adhesion between the brush and the hydrogel. If they are equilibrated above pH 3, they adhere very strongly, marked by a large increase in contact diameter after the load is removed than before it was applied; the only way to separate the two components is to tear the brush off the surface, or to rupture the gel. If they are equilibrated at pH 3.4 the final value of contact diameter, after the unloading, is larger than at the beginning but smaller than at pH 5.8.

At the same time, we demonstrate that the adhesion is switchable and triggered by the pH; If the two components initially in contact at pH 5.8 (strong adhesion) are equilibrated at pH 1 the gel detaches from the brush without damaging either and the system may be used again.

To quantify the adhesion between the brush and the hydrogel we used the JKR equation where the thermodynamic work of adhesion is a function of the radius of curvature of the hydrogel lens, the applied load, the bulk modulus of the lens and the area of contact between the brush and the hydrogel after that the load is removed (unloading stage). We performed the experiments by applying different loads and we observe that the interaction between the brush and the gel has a "pressure effect" in that adhesion energy increases as larger loads are applied and removed. This suggests that probably more than one mechanism is involved in the adhesion process. We therefore hypothesize that the interaction between the brush and hydrogel could be pressure sensitive due to interfacial (e.g. electrostatic) or for interdigitation effects or the actual mechanism could be a mixture of both interfacial and interdigitation effects whose contributions may vary over a range of applied pressures.

We performed some other experiments and the interfacial (surface) mechanism seems to be the dominant mechanism in the interaction between the brush and the hydrogel.

The neutron reflectivity experiments of the brush in contact with the hydrogel when the pressure is applied and released allow observation of the behaviour of the brush under the same condition as we performed the JKR adhesion experiments. From the neutron reflectivity profile, there is no evidence of any interpenetration of the brush chains into the hydrogel, because for each increased value of applied pressure, the data show a sharp profile close to where we expect the hydrogel to be located. The comparison of the brush profile at different brush thickness (111, 147 and 200 Å) shows that the composition of the polymer at the interface is the same and is independent of the brush thickness. The amount of polymer swollen is larger for thicker brushes suggesting a large contribution of long-range interaction between the amino group of the brush chains and the carboxylic group of the PMAA hydrogel as the thickness of the brush increases. To confirm this behaviour, we performed adhesion experiments to understand if the thermodynamic work of adhesion between the brush and the hydrogel is a function of the brush thickness. The comparison of the thermodynamic work of adhesion for a 200 and 90 Å thick brush in contact with the hydrogel show the thicker brush has a large value of the thermodynamic work of adhesion. This result is in agreement with the volume fraction profile of the brush because a thicker brush has a larger number of available amino groups that can interact with the carboxylic groups of the PMAA hydrogel than the brush of smaller thickness. Finally, to exclude any interpenetration of the brush chains into the hydrogel, we performed some experiments with the JKR set-up by substituting the PDMAEMA brush system with a PDMAEMA gel thin film in contact with the PMAA hydrogel in the same range of thickness. A comparison of the thermodynamic work of adhesion between the systems containing PDMAEMA brush and gel films does not show any dependence on the topology of the polymer suggesting that the interpenetration mechanism it is unlikely to happen and confirms that the surface effect is the main mechanism of interaction.

1. Gil, E.S. and S.M. Hudson, *Stimuli-reponsive polymers and their bioconjugates.* Prog. Polym. Sci., 2004. **29**: p. 1173-1222.
2. Ryan, A.J., et al., *Responsive brushes and gels as components of soft nanotechnology.* Faraday Discuss., 2005. **128**: p. 55-74.
3. Zhou, F., et al., *Highly reversible and multi-stage cantilever actuation driven by polyelectrolyte brushes.* J. Am. Chem. Soc., 2006. **128**: p. 5326-5327.
4. Ruiz-Pérez, L., et al., *The conformation of poly(methacrylic acid) chains in dilute aqueous solution.* Macromolecules, 2008. **41**: p. 2203-2211.
5. Khare, A.R. and N.A. Peppas, *Swelling/deswelling of anionic copolymer gels.* Biomaterials, 1995. **16**: p. 559-567.
6. La Spina, R., et al., *Controlling network-brush interactions to achieve switchable adhesion.* Angew. Chem. Int. Ed., 2007. **46**: p. 6460-6463.
7. Wesley, R.D., et al., *Structure of polymer/surfactant complex formed by poly(2-(dimethylamino)ethyl methacrylate) and sodium dodecyl sulfate.* Langmuir, 2002. **18**: p. 5704-5707.
8. Woerdeman, D.L., et al., *Characterization of glass–epoxy adhesion using JKR methods and atomic force microscopy.* Composites A, 1999. **30**: p. 95-109.
9. Johnson, K.L., K. Kendall, and A.D. Roberts, *Surface energy and the contact of elastic solids.* Proc. R. Soc. London A, 1971. **324**: p. 301-313.
10. O'Connor, K.P. and T.C.B. McLeish, *"Molecular Velcro": Dynamics of a constrained chain into an elastomer network.* Macromolecules, 1993. **26**: p. 7322-7325.
11. Ostroha, J., et al., *Controlling the colapse/swelling transition in charged hydrogel.* Biomaterials, 2004. **25**: p. 4345-4353.
12. Geoghegan, M., et al., *The pH-induced swelling and collapse of a polybase brush synthesized by atom transfer radical polymerization.* Soft Matter, 2006. **2**: p. 1076-1080.
13. Silberzan, P., et al., *Study of the self-adhesion hysteresis of a siloxane elastomer using the JKR method.* Langmuir, 1994. **10**: p. 2466-2470.
14. Kusumo, A., et al., *High Capacity, Charge-selective protein uptake by polyelectrolyte brushes.* Langmuir, 2007. **23**: p. 4448-4454.
15. Seidel, C., *Strongly stretched polyelectrolyte brushes.* Macromolecules, 2003. **36**: p. 2536-2543.
16. Huang, J., et al., *Synthesis and in situ atomic force microscopy characterization of temperature-responsive hydrogels based on poly(2-(dimethylamino)ethyl methacrylate) prepared by atom transfer radical polymerization.* Langmuir, 2007. **23**: p. 241-249.
17. Tokarev, I. and S. Minko, *Stimuli-responsive hydrogel thin films.* Soft Matter, 2009. **5**: p. 511-524.

Chapter 6

Total work of adhesion

6.1 Introduction

Adhesion is a well-studied phenomenon, mainly due to its industrial importance. In our research we are studying a smart water-based adhesive that is switchable, i.e. the adhesion may be turned on and off by a change in pH.

In the previous chapter, we discussed the phenomenological effect of when an oppositely charged polyelectrolyte brush and hydrogel are brought into in contact.

The investigated interaction is between poly[2-(dimethyl amino)ethyl methacrylate] (PDMAEMA, the weak polybase) brushes chemically grafted to planar silicon substrates by atom transfer radical polymerization, and a weak polyacid hydrogel of poly(methacrylic acid) (PMAA). We identified that below pH 2, the brush and the hydrogel do not adhere but, above pH 3, the brush and the hydrogel interact strongly and they can be separated only by ripping them apart, damaging one or both of the two components [1].

The interaction between brush and gel is switchable if the system, after the two components are brought into contact, is equilibrated in acid pH, such as pH 1, when the brush and the gel are released without any damage.

We also discovered that the interaction between the brush and hydrogel is pressure sensitive [2] and that the work of adhesion is a function of the applied load.

The experimental data, described in the previous chapter, suggest that the dominant mechanism of interaction between the brush and the hydrogel is an interfacial effect between the amino group of the brush side chains and the carboxylic groups of the PMAA hydrogel; there is no clear evidence of any interpenetration mechanism of the brush chains into the hydrogel. The brush volume fraction profiles, obtained by neutron reflectivity experiments show that, at the hydrogel/brush interface the brush has the same composition of polymer and water independently of the brush thicknesses, 50% polymer and 50% water. On the other hand, the amount of swollen polymer is a function of the brush thickness. In particular, in fig 5.17, we have compared the behaviour of 111, 147 and 200 Å thick brushes in contact with the hydrogel in water solution after a known load has been applied and released. The brush chains at 111 and 147 Å thickness are stretched reaching a value of 286-306 Å, while at 200 Å thick brush the chains are extended to 422 Å [4]. The JKR experiments show a dependence of the thermodynamic work of adhesion as a function of increasing brush thickness, due to the long-range interaction between the charged and uncharged amino groups in the brush chains and the charged and uncharged carboxylic groups in the hydrogel.

In the previous chapter we described experiments using a modified JKR apparatus where observed changes in the contact diameter of the hydrogel in contact with the brush surface, using a camera and a light source placed beside the gel. To increase the interaction between the brush and the hydrogel some known loads were applied on the top of the gel for 15 min and then they were removed quickly. During the unloading stage, the hydrogel would release part of the energy gained during the application of the load. Using the JKR equation, we calculate the thermodynamic work of adhesion in the unloading regime taking into account the value of contact radius after the load was removed; we also deduce the radius of curvature and the elastic modulus of the lens.

In this chapter, we introduce a similar kind of experiment but in this case we want to calculate the energy necessary to separate the hydrogel from the brush after a known force has been applied to increase their contact. This energy is especially important for industrial application because it gives a real idea of the strength of the adhesion between the brush and the hydrogel.

In the literature the work closest to our study is the measurement of the work of adhesion of two oppositely charged hard spheres of mica and silica in air [5]. These experiments were performed at the contact between the two spheres where a maximum force of 200 mN, corresponded to a contact radius of 65 μm. In this condition, the pull-off force in the unloading stage was equal to 73 mN, and the work of adhesion, calculated using the JKR model, was equal to 1000 mJ/m^2, while the work of adhesion calculated by integrating the force-distance curve was equal to 6000 mJ/m^2. This difference may be explained by considering that the silica and mica interaction is due to the contribution van der Waals and electrostatic forces. Barthel [6] showed that the contribution of each component on the total work of adhesion can be isolated if they are different by at least an order of magnitude. This principle, when applied to the mica/silica system, showed that the JKR model takes into account the short range contribution while the pull-off force and force-distance integral takes into account both short and long range forces.

In our case, we cannot use the JKR equation to calculate the contribution of the short range interaction in the hydrogel/brush system because the hydrogel is a soft material, and it dissipates energy when it is pulled off from the surface and the JKR mathematical model is only valid for pure elastic bodies. For this reason, the work of adhesion of the hydrogel-brush system has been calculated as the integral of force-displacement curves, which takes into account all of the contributions that participate in the adhesion between the two surfaces, such as viscoelastic dissipation in the hydrogel, and long and short range interactions. The contribution of the different effects was analysed by changing the thickness of the brush surface; the three-dimensional structure of the film on the surface; the kind of polymer in contact with the hydrogel; and the amount of crosslinker in the hydrogel.

6.2 Content of the chapter

Our experiments show that there is a dependence of the brush thickness on the work of adhesion obtained for the same pH and percentage of crosslinker in the hydrogel. For different brush thicknesses, the relative contributions to the adhesion from charges, and hydrogen bonds vary as shown in the previous chapter. For this reason we performed experiments to isolate, as much as possible, the contribution of each

parameter to the total work of adhesion. This strategy included changing the topology of the polymer on the silicon surface from a brush to a crosslinked polymer film, which we shall refer to as a gel film, and varying the crosslinker density of the hydrogel. Another important parameter that contributes to the energy to separate the hydrogel from the brush is the viscoelastic dissipation of the hydrogel. Viscoelasticity concerns the behaviour of a polymer when subject to a deformation and implies a mixture of liquid like viscous properties with a solid like elastic behaviour; in general, the material loses energy when a mechanical stress is applied and released [7]. The latter is a key parameter in the total work of adhesion, because the stronger the interaction at the interface between the hydrogel and brush, the larger the contribution of the viscoelastic dissipation of the hydrogel. This is because the polymer network, strongly bonded to the brush surface, can be highly stretched.

To study the contribution of changes on the total work of adhesion in the brush-hydrogel system, we performed pull-off experiments between the PDMAEMA gel film of different thicknesses with a more crosslinked PMAA hydrogel to increase the mechanical strength of the network [7] and consequently minimize the contributions of viscoelastic dissipation of the hydrogel and the interpenetration effect. The contribution of the interpenetration effect on the total work of adhesion is studied by neutron reflectivity experiments by comparing the conformation of the brush as a function of thickness under the same condition of pH, hydrogel crosslinking and load applied at the interface. The neutron reflectivity results show no conclusive evidence of interpenetration, but do not exclude a contribution especially at larger brush thicknesses; so to eliminate any possibility of interpenetration, we studied the contribution of the electrostatic charge on the PDMAEMA gel film instead of the brush.

The brushes, with extended chains in the z direction, i.e. perpendicular to the surface, are, in principle, able to penetrate into hydrogel. The gel film [8], on the other hand, is photo-crosslinked on a modified silicon surface and can respond to changes in pH but, in contrast to the brush, there is a very low possibility that free chains can interpenetrate the gel.

These experiments show that an increased electrostatic contribution contributes significantly to the brush-hydrogel total work of adhesion with the increasing larger thickness.

The contribution of hydrogen bonding in the PDMAEMA brush-hydrogel system is studied by substituting the PDMAEMA brush with a PHEMA (poly[2-(hydroxyethyl methacrylate)]) gel film [9] photo-crosslinked on an initiator modified silicon surface. PHEMA has a similar chemical structure to PDMAEMA and is soluble in water. It is characterized by an alcohol functional group that makes the PHEMA a much weaker polyacid than the PMAA . PHEMA can chemically interact with a PMAA hydrogel through hydrogen bonding. The experiments show a small contribution of hydrogen bonding to the total work of adhesion.

As we pointed out earlier in this chapter we are mainly considering pull-off experiments where the thickness of the PDMAEMA brush, PDMAEMA gel film, and the crosslink percentage of the PMAA hydrogel are all varied.
The kind of surfaces, brush or gel film, the thicknesses of the polymer layer and the crosslinker densities of the hydrogel are listed in Table 6.1.

sample	system	%crosslinker (w/w)	Monomer/crosslinker
PMAA045	PMAA hydrogel	0.45	123
PMAA069	PMAA hydrogel	0.69	81
PMAA093	PMAA hydrogel	0.93	60
PMAA3	PMAA hydrogel	3	18

sample	system	Thickness (Å)
PDB28	PDMAEMA brush	28
PDB132	PDMAEMA brush	132
PDB165	PDMAEMA brush	165
PDB311	PDMAEMA brush	311
PDG23	PDMAEMA gel film	23
PDG119	PDMAEMA gel film	119
PDG340	PDMAEMA gel film	340
PHEMA40	PHEMA gel film	40

Table 6.1 PMAA045, PMAA093, PMAA069, PMAA3 refer to a PMAA hydrogel synthesised with respectively 0.45%, 0.93%, 0.69%, and 3% (w/w) crosslinker by weight in the *total* solution. Those quantities of crosslinker means that the gels have an average number of monomers per crosslinker as shown in the fourth column. PDB28, PDB132, PDB165, and PDB311 are PDMAEMA brushes with respective thickness of 28, 132, 165, and 311 Å. PDG28, PDG119, and PDG340 are the PDMAEMA gel films with respective thickness of 28, 119, 340 Å. PHEMA40 is the PHEMA gel film of 40 Å thickness.

6.3 Interaction of the PDMAEMA brush with the PMAA hydrogel.

In the previous chapter we described experiments whereby the PDMAEMA brush and the PMAA hydrogel adhere strongly at neutral pH conditions, but if the system is equilibrated in acid conditions, such as pH 1, the brush and hydrogel come apart without any damage. In this section, we shall focus on the contribution of the different parameters to the total adhesion of the brush-hydrogel system in water at pH 5.8. The total work of adhesion is measured using a mechanical tester as described in section

4.4.2. This set-up constitutes three parts: a light source, a camera and a liquid cell, as shown in Fig 6.1 .

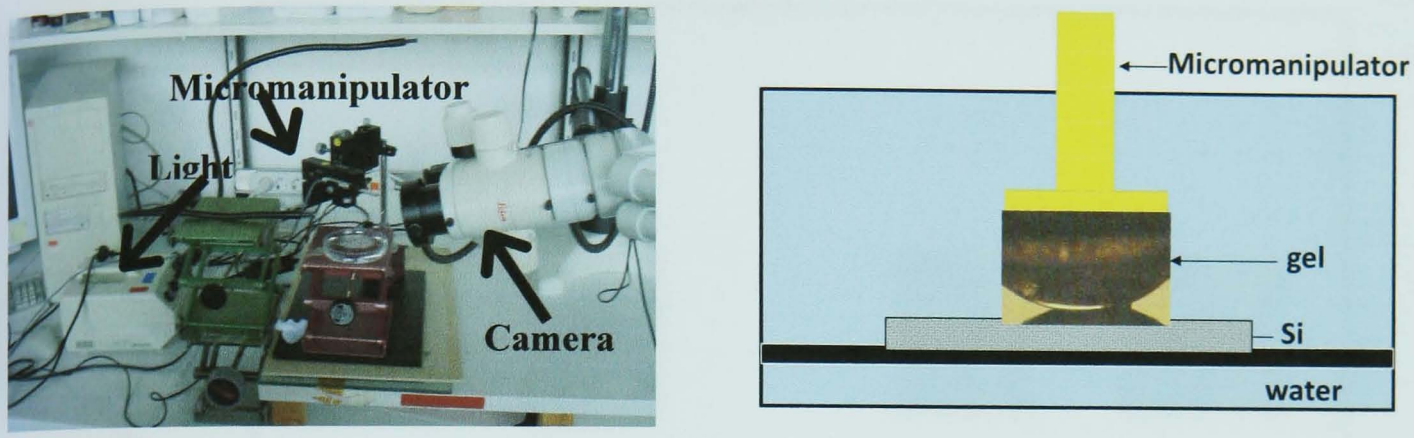

A)

B)

Fig 6.1 A)The pull-off set-up with the camera on the right, the light on the left and the liquid cell in the centre. The liquid cell contains the silicon wafer covered with a polymer film. Behind the liquid cell, the micromanipulator with the force tester brings the gel into contact and pull-off from the surface. B) Schematic representation of the liquid cell for the pull-off experiments. The hydrogel is connected by a sample holder to the micromanipulator that brings the gel into contact with and pulls off from the polymer-coated silicon wafer.

The liquid cell, where the experiments are performed, is situated between the light and a high resolution camera, and the gel is observed from the side. The silicon disk is fixed onto a glass cell of 7 cm diameter with two glass clamps. The hydrogel lens, mechanically attached to the force tester using a Perspex support, is brought into contact with the silicon disk and pulled off by a micromanipulator connected to a 100 g force transducer. The micromanipulator is set to a speed of 20 μm/s in both the loading and the unloading stage. The experimental procedure consists of clamping the disk onto the glass support and leaving the solution to equilibrate for two hours, after which a hemispherical gel is clamped onto the Perspex support and brought into contact with the wafer until the chosen force is reached. The gel and the wafer are left in contact for 15 min and then the gel is pulled upwards until it is detached from the surface.

The micromanipulator machine, connected to a computer, measures the variation of force as a function of time. In Fig 6.2 we show typical data.

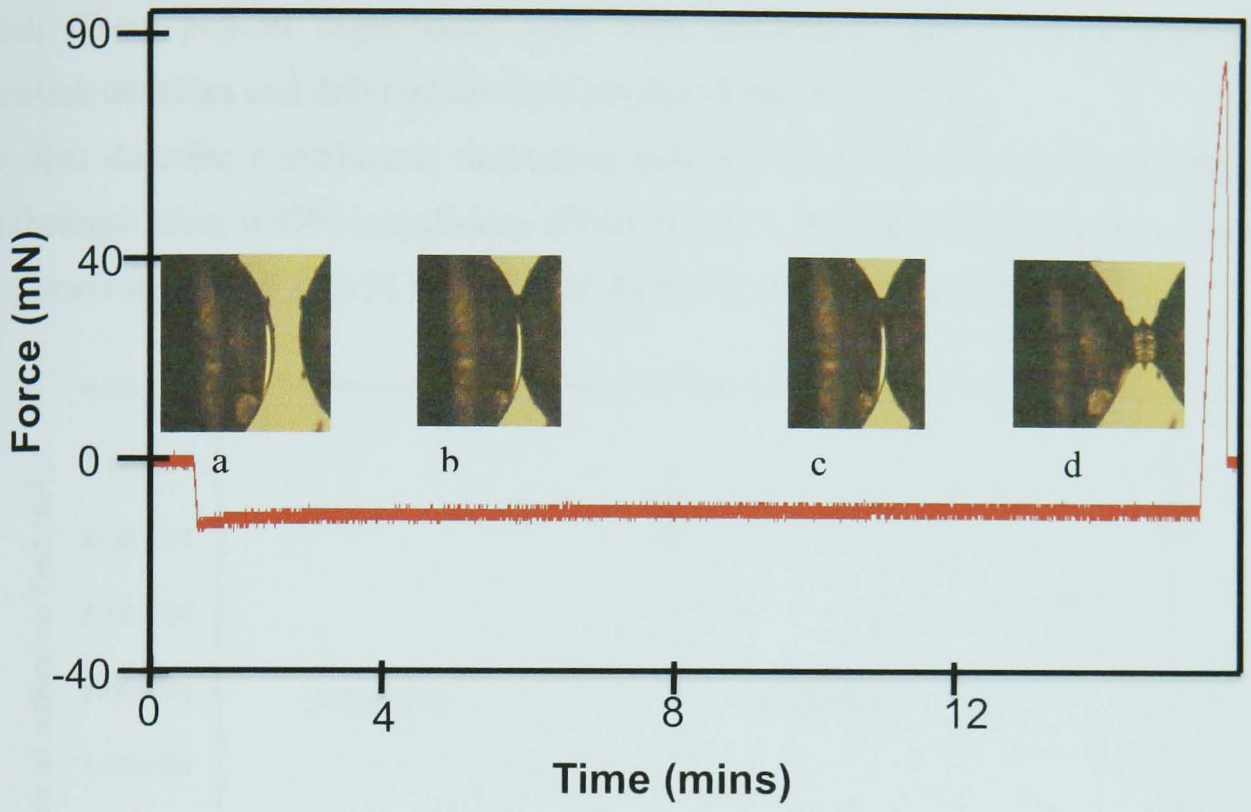

Fig 6.2 Typical data from the pull-off apparatus, showing the variation of the applied force on the hydrogel-brush system as a function of time. (a) The gel is close to the surface but is not in contact; this part gives the background of the experiment. Afterwards, (b) the gel is brought into contact with the surface at 14 μm/s until a final forces of 20 mN is applied. This force is kept constant for 15 mins (c) and then the gel is retracted with a velocity of 14 μm/s until (d) it is ripped off.

The graph, shown in Fig 6.2, can be divided into 4 parts:

a) the background, when the gel is close to the surface but not in contact;

b) the loading regime, when the gel is brought into contact with the surface;

c) equilibration, when the gel is kept for 15 min in contact with the surface under a constant applied force; and

d) the unloading regime, where the gel is pulled until it is detached from the surface.

For each sample surface, these experiments are performed with three different hydrogel lens where the values of total work of adhesion have been averaged to a final result and the error bars are presented as the standard deviation of these three measurements; any possible systematic uncertainties are not therefore included. The work of adhesion has been calculated in the unloading regime by integrating the

variation of the force with respect to displacement, calculated by multiplying the time for the velocity of pull-off. The camera and the light, placed on either side of the liquid cell are used to monitor the variation of contact diameter of the lens with the brush. These pull-off experiments have been performed using different hydrogel crosslink densities and different kinds of polymer brush or gel films.

We first describe experiments measuring pull-off forces for the PMAA hydrogel synthesised using 0.45% crosslinker, (PMAA045), with PDMAEMA brushes in the thickness range of 28 Å to 311 Å, PDB28, PDB132, PDB165, and PDB311.

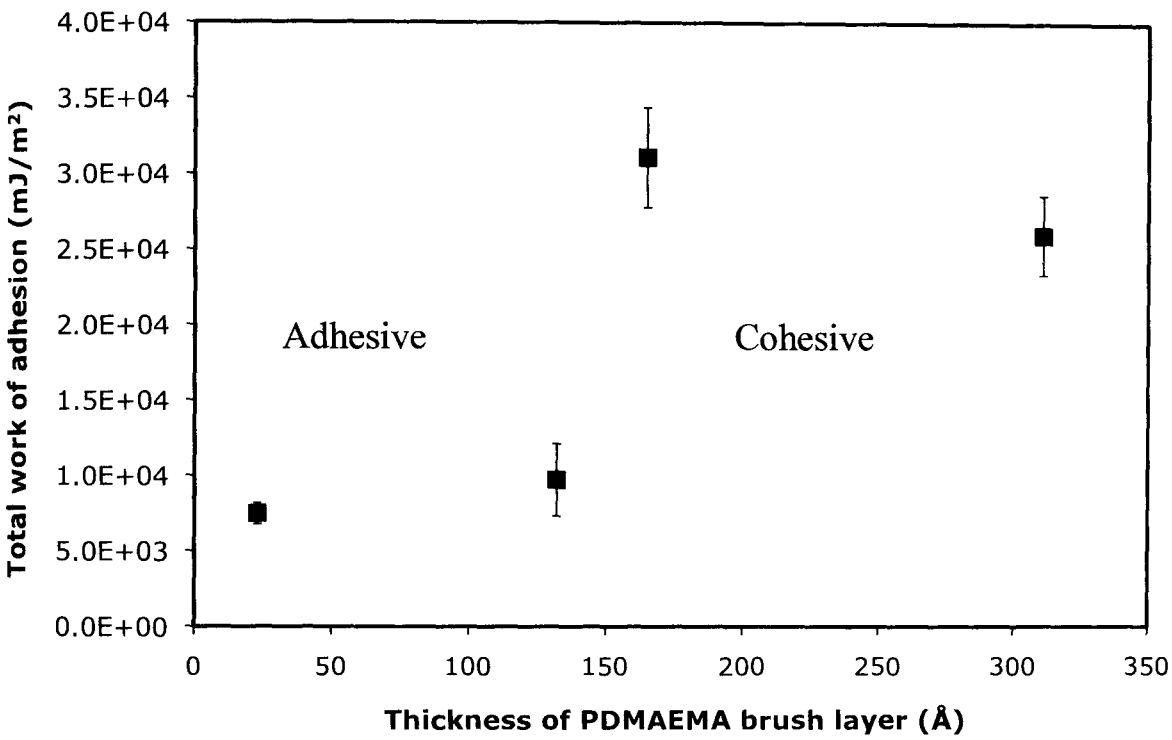

Fig 6.3 The dependence of the work of adhesion as a function of the PDMAEMA brush thickness. The PMAA was synthesised with 0.45 % of crosslinker (PMAA045), the same hydrogel as that used for the experiments described in the previous chapter.

The graph in Fig 6.3, shows a strong dependence of the work of adhesion of PMAA045 with the PDMAEMA brushes as a function of the brush thickness, of which two different regions can be recognized. In the region PDB28-140, the value of the work of adhesion is a third of the value in the region from PDB165 which allows us to conclude that two different kinds of mechanism are involved in the detachment process. In the unloading process, in the range PDB28-140, the failure of the hydrogel takes place at the interface between the hydrogel and the brush and the mechanism is adhesive. In the range from PDB165 to PDB311, the fracture is cohesive with the hydrogel breaking. Here, the chemical bonds in the hydrogel are weaker than the interface between the hydrogel and the brush and so the hydrogel is broken before the

interface is separated. The work of adhesion at the interface, calculated in this range of thickness, is greater than the total work of adhesion measured here because the hydrogel breaks before it can be separated from the interface, but it gives an idea how strong the brush-hydrogel interface is at larger brush thicknesses.

We observe adhesive and cohesive mechanisms *in situ* by a camera just before the hydrogel is pulled off and by a microscope, where we analyse under dry conditions, the surface at the location where the gel was in contact.

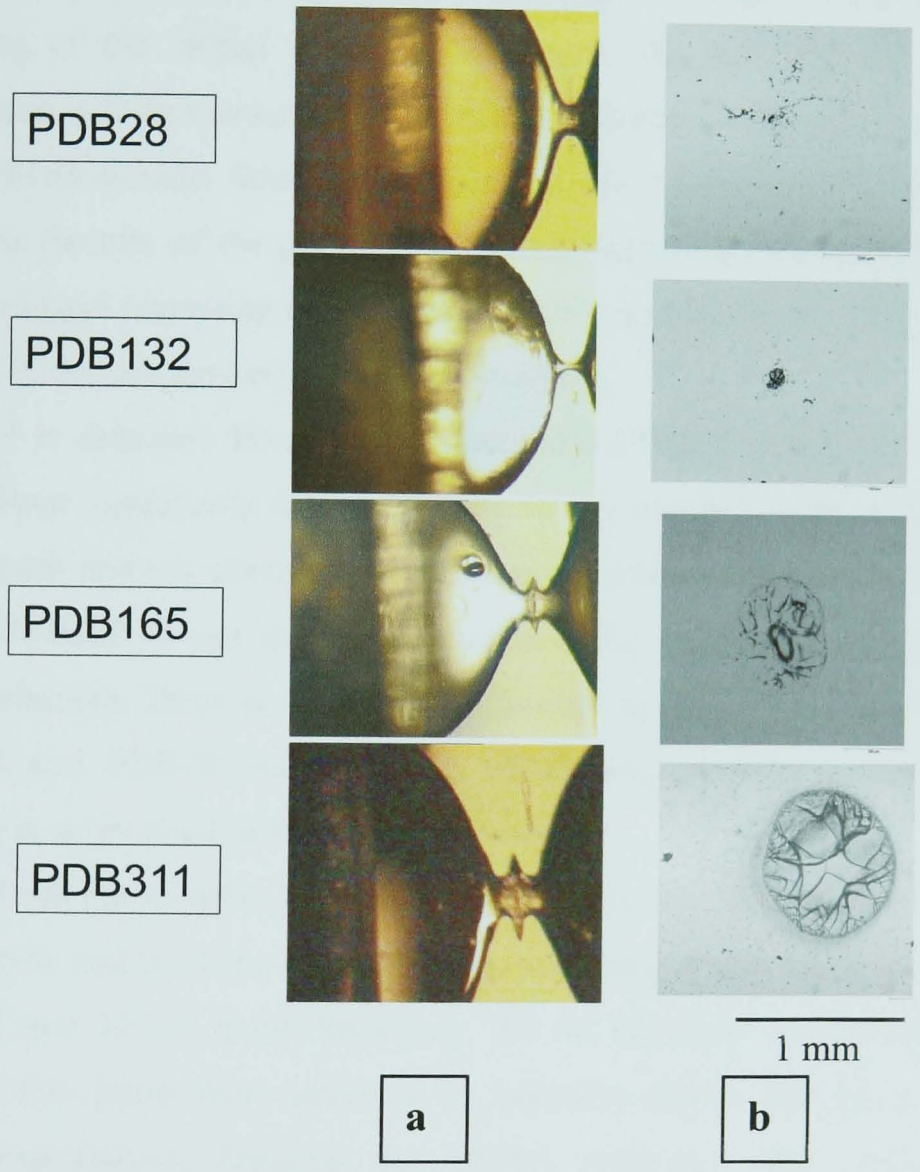

Fig 6.4 Photographs showing (a) the hydrogel in contact with the surface, just before being separated, for different brush thicknesses. These images are collected *in situ* by a camera. The neck, visible for PDB165 and PDB311, shows the cohesive mechanism of failure into the hydrogel. This neck is absent for PDB28 and PDB132, and so the mechanism of failure is adhesive at the hydrogel-brush interface. The microscope pictures (b) show the spot of the surface from where the hydrogel was removed. These spots highlight the cohesive mechanism for PDB165 and PDB311 because there are

pieces of gel remaining on the surface. By the same reasoning the mechanism is adhesive for PDB28 and PDB132 Å because there is no remaining hydrogel on the surface.

The microscope pictures Fig 6.4 (b) of the brush surface, after the gel has been pulled off, show pieces of gel on the surfaces (PDB165 and PDB311) that are actually visible by eye as well. This means that the chemical bonds in the hydrogel are weaker than the interface brush-gel, and so the failure is cohesive. The interface hydrogel-brush is so strong that the hydrogel, before breakage, is visibly deformed [10] due to the stretching of the chains inside the hydrogel. The gel (Fig 6.4 (a)) is more deformed when it is in contact with the PDB340 surface than when it is in contact with the PDB165 surface. Some differences can also be observed in the microscope images of the fracture of the gel on the PDB165 and PDB340 surfaces such as the amount of hydrogel remaining on the surface where there is much more gel remaining on the PDB340 surface than on the PDB165 surface.

The hydrogel is detached from the interface with PDB28 and PDB132 apparently without any large viscoelastic dissipation; any strong lens deformation such as that for the thicker brush was not observed. In addition, the microscope images of the surface PDB28 and PDB132 do not show any remains of the hydrogel, Fig 6.4, making the mechanism adhesive. There is not a great difference in the work of adhesion between the hydrogel and PDB28 and PDB132; which suggests that probably only the interfacial layer is involved in the adhesion process.

From Fig 6.3 we can observe that the threshold between the adhesive and cohesive failure is narrow and is of the order of 30 Å, switching from one to the other in the range of 132 and 165 Å brush thickness. We do not have an explanation for the sharpness of this jump from adhesive to cohesive failure but from the neutron reflectivity experiments, bringing the PMAA hydrogel into contact with the PDMAEMA brush for different thicknesses, we can offer speculative suggestions, also these are discussed below.

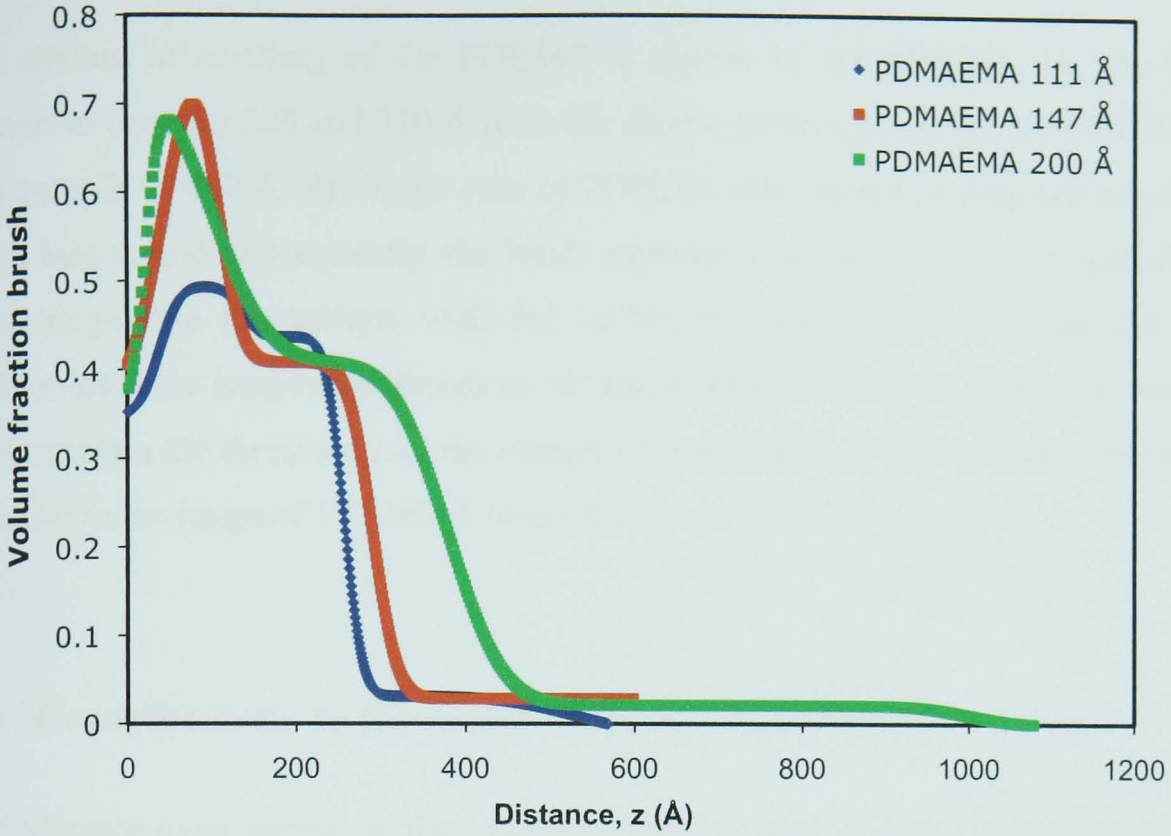

Fig 6.5 The conformation of brushes of thickness 111, 147 and 200 Å in contact with the hydrogel, in water environment, after a pressure of 150 mN was applied for 15 min and then released.

Fig 6.5 shows the conformation of brushes of 111, 147 and 200 Å thickness, indicated as PDB111, PDB147 and PDB200; the ordinates represent the volume fraction of the polymer, as a function of the distance from the silicon wafer at $z = 0$. We have already explained this conformation in section 5.5.2, observing that the applied pressure pushes the polyelectrolyte brush film close to the silicon wafer. We shall analyze the conformation from a different point of view, by correlating the brush conformation to the work of adhesion, which should help understand the jump in the total work of adhesion between 132 and 165 Å.

The conformation of the brushes PDB111, PDB147 and PDB200 show a sharp interface in the direction of the hydrogel with a consistent composition of 50% water and 50% polymer showing that the concentration of polymer and consequently the degree of ionization at the interface is the same and is independent of the brush thickness. The brush composition at the hydrogel/brush interface might explain the results for PDB28 and PDB132, which does not show any large difference in energy of adhesion; this suggests that only the interface of the hydrogel with the polymer brush layer is involved in the adhesion process in this range of thickness.

The amount of swelling of the PDB147 is similar to the PDB111, i.e. the brush extends to between 280 and 310 Å from the silicon surface, while for the PDB200 the film extends to 420 Å [4]. In the case of PDB200, the amount of polymer swollen is much larger, and consequently the brush presents more amino groups available to form long-range interactions with the carboxylic groups into the hydrogel. The addition of these long-range forces to the interaction at the brush/hydrogel interface might explain the threshold and the change of mechanism of failure from adhesive to cohesive in the range of 132-165 Å brush thickness.

6.4 Contributions to the brush-hydrogel interaction

The adhesion experiments, in the unloading regime, show a strong dependence of the work of adhesion on the brush thickness. We suppose that the main parameters, responsible for the large adhesion energy, are:

- viscoelastic dissipation of the hydrogel;
- the electrostatic effect; and
- hydrogen bonding.

Each parameter is discussed separately to understand its contribution to the total work of adhesion in the unloading regime. In this chapter, we dismiss the contribution of the interpenetration of the brush chains the hydrogel because, from the neutron reflectivity experiments, shown in section 5.5.2, we have no conclusive evidence of this effect. Further experiments, comparing the thermodynamic work of adhesion for the brush and gel film in the same range of thicknesses, show no difference in value. This evidence supports the statement that the interpenetration effect is unlikely to happen.

6.4.1 Contribution of the viscoelastic dissipation of the hydrogel

In section 6.3 we showed the dependence of the work of adhesion as a function of the brush thickness. We qualitatively discussed the contribution of the viscoelastic dissipation to the total work of adhesion, comparing the deformed shape of the hydrogel for different brush thicknesses before being separated from the brush surface

(Fig 6.4). When the hydrogel is pulled from the brush surface, the polymer chains inside the hydrogel can be highly stretched, losing more energy before being separated from the brush surface. The contribution of viscoelastic dissipation of the hydrogel is a function of the strength of the brush/hydrogel interface. We demonstrate here that the hydrogel dissipates more energy as the brush thickness increases because the hydrogel-brush interface is stronger than that for thinner brushes and the rupture may not take place at the hydrogel-brush interface but within the hydrogel.

In Fig 6.6 we compare the behaviour of the PMAA045 in contact with PDB311 and PDB132. This graph shows the variation of contact diameter and pull-off force, as a function of time, in the unloading stage, after the hydrogel had been kept in contact with the brush surface for 15 min at constant force to ensure equilibration.

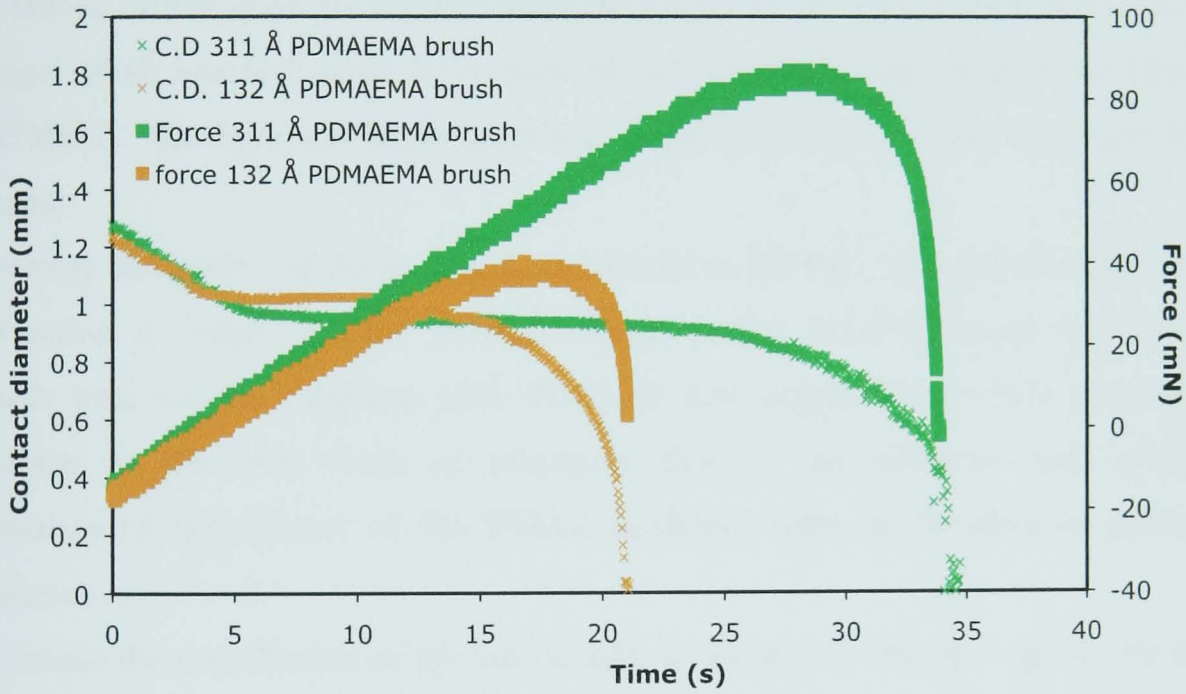

Fig 6.6 Variation of contact diameter and pull-off force as a function of time in the unloading stage for brushes of thickness 132 and 311 Å in contact with the PMAA hydrogel with 0.45 % of crosslinker (PMAA045).

In the case of the PDB311, the pull-off force increases monotonically until it reaches a maximum of 85 mN and then the force drops to zero. At the same time the contact diameter is reduced from 1.3 to 0.95 mm and then remains constant for 20 s before decreasing quickly until it reaches zero, when the gel detaches from the surface. In the particular case of PDB311, the hydrogel is detached from the surface cohesively because the chemical bonds of the hydrogel are weaker than the hydrogel brush interface; evidence of this mechanism is shown in Fig 6.4.

In the case of PDB132, the same trend is observed as for the PDB311; the force increases monotonically until a maximum of 35 mN is reached and then it decreases quickly to zero. The contact diameter decreases from 1.2 to 1 mm, is constant for 10 s and then decreases until the gel is detached from the surface in an adhesive mechanism. It is important to notice that for both thicknesses, the contact diameter is constant while the force increases monotonically; this trend shows that the hydrogel is deformed without affecting the interface, and releases energy (eventually by heat) by stretching the chains inside the hydrogel as viscoelastic dissipation. The dissipation energy is larger in the case of PDB311, where the contact diameter is constant for 20 s, than for the PDB132, where the contact diameter is constant for 10 s. When the pull-off energy becomes too large, the hydrogel-brush interface fails with a different mechanism, which depends on the brush thickness. In the case of the PDB132, the hydrogel-brush interface starts to be torn off and eventually separated. In the case of the PDB311, the hydrogel-brush interface is not modified but the hydrogel itself ruptures.

The energy dissipation of the hydrogel contributes to the total work of adhesion but its contribution is larger for the PDB311, because the brush-hydrogel interface is stronger than for the interface with PDB132; this suggests that other parameters contribute to the total work of adhesion, causing the adhesive and cohesive mechanism of detachment of the PMAA hydrogel with the brushes of different thickness.

To estimate the contribution of the viscoelastic dissipation in the hydrogel to the total work of adhesion, we performed adhesion experiments by using identical brush samples but changing the crosslink percentage of the PMAA hydrogel.

In order to analyse our data concerning the effect of the viscoelastic dissipation, we need the modulus of the hydrogel, which is calculated by measuring the variation of the contact diameter when known loads are applied. These experiments have been performed on a silicon surface in the loading regime and the experimental points are fitted using the Hertz equation [11]. The moduli are of the order of MPa and are listed in Table 6.2.

Hydrogel	Elastic Modulus (MPa)
PMAA3	5.58
PMAA093	0.25
PMAA069	0.18
PMAA045	0.17

Table 6.2 Elastic moduli of the PMAA hydrogels of different crosslinking densities.

The contribution of the dissipation energy can be demonstrated by comparing the trend of the contact diameter as a function of the pull-off force in the unloading stage for the 311 Å thick PDMAEMA brush bought into contact with PMAA045 or PMAA3.

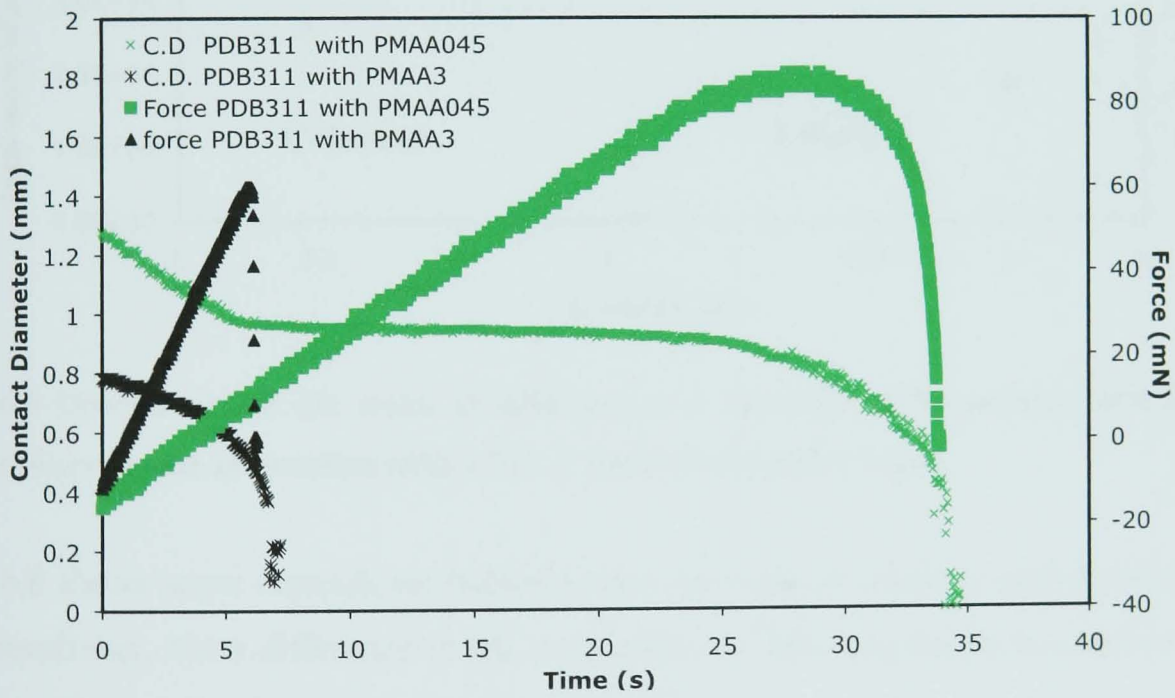

Fig 6.7 Comparison of the variation of the force and contact diameter (C.D.) as a function of the time for the 311 Å thick PDMAEMA brush in contact with the PMAA3 and PMAA045 hydrogels.

As can be seen in Fig 6.7, the PMAA3 does not establish a constant contact diameter as the force increases monotonically, unlike the PMAA045. This demonstrates that the contribution of the viscoelastic dissipation to the total work of adhesion is lower at large hydrogel crosslinking because its material strength is increasing. We also

investigated different PMAA crosslinking densities to understand if this parameter also influences the mechanism of detachment of the hydrogel from the brush.

Fig 6.8 shows the total work of adhesion for the PDB311 in contact with PMAA hydrogel at 0.45, 0.69, 0.93 and 3% crosslinking percentage. The amount of crosslinker influences the swelling of the hydrogel as well such that the hydrogel with the greater percentage of crosslinker has the lowest radius of curvature and radius of contact between brush and gel for the same applied force in comparison with the other crosslinking densities studied.

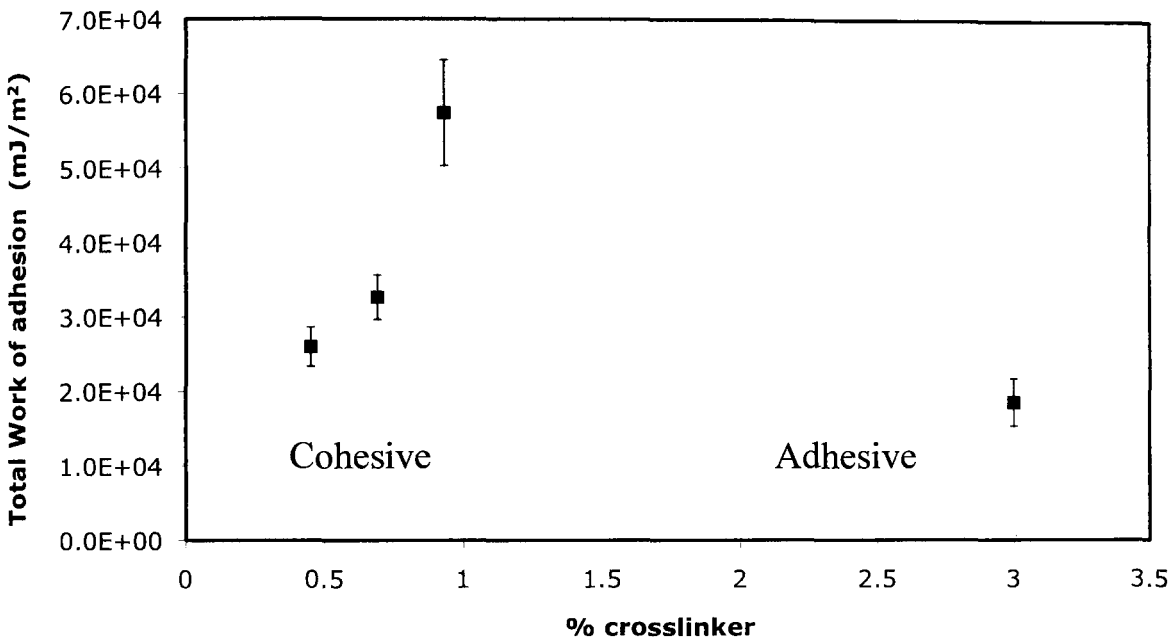

Fig 6.8 Dependence of the work of adhesion as a function of the amount of PMAA crosslinker for the interaction with a 311 Å thick PDMAEMA brush.

Fig 6.8 shows some dependence between the total work of adhesion and the amount of crosslinker, but a difference in the mechanism of detachment can be observed as the crosslinking density changes as shown in Fig 6.9.

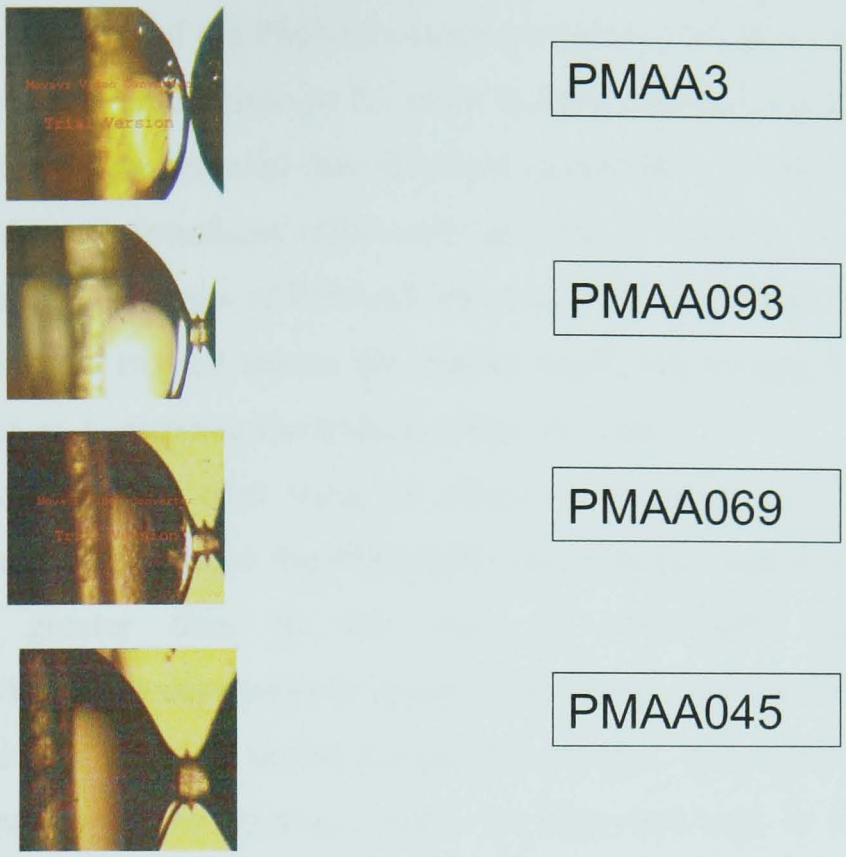

Fig 6.9 Gels of different crosslinking densities just before being detached from the PDB311. These images are collected *in situ* by a camera. The neck shows the cohesive mechanism of failure of the chemical bonds of the hydrogel for PMAA093 PMAA069 and PMAA045, while it is absent for PMAA3 in which case the mechanism of rupture is adhesive at the hydrogel-brush interface.

The mechanism of failure is adhesive for the PMAA3 and cohesive for the PMAA093-PMAA045. This means the value of the total work of adhesion for the PMAA093, PMAA069, and PMAA045 is underestimated because the chemical bonds in the hydrogel fail before the gel-brush interface. We discuss below a few possible explanations for these different mechanisms of detachment as a function of the crosslinking percentage.

One explanation could be related to the local force applied on the edge of the hydrogel. The PMAA045, PMAA069 and PMAA093 all have a lower modulus than that of PMAA3 and so the lenses are softer and more deformable, and consequently the force applied at the edge of the lens is locally larger for the lower crosslinking percentage hydrogel leading to a breakage inside the hydrogel instead of at the hydrogel-brush interface. In the case of the PMAA3, the lens is stiffer and elastic and

the local force at the edge is not too high, leading to a breakage at the hydrogel-brush interface. The stiffness of the PMAA3 causes a much lower value (around 40% lower) of area of contact in comparison to the other studied hydrogel when the same force is applied. We have demonstrated that the main mechanism of interaction between the hydrogel/brush is the interfacial effect and the work of adhesion increases as the area of contact arises. In the case of PMAA3, the smaller area of contact in comparison to the other hydrogels studied means the system needs less energy, i.e. a smaller total work of adhesion, to separate the hydrogel from the brush.

Fig 6.8 shows that the total work of adhesion is greater at PMAA093 than at PMAA045, probably because the PMAA093 has a larger modulus and the hydrogel strength is greater than in the case of PMAA045. Consequently the PDB311/PMAA093 system needs to spend more energy than the PDB311/PMAA045 before the network is broken during the pull-off process. To conclude, the viscoelastic energy dissipation of the hydrogel plays an important role in the total work of adhesion between the hydrogel and the PDMAEMA brush, unlike for the systems shown in Fig 6.6 where the contact diameter and pull-off force change as a function of time for the 132 Å and 311 Å thick PDMAEMA brushes in contact with PMAA045. For these two samples, (PMAA045 / PDB311 and PMAA045 / PDB132), the contact diameter is constant while the pull-off force increases monotonically; the pull-off force reaches a maximum and then drops to zero while the contact diameter of the hydrogel decreases until it reaches zero. The constant contact diameter is due to the viscoelastic dissipation of the hydrogel, which stretches the chains inside the network. This contribution is higher in the case of the PDB311 than for the PDB132, because for thicker brushes there may be an increasing contribution of other parameters to the total work of adhesion such as electrostatic and hydrogen bonding, raising the strength of the hydrogel-brush interface. We performed some other experiments keeping the same brush samples and changing the crosslinking densities on the PMAA hydrogel. These experiments show that the crosslinking percentage influences the mechanism of detachment of the hydrogel from the brush. At 3% crosslinker the failure mechanism is adhesive and at 0.93, 0.69 and 0.45% crosslinker, the mechanism is cohesive.

6.4.2 Electrostatic effect

The brush and hydrogel are weak polyelectrolytes and consequently both electrostatic and hydrogen bond interactions should play an important role in the adhesion process. We have already shown that viscoelastic dissipation of the hydrogel contributes significantly to the total work of adhesion for thicker brushes. In this case the dissipation energy is larger, probably because there is a large amount of polymer chains that contribute through long-range forces to the adhesion with the hydrogel in comparison to the thinner brush. The volume fraction depth profile measured by neutron reflectivity, (Fig 6.5), shows the conformation of the brush for different brush thicknesses. The difference in conformation between the PDB111 and PDB147 lies in the brush volume fraction close to the silicon wafer: 50% for the PDB111 and 75% for the PDB147. The two conformations show the same value of volume fraction, close to the hydrogel, 0.45, and a similar extension of ~300 Å from the substrate. The PDB200 has the same volume fraction as for the PDB147, with $\phi = 0.70$, close to the silicon wafer and the same volume fraction as for the PDB111 and PDB147, 0.45, in the vicinity of the hydrogel, but it shows a greater thickness of swelling, 400 Å. A polymer brush with a greater swelling thickness but with the same volume fraction profile suggests that a larger number of monomers are available to bind with the hydrogel via long-range interactions. To study the electrostatic contribution, we need to isolate it from any other parameters such as the viscoelastic dissipation of the hydrogel, and any possible interpenetration effect of the brush into the hydrogel.

For this reason, we performed adhesion experiments using the PDMAEMA gel film instead of the PDMAEMA brush in contact with the PMAA3. The brush and gel film are based on the same monomer but they have different topologies. The gel film is a random copolymer of DMAEMA and BPMA monomers. The BPMA, in a concentration of 5% respect to the amount of DMAEMA, is a photocrosslinking agent that allows the PDMAEMA to be chemically attached to a modified silicon wafer. Due to its structure, the free chains of the PDMAEMA gel film have less chance to interpenetrate the hydrogel, unlike the brush. The adhesion experiments have been performed for the same thicknesses as the brush, 28, 119 and 340 Å, denoted as PDG28, PDG119 and PDG340.

In the Fig 6.10 we show the work of adhesion as a function of the thickness for the PDMAEMA gel film. These experiments were performed following the same

procedure as for the brush. The gel films were equilibrated for two hours and then PMAA3 was brought into contact for 15 min, with a force of 20 mN applied, and then detached. The total work of adhesion is calculated by integrating the force-displacement curve in the unloading process.

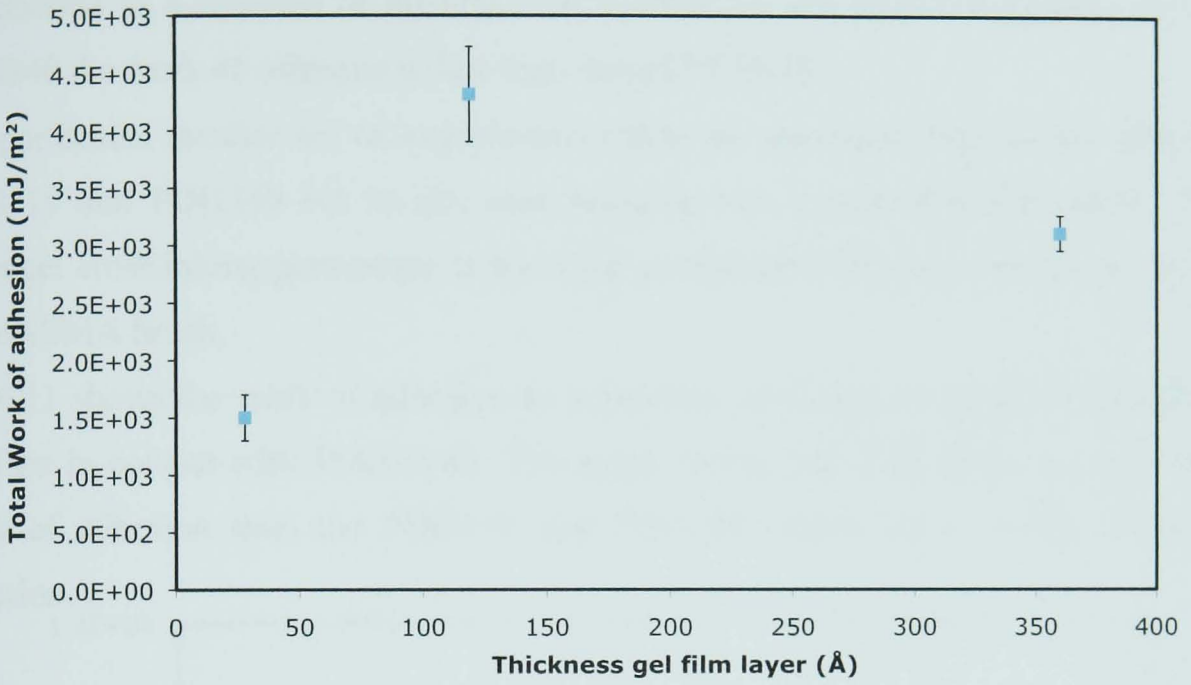

Fig 6.10 Work of adhesion as a function of the gel film thickness. The PMAA gel is synthesized with 3% crosslinker by weight (PMAA3).

The total work of adhesion is a function of the gel film thickness. The energy to separate the gel film / hydrogel interface is greater for the PDG28 than the PDG119 with that for the PDG340 in between these values. The higher charge density as a function of the gel film thickness could justify an increase of the work of adhesion for the hydrogel with the PDG119 than with PDG28, but we cannot explain why it decreases again for the PDG340. In the case of the gel film, we could expect a slightly greater dependence of thickness in comparison with PDMAEMA brush in the range of thickness corresponding to adhesive failure (Fig 6.8), because the topology of the two surfaces is different. We do not have any information about the conformation of the gel film but, from the AFM experiments, (Table 6.3), we know that the gel film swells 30 % more than the brush under the same pH conditions and range of thickness. This suggests that the gel film has probably more charged groups than the brush and consequently a different conformation. Because we have observed an electrostatic effect on the gel film (Fig 5.10) with PMAA3, we can conclude that the same effect is important for the brush film, since the two polymers are the same.

To summarise, to estimate the role of the charge effect on the hydrogel-brush interaction, we performed adhesion experiments between PDMAEMA gel films of different thicknesses in contact with the PMAA3. We chose this system to minimize the contribution of the dissipation energy. The results show a dependence of the work of adhesion as a function of thickness for the PDG28 and PDG119 samples but for PDG340 the work of adhesion is less than that of PDG119.

We performed another set of experiments using the same gel film surface PDG28, PDG119 and PDG340 but in this case bringing into contact the PMAA045. This hydrogel crosslinking percentage is the same as that used for the experiments on the PDMAEMA brush.

Fig 6.11 shows the work of adhesion as a function of thickness for the PDMAEMA gel film in contact with PMAA045. The graph shows that PDG28 has a larger total work of adhesion than the PDG119 and PDG340, which have similar works of adhesion.

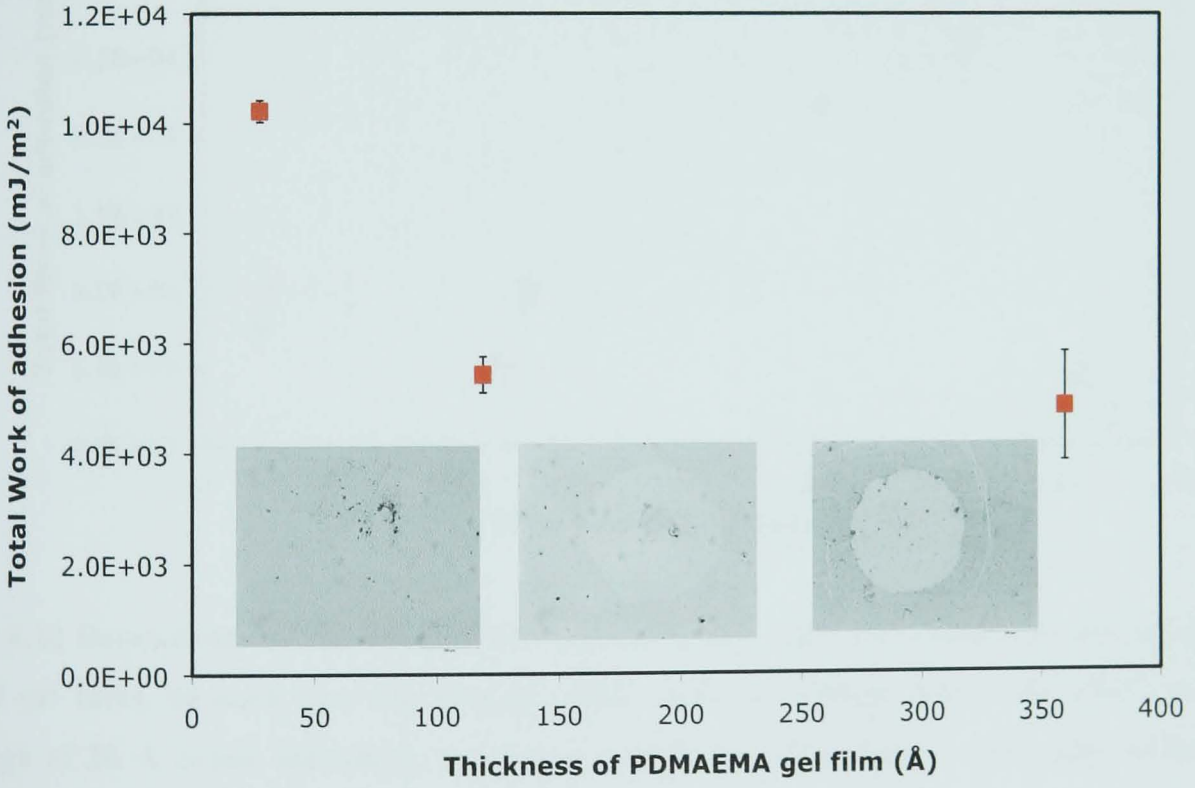

Fig 6.11 Variation of the work of adhesion as a function of the gel film thickness in contact with PMAA045. The microscope images, below each point, show that, for PDG119 and PDG340, the gel film is ripped off during the unloading stage of the hydrogel. The same effect is not recorded for the PDG28 where the failure is at the hydrogel-gel film interface.

We analyzed the film surface with optical microscopy after the gel film was in contact with the hydrogel PMAA045 to have some information about the mechanism of

failure. The microscopy images, shown in Fig 6.11, reveal that, in the case of PDG119 and PDG340, the gel film itself is ruptured and detached from the silicon wafer. This is confirmed by performing the same experiments again using the same gel on the same spot. The work of adhesion for the second trial dropped to zero as expected for a silicon surface. The same result is not observed for the PDG28 where the value of total work of adhesion for the first and second trials was comparable. The hydrogel-gel film interface seems to be stronger than the silicon-gel film interface for the PDG119 and PDG340, but this is not the case for the PDG28. The graph in Fig 6.12 allow us to compare the work of adhesion of the brush and gel films in contact with PMAA045 as a function of polymer layer thickness.

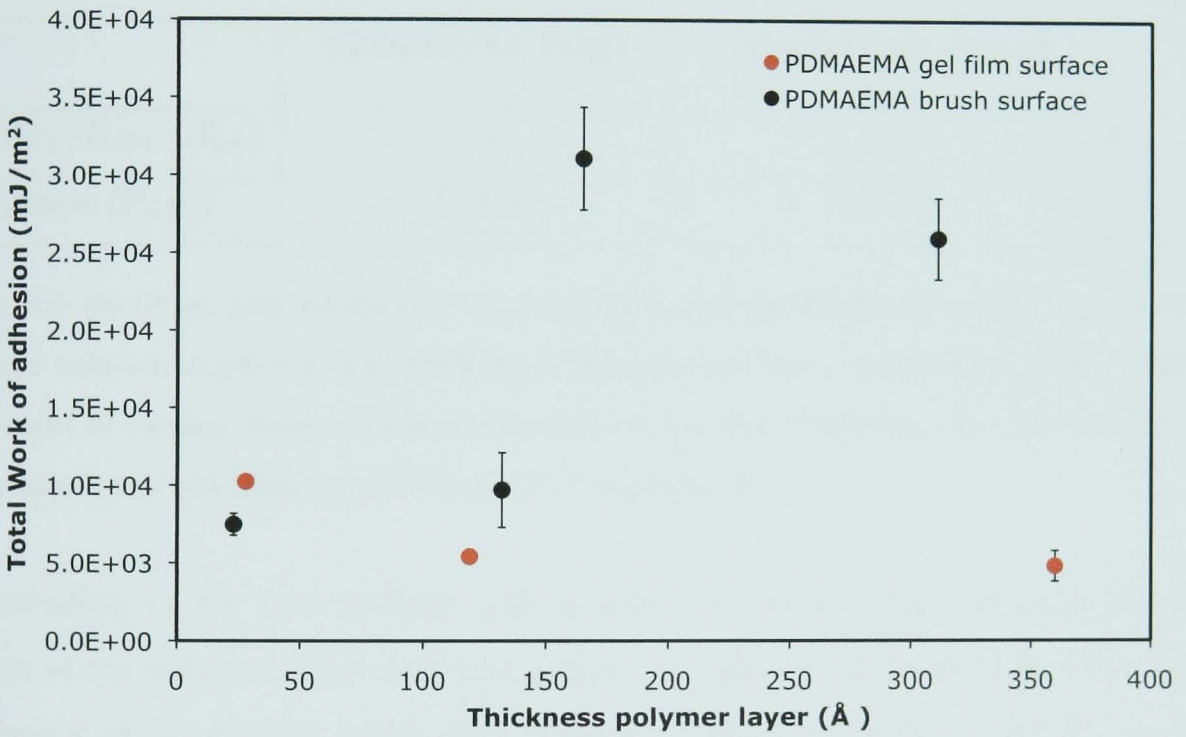

Fig 6.12 Dependence of the work of adhesion as a function of the thickness of the brush and gel films. In each case the polymer films were in contact with PMAA045. In the range of 20 Å brush thickness, the brush and the gel film have comparable adhesion energies but for 119 and 340 Å gel film thicknesses, the measured work of adhesion is smaller than the interfacial works of adhesion because the gel film-silicon interface debonds before the gel film-hydrogel interface can rupture.

Fig 6.12 shows that the work of adhesion for the thinner brush and gel films (23 and 28 Å thick respectively), is comparable, while at thicknesses greater than 100 Å, the gel film work of adhesion is smaller than that of the brush; we observe that the mechanism of rupture is different for the brush and the gel film. For the brush, the

mechanism is cohesive and the chemical bonds inside the hydrogel are weaker than the interface hydrogel-brush. In the case of the gel film, the silicon-gel film interface is weaker than the hydrogel-gel film interface. To understand the behaviour of the gel film at the interface, we performed an AFM study to compare the swelling and the roughness of the brush and gel film in water. These AFM experiments give a qualitative idea about the swelling of the two surfaces, which is related to the conformation of the brush and gel film polymer and to the amount of polymer per unit surface area. Any swelling difference is due to the way that brush and the gel film are synthesized. The brush is synthesized by the "grafting from " method that gives a high grafting density and the gel film by the "grafting to" method that gives a less dense polymer surface.

	PDMAEMA brush	**PDMAEMA gel film**
Swelling (H_{H20}/H_{dry})	1.23	1.60
Roughness (R_{RMS})	10.64 Å	8.70 Å

Table 6.3 Swelling and roughness of the brush and gel films measured by AFM in aqueous solution at pH = 6. The swelling of the polymer layer is calculated as the ratio of the height of swollen water thickness divided by the dry thickness. The dry thicknesses of the brush and gel films are 207 and 277 Å respectively.

The swelling of the two surfaces was studied by AFM in aqueous solution. The surface of the polymer films was scratched using a blade and the thickness measured (the height of the scratch) under dry conditions. Then pure water was added and the thickness measured again in equilibrium. The value of swelling, indicated in Table 6.3, is the ratio of the film thickness in water over the thickness in dry conditions. The same procedure is used for both the brush and the gel film samples. The thickness in the dry condition is 277 Å for the brush and 207 Å for the gel film. The gel film, under the same pH condition, swells 30% more than the brush, confirming that the gel film has a smaller amount of polymer per unit surface area. This is because the gel film is chemically anchored on the surface through the photocrosslinker monomers at a weight fraction of 5%, while, for the brush, each chain is covalently bound to the surface and consequently the brush layer is more strongly attached onto the silicon surface than the gel film. This difference could explain why for the brush the failure is at the interface hydrogel-brush or inside the hydrogel, unlike for the gel film where

the failure is at the gel film-silicon or at the hydrogel-gel film interface. When the hydrogel is pulled-off, the gel film chains, not as strongly attached to the surface as the brush, can be stretched more than the brush and it costs more energy to break the hydrogel-gel film interface than the silicon-gel film interface because more energy can be dissipated in the film than the brush. The same effect is not observed for the PDG28. Due to the sample preparation the gel film PDG28 has a larger fraction of crosslinks to the surface than the PDG119 and PDG340 sample. The gel film is made of a random copolymer of DMAEMA and BPMA. When the spin coated film is exposed to the UV lamp [9], the photo-crosslinker reacts with the initiator layer on the silicon wafer and with other monomers to form the network. If the film is thinner (as when prepared from a dilute solution), the ratio of initiator molecules to BPMA is higher than for a thicker film, made from a more concentrated solution. Consequently the thinner film is highly covalent bound with the surface and so remains attached to the silicon in the pull-off process.

The comparison of the roughness for the gel film and brush in the same conditions of pH does not show any appreciable difference, demonstrating that this parameter is not responsible for any difference in the mechanism of adhesion between the two processes.

To summarize, the analysis shows that the total work of adhesion of the PDMAEMA gel film has a different behaviour as a function of thickness with respect to that of the brush. The work of adhesion is greater for PDG28 and then decreases and assumes a constant value for PDG119 and PDG340. The comparison of the work of adhesion for the brush and the gel film shows that for a thickness of 28 Å the brush and gel films have comparable works of adhesion but for thicknesses of 119 Å and 340 Å, the gel film has a smaller work of adhesion than for the brush of comparable thickness. The microscope images (Fig 6.11) of the gel film after being in contact with the PMAA045 show that the polymer gel film is torn off when the hydrogel lens is removed. This can be explain the low value of the total energy of adhesion for the gel film with the silicon substrate in comparison with the PDMAEMA brush, especially at greater thicknesses. A different mechanism of failure is observed when the gel films are added in contact with the PMAA3. Under these experimental conditions, the gel film is stable and does not rupture at the silicon interface but experience adhesive failure at the interface with the hydrogel. To demonstrate this we performed the pull-

off experiments with the same gel on the same spot twice; these experiments showed that there is no significant difference in the work of adhesion between the two trials of PMAA synthesized with 3% crosslinker. This different mechanism of failure as a function of the percentage of crosslinker is likely to be due to the local force applied at the edges of the hydrogel. The PMAA3 is stiffer than the PMAA045 and, consequently, the local force at the edges of the hydrogel, during the pull off process, is lower than that for the PMAA045, initiating the crack at the hydrogel-gel film interface.

6.4.3 Hydrogen bonding

To estimate the contribution of hydrogen bonds we performed pull-off experiments, bringing the PHEMA gel film into contact with PMAA hydrogel of different crosslinking densities. PHEMA is a water-soluble polymer with a similar chemical structure to the PDMAEMA. The PHEMA interacts with the PMAA hydrogel forming mainly hydrogen bonds [12]. In Fig 6.13, we show the variation of the total work of adhesion for a 40 Å thick PHEMA gel film as a function of the hydrogel crosslinking density.

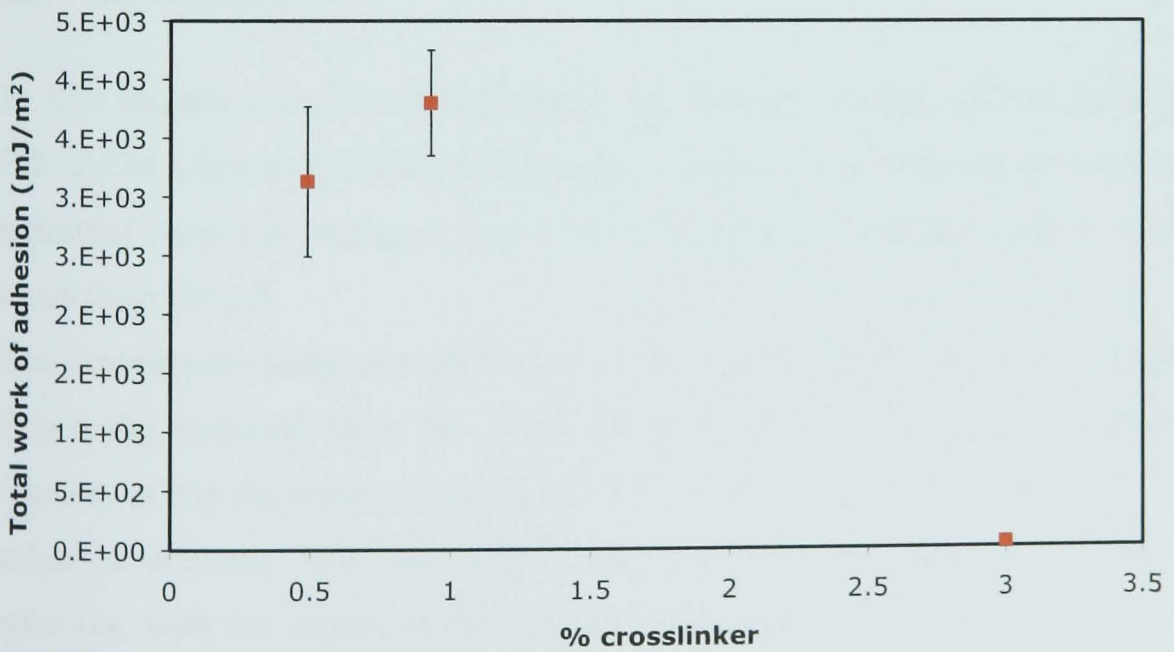

Fig 6.13 Work of adhesion for the PHEMA gel film (40 Å thickness) as a function of the percentage of crosslinker in the PMAA hydrogel.

From the mechanical measurements, the work of adhesion is in the order of 70 mJ/m^2 [13] when the PHEMA40, is in contact with PMAA3, while it increases by a factor of between 40 and 50 when the hydrogel is brought into contact with the PMAA093 and PMAA045. In the case of PMAA045 and PMAA093, the modulus of the gel decreases and the hydrogel has a larger radius of curvature and therefore area of contact with the surface. Consequently, the gel film and the hydrogel have more points of contact than for the PMAA3 to interact via hydrogen bonds which use a large amount of energy to separate the hydrogel from the PHEMA40 surface. In this condition, contribution of the dissipation energy is larger for less crosslinked PMAA gels, explaining the greater work of adhesion for PHEMA in contact with PMAA045 and PMAA093. To conclude, hydrogen bonding seems not to play any major role in the adhesion between the PHEMA and consequently the PDMAEMA brushes and the hydrogel if viscoelastic dissipation is not significant. This is exemplified by the total work of adhesion being significantly greater for less crosslinked PMAA gels than the most crosslinked gel (PMAA3) studied.

6.5 Conclusion

In this chapter we described pull-off experiments of the PMAA hydrogel from PDMAEMA brush of different thicknesses. This kind of experiment is important for industrial purposes because it gives an idea of the real energy spent to separate the brush from the gel.

The experiments show a brush thickness dependence of the total work of adhesion to detach the hydrogel from the brush. In particular it is possible to recognize two regions. In the thickness range of 28-132 Å, the total work of adhesion assumes a value of between 7000 and 10000 mJ/m^2 and the mechanism of detachment is adhesive, with the failure at the hydrogel-brush interface. In the region thickness of 165-311 Å the total work of adhesion reaches a value of between 25000 and 30000 mJ/m^2, three times more than in the region where the adhesive failure is observed and the detachment has a cohesive mechanism; the failure is with the hydrogel. This means that the chemical bonds inside the hydrogel are weaker than the hydrogel-brush

interface. To understand this different mechanism of detachment and total work of adhesion, we hypothesised that the main parameters, responsible could be:

- viscoelastic dissipation of the hydrogel;
- an electrostatic (charge) effect; and
- hydrogen bonding.

The strategy used was to isolate, as well as possible, each effect to estimate each contribution to the total work of adhesion of the PMAA hydrogel and PDMAEMA brush system.

To estimate the viscoelastic dissipation energy of the hydrogel, we studied the change of contact diameter of the PMAA as a function of the crosslinker percentage in contact with the PDB132 and PDB311 as a function of the pull-off force. The comparison shows that the viscoelastic dissipation contributes more for the PDB311 than for the PDB132. In the case of the PDB311 the contact diameter is constant for 20 s while for the PDMA132 the contact diameter is constant for 10 s; in both cases, the pull off force increases monotonically, stretching the chains of the network while the contact diameter is constant.

This means that increasing viscoelastic dissipation is a consequence of the larger strength of the hydrogel-brush interface at PDB311 than PDB132, due to other contributions such as electrostatic and/or hydrogen bonding.

To study the electrostatic interaction between the brush and the hydrogel as a function of the thickness we performed pull-off experiments by bringing into contact the PMAA3, the most crosslinked gel, with a PDMAEMA gel film. The reasoning behind these experiments is to quantity the electrostatic forces by inhibiting the effect of viscoelastic dissipation of the hydrogel and the interpenetration effect of the brush into the hydrogel. The total work of adhesion of the PMAA3 in contact with the PDMAEMA gel film at different thickness increases with the gel film thickness and then decreases slightly. This suggests that electrostatic forces are an important parameter in the hydrogel-brush interaction. To quantify the hydrogen bonding interaction between the brush and the hydrogel we performed pull-off experiments with PMAA hydrogel and PHEMA gel film. This polymer is weak polyacid much weaker than the PMAA hydrogel, soluble in water and with a similar structure to the PDMAEMA. PHEMA can interact with the PMAA only through hydrogen bonding. These experiments show that there is hydrogen bonding between the hydrogel and the

brush but their contribution to the total work of adhesion is small in comparison to the electrostatic interaction between the PDMAEMA brush and the hydrogel.

1. La Spina, R., et al., *Controlling network-brush interactions to achieve switchable adhesion.* Angew. Chem. Int. Ed., 2007. **46**: p. 6460-6463.
2. Silberzan, P., et al., *Study of the self-adhesion hysteresis of a siloxane elastomer using the JKR method.* Langmuir, 1994. **10**: p. 2466-2470.
3. O'Connor, K.P. and T.C.B. McLeish, *"Molecular Velcro": Dynamics of a constrained chain into an elastomer network.* Macromolecules, 1993. **26**: p. 7322-7325.
4. Seidel, C., *Strongly stretched polyelectrolyte brushes.* Macromolecules, 2003. **36**: p. 2536-2543.
5. McGuiggan, P.M., *Stick slip contact mechanics between dissimilar materials: Effect of charging and large friction.* Langmuir, 2008. **24**: p. 3970-3976.
6. Barthel, B., *Modelling the adhesion of spheres: when the form of the interaction is complex.* Colloids and Surfaces, 1999. **149**: p. 99-105.
7. Anseth, K.S., C.N. Bowman, and L. Brannon-Peppas, *Mechanical properties of hydrogels and their experimental determination.* Biomaterials, 1996. **17**: p. 1647-1657.
8. Tokarev, I. and S. Minko, *Stimuli-responsive hydrogel thin films.* Soft Matter, 2009. **5**: p. 511-524.
9. Huang, J., et al., *Synthesis and in situ atomic force microscopy characterization of temperature-responsive hydrogels based on poly(2-(dimethylamino)ethyl methacrylate) prepared by atom transfer radical polymerization.* Langmuir, 2007. **23**: p. 241-249.
10. Johnson, K.L., *Mechanics of adhesion.* Tribol. Int., 1998. **31**: p. 413-418.
11. Johnson, K.L., K. Kendall, and A.D. Roberts, *Surface energy and the contact of elastic solids.* Proc. R. Soc. London A, 1971. **324**: p. 301-313.
12. Ferreira, L., M.M. Vidal, and M.H. Gil, *Evaluation of poly(2-hydroxyethyl methacrylate) gels as drug delivery systems at different pH values.* Int. J. of Pharmac., 2000. **194**: p. 169-180.
13. Falsafi, A., M. Tirrell, and A.V. Pocius, *Compositional effects on the adhesion of acrylic pressure sensitive adhesives.* Langmuir, 2000. **16**: p. 1816-1824.

Summary and future work

In this project, we studied the adhesion between a weak base brush, PDMAEMA, grafted from a silicon surface and a weak polyacid hydrogel, synthesised from MAA monomer. The brush and gel are both pH responsive but to different pH triggers. The weak polybase brush is positively charged in acid pH and uncharged in base pH while the weak polyacid hydrogel is charged in basic condition and uncharged in acid pH. The amount of charges influences the swelling of the polymer chains because the polymers uptake water to minimize the repulsion forces between the charges.

To quantify the adhesion between the brush and the hydrogel we performed kinetics experiments using a modified JKR set up. The hydrogel was synthesised in a hemispherical shape with 3.5 mm radius of curvature. The experimental procedure consists of leaving the brush sample to equilibrate for two hours inside the liquid cell, filled with the pH solution that we want to study. Using the camera and with gel illuminated from the other side by a light source we can observe and collect the variation of contact diameter of the hydrogel at the beginning, when the hydrogel is added on the brush surface, when the load is applied and when it is removed. We performed these experiments at pH 2, 3.4 and 5.8. We observe that:

the interaction between the brush and the hydrogel is dependent on the pH.

If the gel and the brush are equilibrated at pH 2 they do not adhere, i.e. the value of the contact diameter after the load is removed is the same as that before it was applied, showing no adhesion between the brush and the hydrogel. If they are equilibrated above pH 3 they adhere very strongly, marked by a large increase in contact diameter after the load is removed compared to before it was applied; the only way to separate the two components is to tear the brush off the surface, or to rupture the gel. If they are equilibrated at pH 3.4 the final value of contact diameter, after the unloading, is larger than at the beginning but smaller than at pH 5.8.

We observed that

the adhesion is switchable and triggered by the pH;

If the two components initially in contact at pH 5.8 (strong adhesion) are equilibrated at pH 1 the gel detaches from the brush without damaging either and the system may be used again.

To quantify the adhesion between the brush and the hydrogel we used the JKR equation where the thermodynamic work of adhesion is a function of the radius of curvature of the hydrogel lens, the applied load, the bulk modulus of the lens and the area of contact between the brush and the hydrogel after that the load is removed (unloading stage). We performed the experiments by applying different loads and we observed that the interaction between the brush and the gel is pressure sensitive; the adhesion energy increases as larger loads are applied and removed. This suggests that probably more than one mechanism is involved in the adhesion process. We therefore hypothesize that the interaction between the brush and hydrogel may be pressure sensitive due to interfacial (e.g. electrostatic) or interdigitation effects.

- Interfacial (surface) effect

  The force applied produces an increase in the contact area between the brush and hydrogel, creating more surface available for electrostatic or hydrogen bond interactions between the amino and carboxylic groups of the polybase and polyacid respectively.

- Interdigitation effect

  The Velcro^{TM} effect could be another mechanism involved where the increase in the applied load generates an interdigitation of the brush into the hydrogel.

The actual mechanism could be a mixture of both interfacial and interdigitation effects whose contributions may vary over a range of applied pressures.

We conclude

the interfacial (surface) mechanism is the dominant mechanism in the interaction between the brush and the hydrogel.

The neutron reflectivity experiments of the brush in contact with the hydrogel when the pressure is applied and released allow an observation of the behaviour of the brush under the same conditions as those for the JKR adhesion experiments. From volume fraction-depth profiles, obtained using neutron reflectivity, there is no evidence of any interpenetration of the brush chains into the hydrogel, because for each increase in applied pressure, the data show a sharp interface close to where we expect the hydrogel to be located. The comparison of the brush profile at different brush

thickness, (111, 147 and 200 Å), show that the composition of the polymer at the interface with the hydrogel is the same and is independent of the brush thickness. The amount of polymer swollen is larger for thicker brushes suggesting a large contribution of long-range interactions between the amino group of the brush chains and the carboxylic group of the PMAA hydrogel as the thickness of the brush increases. To confirm this behaviour, we performed adhesion experiments to understand if the thermodynamic work of adhesion between the brush and the hydrogel is a function of the brush thickness. The comparison of the thermodynamic work of adhesion for a 200 and 90 Å thick brush in contact with the hydrogel shows the brush with higher thickness has a large value of thermodynamic work of adhesion. This result is in agreement with the volume fraction profile of the brush because a thicker brush has a larger number of available amino to interact with the carboxylic groups of the PMAA hydrogel than the brush of smaller thickness. Finally, to exclude any interpenetration of the brush chains into the hydrogel, we performed some experiments with the JKR set up by substituting the PDMAEMA brush system with a PDMAEMA gel thin film in contact with the PMAA hydrogel in the same range of thickness. A comparison of the thermodynamic work of adhesion between the brush and a gel film made by the same polymer but with comparable thickness does not show that the adhesion has any dependence on the topology of the polymer.

The interpenetration mechanism it is unlikely to happen and confirms that the surface effect is the main mechanism of interaction.

To have a better idea about the applicability of this switchable glue, we performed some experiments to measure the energy to separate the PMAA hydrogel from the PDMAEMA brush after a known force was applied.

The set-up is similar to the one describe above but in this case a micromanipulator is used to bring the gel into contact with the brush and then to separate them.

These experiments show that

there is a brush thickness dependence of the total work of adhesion to detach the hydrogel from the brush.

In particular it is possible to recognize two regions characterized by two different mechanism of detachment. In the thickness range of 28-132 Å, the mechanism of detachment is adhesive, with the failure at the hydrogel-brush interface and the energy is in the order of 10000 mJ/m^2. In the brush thickness region of 165-311 Å the

detachment has a cohesive mechanism; the failure is with the hydrogel and the energy is in the order of 30000 mJ/m^2. This means that the chemical bonds inside the hydrogel are weaker than the hydrogel-brush interface. To understand this different mechanism of detachment and total work of adhesion, we hypothesised that the main parameters responsible could be:

- viscoelastic dissipation of the hydrogel;
- an electrostatic (charge) effect; and
- hydrogen bonding.

The strategy used was to isolate, as well as possible, each effect to estimate each contribution to the total work of adhesion of the PMAA hydrogel and PDMAEMA brush system.

To estimate the viscoelastic dissipation energy of the hydrogel, we studied the change of contact diameter and pull-off force of the PMAA in contact with the PDB132 and PDB311 as a function of the crosslinker percentage of the hydrogel.

The comparison shows that

the viscoelastic dissipation contributes more for the at large value of 165-300 Å brush thickness than for a thinner one, 28-132 Å.

In the case of the PDB311 the contact diameter is constant for 20 s while for the PDMA132 the contact diameter is constant for 10 s; in both cases, the pull off force increases monotonically, stretching the chains of the network while the contact diameter remains constant.

This means that increasing viscoelastic dissipation is a consequence of the larger strength of the hydrogel-brush interface at PDB311 than PDB132, due to other contributions such as electrostatic and/or hydrogen bonding.

To study the electrostatic interaction between the brush and the hydrogel as a function of the thickness, we performed pull-off experiments by bringing into contact the PMAA3, the most crosslinked gel, with a PDMAEMA gel film. The reasoning behind these experiments is to quantity the electrostatic forces by inhibiting the effect of viscoelastic dissipation of the hydrogel and the interpenetration effect of the brush into the hydrogel. The total work of adhesion of the PMAA3 in contact with the PDMAEMA gel film at different thickness increases with the gel film thickness and then decreases slightly. This suggests that

electrostatic forces are an important parameter in the hydrogel-brush interaction.

To quantify the hydrogen bonding interaction between the brush and the hydrogel we performed pull off experiments with PMAA hydrogel and PHEMA gel film, which can interact with the PMAA only through hydrogen bonding. These experiments show that there is

hydrogen bonding between the hydrogel and the brush but their contribution to the total work of adhesion is small in comparison to the electrostatic interaction between the PDMAEMA brush and the hydrogel.

Future work should include a systematic study of the adhesion of the brush and hydrogel in both basic conditions and as a function of ionic strength. In the case of the pH this might include the use of buffer to keep the pH of the solution constant. The buffer, and the addition of salt could screen charges in the brush and hydrogel, changing the adhesion and the mechanism of interaction between the brush and the hydrogel.

Other studies could concern the switching behaviour of the brush/gel system in basic pH.

We have performed these experiments qualitatively and we observed the switching in basic condition; but in these pH environments, other effects can be involved because the hydrogel swells, increasing the stress into the gel-brush interface and favouring the rupture.

The same kind of experiments in acid and basic condition could be performed by changing the grafting density of the PDMAEMA brush by mixing the initiator, deposited on the surface with a non active one and then performing the adhesion and switching experiments quantitatively. The grafting density of the polymer can also be changed by mixing the PDMAEMA with PHEMA polymers. Qualitatively these experiments show that the pH of switching is dependent on the amount of PDMAEMA grafted on the surface but we do not have any quantitatively information.

Other experiments could regard the use of the pull-off set-up to understand more about the adhesion between the brush and the hydrogel. Some other experiments could be performed using a hard sphere of silicon in contact with the PDMAEMA brush. Silicon spheres are covered in a thin oxide layer which shows acid behaviour. This would avoid any contribution of viscoelastic dissipation and interpenetration and would help to calculate the dependence of the adhesion between the brush and gel as a

function of the brush thickness. The same experiments could be performed on brushes with different grafting density, pH conditions and ionic strength.